Platinum sponsor

Celanese

2024 Implant Polymers:

UHMWPE & PEEK conference

June 20 – 21, 2024

Barcelona, Spain - World Trade Center

Additional sponsors:

MITSUBISHI CHEMICAL GROUP
Mitsubishi Chemical Advanced Materials GmbH

Invibio
BIOMATERIAL SOLUTIONS

Orthoplastics
A VIANT COMPANY

EVONIK
Leading Beyond Chemistry

CeramTec
THE CERAMIC EXPERTS

3D SYSTEMS

SEQENS
OUR SCIENCE FOR YOUR FUTURE

2024 Implant Polymers: **UHMWPE & PEEK conference**

June 20 – 21, 2024
Barcelona, Spain - World Trade Center
Port Vell Meeting Room

The purpose of the meeting is to bring together engineers, scientists, regulators, and clinicians from academia, industry, and government to present leading edge research on advancements in medical grade UHMWPE, PEEK, and the rapidly growing field of polymer implant additive manufacturing technology. In addition to UHMWPE and PEEK, the Combined Meeting will also broadly showcase point-of-care additive manufacturing of implantable polymers.

2024 Organizing and Scientific Committee:

Co-Presidents: Pierangiola Bracco, Ph.D. and Steven Kurtz, Ph.D.
Organizers: Hannah Spece, Ph.D. and Francisco Medel, Ph.D.

Mark Allen
Matthew Di Prima, Ph.D.
Ebru Oral, Ph.D.
Heather Prentice, Ph.D.
Claude Rieker, Ph.D.
Neha Sharma, Ph.D.

Sponsorship

We are pleased to announce that Celanese will be supporting the 2024 Combined Meeting as a Platinum Sponsor. We also welcome the sponsorship of Invibio as Silver Sponsor; and Orthoplastics, Evonik, Mitsubishi Chemical Advanced Materials, CeramTec GmbH, 3D Systems, and Seqens as Bronze Sponsors.

Interested in sponsoring our 2026 edition?
Please contact Steve Kurtz - skurtz@drexel.edu.

Celanese

Thursday, June 20, 2024 I Day One

Time	Subject	Presenter
8:00 AM	On-site Registration Opens	
9:00 AM	Opening Remarks	Steven Kurtz, Ph.D.
9:10 AM	Welcome	Amanda Dresch, Celanese
	SESSION I: UHMWPE as a Bearing Material	
	Session Co-Moderators: Steven Kurtz and Francisco Medel	
9:15 AM	**Invited Talk 1:** Introduction of Alumina Modular Heads for Ceramic on Polyethylene in Orthopaedics	Claude Rieker, Ph.D.
9:35 AM	**Podium Talk 1:** Role of implant bearing surfaces on non-revision re-operation, rehospitalisation and mortality outcomes following primary total hip replacement across a national healthcare system: evidences from the National Joint Registry	Alessandro Alan Porporati, Ph.D., CeramTec GmbH
9:50 AM	**Podium Talk 2:** The Tribological Performance of Crosslinked UHMWPE on Coated Titanium	Ryan Siskey, M.S., Exponent Inc
10:05 AM	**Podium Talk 3:** Formal Risk-Informed Validation of a Finite Element Model for Lumbar Spine Total Joint Replacement Under Normal and Impingement Conditions	Steven Kurtz, Ph.D., Drexel University
10:20 AM	**Podium Talk 4:** Correlation of crosslinking measured with the trans-vinylene index and wear as measured by a pin-on-disc test of polyethylene liners from various manufacturers used in total hip arthroplasty	Peter Wahl, Cantonal Hospital Winterthur
10:35 AM	Morning Coffee Break	
	SESSION II: UHMWPE Emerging Trends	
	Session Co-Moderators: Pierangiola Bracco and Anuj Bellare	
11:20 AM	**Invited Talk 2:** Celanese Sustainability Solutions	Alban Hasani M.S., Celanese
11:40 AM	**Invited Talk 3:** Unveiling the Shocking Reality of Rampant UHMWPE Counterfeiting in Today's Supply Chain Management	Mark Allen, Orthoplastics
12:00 PM	**Podium Talk 5:** Long-term revision risk for highly crosslinked versus conventional polyethylene in total knee arthroplasty	Heather Prentice, Ph.D., MPH, Kaiser Permanente
12:15 PM	**Podium Talk 6:** The first antioxidant-stabilized, chemically crosslinked UHMWPE implant: Rationale and preclinical testing	Ebru Oral, Ph.D., Massachusetts General Hospital, Harvard Medical School
12:30 PM	**Rapid Fire Talks:** 3 minute presentations of selected UHMWPE and Implant Polymer posters – no discussion until poster session	
1:00 PM	Buffet Lunch and Poster Session	

Thursday, June 20, 2024 I Day One

Time	Subject	Presenter
	SESSION III: In Vitro Testing and Clinical Performance of UHMWPE	
	Session Co-Moderators: Claude Rieker and Raelene Cowie	
2:30 PM	**Podium Talk 7:** In-Vivo Validation of the UHMWPE Creep Determination in Clinical Radiographs after TKA Using Artificial Intelligence	Ana Laura Puente Reyna, Ph.D., Aesculap
2:45 PM	**Podium Talk 8:** Antioxidant Performance in UHMWPE Knee Bearings: A Mid-Term Report	Peder Solberg, Dartmouth College
3:00 PM	**Podium Talk 9:** Development of a Successive Self-Nucleation and Annealing (SSA) protocol for the characterization of biomedical UHMWPE	Pierangiola Bracco, Ph.D., University of Torino
3:15 PM	**Podium Talk 10:** Comparison of macro-, micro- and nanoscale creep behavior of UHMWPE, crosslinked UHMWPE, and PEEK	Miroslav Slouf, Ph.D., Czech Academy of Sciences
3:30 PM	**Podium Talk 11:** Understanding Izod Impact strength variations as a function of different polymer resins and processing technologies	ir. Harold Smelt, M.S., DSM Biomedical
3:45 PM	Afternoon Coffee Break	
	SESSION IV: Advances in Processing, Crosslinking, and Additives	
	Session Co-Moderators: Miroslav Slouf and Ebru Oral	
4:30 PM	**Podium Talk 12:** Synergistic antibacterial UHMWPE-based materials: mechanical properties and morphology	Nicoletta Inverardi, Ph.D., Massachusetts General Hospital, Harvard Medical School
4:45 PM	**Podium Talk 13:** Toughness Study of Super Gradient Crosslinked UHMWPE	Zongtao Zhang, Ph.D., b-ONE Ortho Corp
5:00 PM	**Podium Talk 14:** Bis-diazirine crosslinked UHMWPE	Anuj Bellare, Ph.D., Polymerix
5:15 PM	**Podium Talk 15:** The synergistic role of beta-carotene in in-vivo oxidation of contemporary UHMWPE tibial liner	Songyun Liu, Ph.D., Rush University Medical Center
5:30 PM	**Podium Talk 16:** 4Degra® - A new surface eroding bioresorbable material for 3D printing medical devices	Tom Robinson, 4D Biomaterials
5:45 PM	**Podium Talk 17:** Investigating the effects of porous topology and feature size on the separation forces of UHMWPE-PEEK structural composites for orthopedic implant applications	James Smith, Ph.D., Drexel University
	Day 1 Meeting Adjourns	
9:00 PM	**Gala Dinner at Casa Batlló** Tours beginning at 9 PM, followed by dinner at 10 PM	

Friday, June 21, 2024 I Day Two

Time	Subject	Presenter
9:00 AM	On-site Registration Opens	
	SESSION V: PAEK-based Orthopaedic and Spinal Implants	
	Session Co-Moderators: Francisco Medel and Cemile Basgul	
9:30 AM	**Podium Talk 18:** Development of Press-Fit polyetheretherketone (PEEK) Hip Prosthesis for Reducing Stress-Shielding and Bone Resorption	Dongmei Yu, Ph.D., The Royal National Orthopaedic Hospital, Tangdu Hospital
9:45 AM	**Podium Talk 19:** Carbon-fibre-reinforced PEEK as biomaterial in a rotating hinge knee design – biotribological testing, retrieval findings & clinical results	Thomas Grupp, Ph.D., Aesculap
10:00 AM	**Podium Talk 20:** Population-based FE study on the primary fixation of a cementless PEEK femoral and tibial component	Corine Post, Radboud University
10:15 AM	**Podium Talk 21:** PEEK spinal cages: Design and Manufacturing considerations	Yu Chen, Ph.D., University of Exeter
10:30 AM	**Podium Talk 22:** Evaluating All-Polymer PEEK Knee Prostheses: A Comparative Imaging Study	MD Cedric Boyhn, AZ Monica Hospital
10:45 AM	Morning Coffee Break	
	SESSION VI: PAEK Additive Manufacturing and Point-of-Care Considerations	
	Session Co-Moderators: Neha Sharma and Francisco Medel	
11:30 AM	**Invited Talk 4:** 3D Printing at the Point of Care: The Medical Device Production System Concept	Matthew Di Prima, Ph.D., US Food and Drug Administration
11:50 AM	**Invited Talk 5:** Update on Implant Grade PEKK: Biocompatibility and Case Studies for Injection Moulding and 3D Printing	Boris Gaillard, Ph.D., Seqens
12:10 PM	**Invited Talk 6:** Exploration of PEEK Polymer materials in Additive Manufacturing for Advanced Medical Applications & Pre-clinical Study data	Dharmesh Patel, Ph.D., Invibio
12:30 PM	**Rapid Fire Talks:** 3 minute presentations of selected PAEK and AM posters – no discussion until poster session	
1:00 PM	Buffet Lunch and Poster Session	

Friday, June 21, 2024 I Day Two

Time	Subject	Presenter
	SESSION VI (continued): PAEK Additive Manufacturing and Point-of-Care Considerations	
	Session Co-Moderators: Steven Kurtz and Oana Ghita	
2:30 PM	**Invited Talk 7:** Bridging Innovation and Patient Care: Point-of-Care 3D Printing of Polymer Implants	Neha Sharma, Ph.D., University of Basel
2:50 PM	**Invited Talk 8:** VESTAKEEP Polymer 3D printing. Why Evonik VESTAKEEP i43DF PEEK Filament is a true alternative to metal for next generation human implants	Marc Knebel, Evonik
3:10 PM	**Invited Talk 9:** PEEK Cranial Implants - a journey from university to 510(k)	Stefan Leonhardt and Ashley Dawson, Ph.D., 3D Systems
3:30 PM	**Podium Talk 23:** Antibacterial Properties of 3D Printed PEKK	Jim Porteus, Oxford Performance Materials
3:45 PM	Afternoon Coffee Break	
	SESSION VII: Functionalization of PAEKs	
	Session Co-Moderators: Steven Kurtz and James Smith	
4:30 PM	**Podium Talk 24:** Lycopene and nano-CaO 2 decorated porous polyetheretherketone scaffold for anti-tumor and osteogenesis	Dongmei Yu, Ph.D., The Royal National Orthopaedic Hospital, Tangdu Hospital
4:45 PM	**Podium Talk 25:** Mechanical, morphological, calorimetric and spectroscopic characterization of 3D printed and annealed PEEK and carbon-fiber reinforced PEEK samples	Francisco Medel, Ph.D., University of Zaragoza
5:00 PM	**Podium Talk 26:** Enhancing Bioactivity of PAEKs for Implantable Device Applications with Silicon Nitride – a Survey of Current Projects	Ryan Bock, Ph.D., SINTX Technologies
5:15 PM	**Closing Remarks**	Steven Kurtz, Ph.D.
Meeting Adjourns		

Poster Presentations I Day One

Title	Presenter
Metrological assessment of tribological properties of a UHMWPE/Al 2 O 3 contact pair relevant for biomedical applications	Francisco Javier Pascual Aranzana, Ph.D., University of Zaragoza
High Demanding Activities Knee Wear Simulation of a PEEK-OPTIMA TM Femoral Component Articulating Against a UHMWPE Gliding Surface	Ana Laura Puente Reyna, Ph.D., Aesculap
Long term wear performance of first generation highly crosslinked polyethylene liners	Stuart Callary, Ph.D., University of Adelaide
An objective evaluation of the quality of UHMWPE in total hip replacements, which we implant in daily practice	Petr Fulin, Ph.D., Charles University and Motol University Hospital
Towards a European database of explanted UHMWPE inserts: potential and challenges	Pierangiola Bracco, Ph.D., University of Torino
Comparison of various UHMWPE formulations in contemporary total knee replacements	Veronika Gajdošová, Ph.D., Czech Academy of Sciences
Technological and Pharmacological considerations for the development of therapeutic UHMWPE	Ebru Oral, Ph.D., Massachusetts General Hospital, Harvard Medical School
Determination of particle induced osteolysis in THA with highly crosslinked polyethylene liners	Songyun Liu, Ph.D., Rush University Medical Center

Poster Presentations I Day Two

Title	Presenter
Optimization of Fused Filament Fabrication (FFF) Process Parameters for PEEK and PEKK Biomaterials for Orthopedic Medical Device Application	Abigail Tetteh, M.S., Drexel University
Fabrication of 3D printed surface-porous PAEK structures	**Yaan Liu**, Ph.D., University of Exeter
Investigations for Implant applications with novel PEAK materials	Sebastian Pammer, 3D Systems
Interlaboratory Validation of Medical 3D Printing for PEEK: A Multicenter Study	Cemile Basgul, Ph.D., Drexel University
Silicon Nitride PEKK Composite Promotes Osteogenic Activity Compared to PEEK in Porous 3D Printed Specimens	Paul DeSantis, M.S., Drexel University
From Print to Performance: Examining CFR-PEKK Composite Properties for Improved Trauma Plate Design	Arjun Sharma, Drexel University
Use of AI-based software for rapid optimization of printing parameters for a novel 3D printer with thermal radiation heating for the production of PEEK samples in small dimensions	Andreas Schwitalla, Charité – Universitätsmedizin Berlin
Taguchi Optimization of Additively Manufactured PEKK and Silicon Nitride Loaded PEKK for Medical Device Applications	Tabitha Derr, Drexel University
3D Printing at the Point of Care: Patient-Specific PEKK Ankle Fusion Implants for Diabetic Patient	Pearle Shah, Drexel University

SPECIAL THANKS

to all the sponsors & attendees
at the 2024 Conference!

Platinum Sponsor: Celanese

Silver Sponsor: Invibio

Bronze Sponsors:
Orthoplastics
Evonik
Mitsubishi Chemical Advanced Materials
CeramTec GmbH
3D Systems
Seqens

Interested in sponsoring our 2026 edition?
Please contact Steve Kurtz - skurtz@drexel.edu.

Introduction of Alumina Modular Heads for Ceramic on Polyethylene in Orthopaedics

Rieker CB[1], Semlitsch M
[1]Zimmer Biomet EMEA, Zug, Switzerland
claude.rieker@zimmerbiomet.com

Introduction:

In the early 1970s, when total hip arthroplasty became commercially available, the ideal bearing for these prostheses was completely unknown. Among the landscape of innovation, alongside the metal-to-metal bearings pioneered in England by McKee/Farrar/Ring in the late 1950s and the metal-to-polyethylene bearings introduced by Charnley in 1962, European orthopaedic surgeons (such as Boutin in France, Salzer in Austria, and Mittelmeier/Griss in Germany) proposed replacing the metal heads of hip prostheses with pure aluminium oxide (alumina Al_2O_3) heads. This innovative approach presented the potential for alumina-alumina bearings or alumina-polyethylene bearings, marking a significant leap forward in prosthetic technology.

Discussion:

The initial phase of this groundbreaking development witnessed a collaborative effort between engineers and orthopaedic surgeons, driven by the shared goal of optimising the mechanical properties of aluminium oxide heads while ensuring the biocompatibility of this ceramic material. In a precise search to mitigate the potential risk of brittle fracture associated with these heads, numerous developmental pathways were explored, encompassing strategies such as grain size reduction and the maximisation of density. Notably, the biocompatibility was rigorously examined under the meticulous scrutiny of Boutin, whose pioneering experiments included the implantation of polished dense alumina spheres beneath the skin of human abdomens, alongside the insertion of dense alumina rods into the trochanters of several canines, providing invaluable insights into the material's suitability for medical applications.

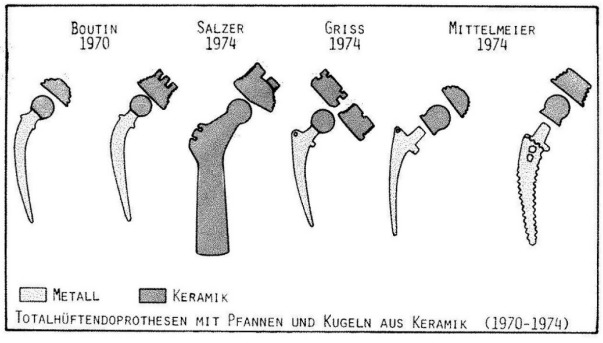

Overview of the early available ceramic components drawn by M. Semlitsch in 1984

The second major development was the introduction of the Morse taper, an innovative design for fixing the alumina head to the femoral stem. This innovative design has resulted in a stable fixation, reducing the risk of disassociation and providing better structural integration between the components. Engineers Dörre in Germany and Semlitsch in Switzerland played a key role in the development and optimisation of the Morse taper, contributing to the overall success of the alumina heads.

The initial introduction of alumina heads, having a diameter of 32mm, marked a significant milestone in 1974, led by Feldmühle (now known as CeramTec) and branded under the name Biolox®. These pioneering components featured a 14/16 Morse taper and offered a choice of three neck lengths, setting a new standard in hip arthroplasty technology. However, recognising the demand for versatility, a decision was made in 1988 to expand the product line by introducing alumina heads with a reduced diameter of 28mm while retaining the option of three neck lengths. This necessitated a corresponding adjustment in the dimensions of the Morse taper, which was revised to 12/14.

The journey of alumina continued, with persistent efforts focused on enhancing its mechanical properties. A decisive breakthrough emerged in the early 1990s with the advent of high-temperature isostatic pressing and the implementation of laser marking techniques. These transformative modifications operated a profound improvement in the toughness of alumina, significantly strengthening its durability and resistance. This remarkable leap forward led in the introduction of a new and improved grade, named Biolox Forte® in 1995.

As Biolox Forte® components reached the limits of what could be achieved with pure alumina, a new composite ceramic (82% alumina / 17% zirconia) was developed in the early 2000s under the name Biolox Delta®. This new ceramic (zirconia toughened alumina) has twice the toughness of pure alumina, further reducing the very low risk of fracture and enabling the development of other types of implants, including femoral components for total knee replacements and hip resurfacing implants.

Conclusion:

In summary, the orthopaedic developments of the 1970s, involving collaboration between visionary surgeons and innovative engineers, laid the foundations for the orthopaedic implants we still use today. The introduction of alumina revolutionised prosthesis design, improving the durability, wear resistance and biocompatibility of implants. In addition, the Morse taper represented a significant advance in component fixation, ensuring optimal structural integrity. These remarkable contributions have had a lasting impact on the quality of life of patients who benefit from orthopaedic prostheses, underlining the importance of interdisciplinary collaboration in medical progress.

Role of implant bearing surfaces on non-revision reoperation, rehospitalisation and mortality outcomes following primary total hip replacement across a national healthcare system: evidences from the National Joint Registry

Alessandro Alan Porporati[1,2,*]

a.porporati@ceramtec.de

1. CeramTec GmbH, Medical Products Division, Plochingen, Germany

2. University of Trieste, Department of Engineering and Architecture, Trieste, Italy

Introduction
We investigated the risk of re-hospitalisation, non-revision re-operations and mortality according to detailed bearing surfaces materials implanted during primary total hip replacement (THR).

Methods
We analysed THR procedures across all orthopaedic units in England using the National Joint Registry and the Hospital Episode Statistics. Re-hospitalisation and re-operation for an orthopaedic indication were identified using ICD-10 and OPCS-4 classifications through linked Hospital Episode Statistics data. We identified primary THRs with heads and monobloc cups or modular acetabular component THRs with head and shell/liner combinations. We used adjusted modified Poisson regression and flexible parametric survival models.

Results
A total of 645,553 primary THRs with modular acetabular component and 378,897 primary THRs with monobloc acetabular component were performed between 2003-2019, with 3.2% and 4.2% re-admitted to hospital respectively, and 0.2% and 0.8% undergoing non-revision re-operations.
For THRs with a modular acetabular component, compared to implants with cobalt chrome head and highly crosslinked polyethylene (HCLPE) liner, the risks of re-hospitalisation and re-operation were higher for all implants with non-HCLPE liner but lower for implants with delta ceramic (BIOLOX®*delta*, CeramTec GmbH) and HCLPE liner or pre-assembled delta ceramic implants.
For monobloc acetabular component THRs, implants with delta ceramic head and HCLPE cup had a lower risk of re-hospitalisation and re-operation than implants with cobalt chrome and HCLPE cup. Implants with a stainless steel or cobalt chrome head and non-HCLPE cup had a higher risk of re-operation.
Mortality was also lower for implants with delta ceramic from the primary THR until 15 years post-surgery.

Conclusion
The risk of re-hospitalisation and re-operation for an orthopaedic indication other than revision is reduced for implants with a delta ceramic head and a HCLPE liner/cup or pre-assembled delta ceramic implants, as is the risk of mortality at different time points following the initial implantation.

* results produced as part of a contract between CeramTec GmbH and the University of Bristol (Research study agreement “The Clinical and Cost Utility Outcomes of Ceramic Bearings in Total Hip Replacement”)

The Tribological Performance of Crosslinked UHMWPE on Coated Titanium

[1,2]Siskey RL, [2]Bertone T, [1,2]Carden, K, J, [3]Hecker, R, [3]Vinciguerra
[1]Drexel University, Philadelphia, PA, [2]Exponent Inc., Philadelphia, PA, [3]Enovis, Austin, TX,
Corresponding author rsiskey@exponent.com

Introduction

Metallic orthopedic bearing materials have remained relatively unchanged for the past two decades. However, market pressures are now forcing manufactures to consider alternative materials to even further reduce the in vivo response to the device and its potential wear debris. One possible direction for device designers to consider is coating traditional biomedical alloys with materials like silicon nitride (SiN), titanium nitride (TiN), titanium niobium nitride (TiNbN) and amorphous diamond-like (ADLC) materials[1-5]. The objective of this study was to evaluate the wear rate of different commercially available UHMWPEs under controlled laboratory conditions and to compare these alternative bearing couples with standard of care bearing couples such as highly-crosslinked polyethylene against CoCr.

Materials and Methods

Twenty pin-on-disc material combinations were tested using a 100 station Phoenix Tribology T87 Multi-station Pin-on-Disc Machine[6-9]. ASTM F732 "Standard Test Method for Wear Testing of Polymeric Materials Used in Total Joint Prostheses" was used as a guide. The pin materials tested were four ultrahigh molecular weight polyethylenes (25 kGy 1050, 75 kGy GUR 1020, 75 kGy 1020-E and 150 kGy 1020-E) and PEEK Optima. The four disc counterfaces were forged ASTM F1108 Ti_6Al_4V coated with SiN, TiN, TiNbN, and ADLC. Each material combination was tested in five wear stations and two load soak stations, which were used to compensate for fluid uptake. The test matrix is summarized in Table 1.

Table 1. Summary of pin and disc material combinations.

Pin Material	Disk Material	Number of Stations
25 kGy 1050	ADLC	n = 5
75 kGy 1020	ADLC	n = 5
75 kGy 1020-E	ADLC	n = 5
150 kGy 1020-E	ADLC	n = 5
PEEK	ADLC	n = 5
25 kGy 1050	SiN	n = 5
75 kGy 1020	SiN	n = 5
75 kGy 1020-E	SiN	n = 5
150 kGy 1020-E	SiN	n = 5
PEEK	SiN	n = 5
25 kGy 1050	TiN	n = 5
75 kGy 1020	TiN	n = 5
75 kGy 1020-E	TiN	n = 5
150 kGy 1020-E	TiN	n = 5
PEEK	TiN	n = 5
25 kGy 1050	TiNbN	n = 5
75 kGy 1020	TiNbN	n = 5
75 kGy 1020-E	TiNbN	n = 5
150 kGy 1020-E	TiNbN	n = 5
PEEK	TiNbN	n = 5

A lubricant chamber (volume 15 ml) was mounted around each disc, so that each station had an independent volume of bovine serum lubricant. Water circulated through the test bath at 37 ± 3^0C. The load applied to each pin was 128 N, giving a nominal contact pressure of 2.01 MPa (pin diameter 9 mm).

An elliptical slide track (10 mm major axis, 5 mm minor axis) was employed to facilitate multidirectional wear at 1 Hz. Sliding speed was 24.2 mm/s. Every 0.25 MC, up to 3.0 MC, the wear test was stopped for interval analysis and the test specimens were removed for characterization. The pins and discs were cleaned, dried and massed using the procedure described in ASTM F1714 "Standard Guide for Gravimetric Wear Assessment of Prosthetic Hip Designs in Simulator Devices." After massing, the pins and counterfaces where photo documented. The resulting mass loss was converted to cumulative volumetric loss using the density of each pin material. The volumetric loss was averaged for the five wear stations (load soak corrected) for each of the 20 material combinations tested. The wear rate (volumetric wear per million cycles) for each pin and disc was calculated by applying a linear regression to the volume loss by cycle count and averaged for each material combination. The wear rates by test group were then compared using a student's t-test.

Results

All polymeric samples demonstrated burnishing of the articulating surfaces. For the pins, the entire surface was burnished, whereas the discs demonstrated different degrees of damage in the region of contact (Figure 1). The ADLC demonstrated negligible changes in the contact regions. The TiN and TiNbN demonstrated consistent abrasive wear patterns in the contact regions as confirmed by the presence of microscratching. The SiN, consistent with the wear rates, demonstrated more significant abrasive damage and changes in surface morphology in the articulating region.

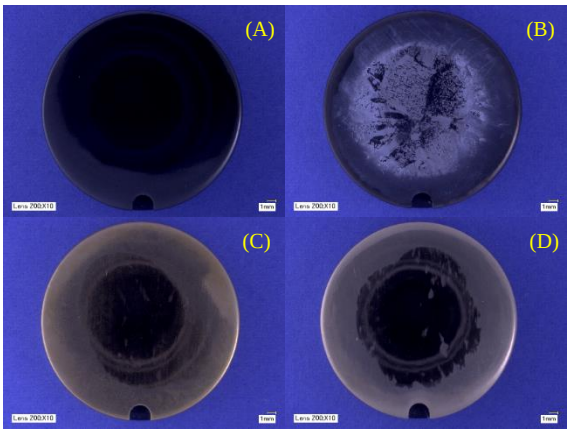

Figure 1. – Representative images of the ADLC (A), SiN (B), TiN (C), and TiNbN (D) counterfaces after 3.0 MC.

The resulting wear rates have been summarized in Table 2. For all four counterface materials, the rank order of average wear rate was consistent and decreasing from PEEK to 25 kGy 1020 to 75 kGy 1020-E to 75 kGy 1020 and to 150 kGy 1020-E. When the wear rates for the four UHMWPE pin materials are stratified by disc material, the SiN counterface results in a statistically higher wear rate than the other counterfaces ($p \leq 0.0116$). For the two highly crosslinked groups, 150 kGy 1020-E and 75kGy 1020, no statistical difference was found between the three remaining counterfaces. For both the 25 kGy 1020 and 75 kGy 1020-E material, the TiNbN demonstrated a statistically higher wear rate when compared to both the TiN and ADLC ($p \leq 0.0292$). While not statistically different, on average the ADLC demonstrated the lowest wear rate for all pin material groups.

Table 2. Summary of wear results for pins and discs by bearing couple after 3.0 MC. The results for the wear test samples were corrected at each interval using the load soak pins. All results are reported as average ± standard deviation.

Pin Material	Disc Material	Wear Rate [mm^3/MC]
150 kGy 1020-E	ADLC	0.3 ± 0.1
75 kGy 1020	ADLC	0.6 ± 0.5
75 kGy 1020-E	ADLC	1.7 ± 0.3
25 kGy 1020	ADLC	4.2 ± 0.5
PEEK	ADLC	4.9 ± 4.1
150 kGy 1020-E	TiN	0.5 ± 0.4
75 kGy 1020	TiN	0.8 ± 0.2
75 kGy 1020-E	TiN	5.0 ± 1.8
25 kGy 1020	TiN	8.6 ± 2.4
PEEK	TiN	32.4 ± 15.5
150 kGy 1020-E	TiNbN	0.4 ± 0.2
75 kGy 1020	TiNbN	0.7 ± 0.4
75 kGy 1020-E	TiNbN	2.7 ± 1.1
25 kGy 1020	TiNbN	6.1 ± 1.3
PEEK	TiNbN	27.2 ± 9.3
150 kGy 1020-E	SiN	13.6 ± 6.2
75 kGy 1020	SiN	10.7 ± 5.2
75 kGy 1020-E	SiN	12.3 ± 4.9
25 kGy 1020	SiN	13.6 ± 4.8
PEEK	SiN	35.4 ± 8.9

Discussion

No remarkable changes to the TiN, TiNbN or ADLC coatings, other than abrasive scratching in the contact region were observed out to 3.0 MC. The SiN demonstrated more significant polishing in the contact region but mass change of the counterfaces was not investigated as part of this study.

The PEEK wear rates were higher for all counterfaces when compared to the performance of the UHMWPE against the same counterface. As expected, the four UHMPWE materials demonstrated decreasing volumetric wear rate as a function of effective crosslinking dose. Note that vitamin E is considered a crosslinking inhibitor so the effective crosslink density for the 75 kGy and 150 kGy 1020-E groups will be less than the crosslinking dose suggests. When the disc materials are compared, consistent with the observed damage, the SiN demonstrated significantly higher wear rates compared to all other test groups, regardless of pin material. The ADLC demonstrated the lowest wear rates on average across all pin materials. A previous study was conducted on the same pin materials against cobalt chromium (CoCr) counterfaces, using the same equipment and methods to a cycle count of 1.0 MC. The resulting wear rates by pin type are provided in Table 3. For the highly crosslinked groups, 150 kGy 1020-E and 75 kGy 1020, the CoCr wear rates are lower than all of the alternate bearings. However, wear rates for the more moderately crosslinked material, 75 kGy 1020-E, are comparable for the CoCr (1.3 ± 1.2 mm^3/MC) and ADLC (1.7 ± 0.3 mm^3/MC).

Table 3. Summary of wear results for the same pin types tested against CoCr to 1.0 MC. The results for the wear test samples were corrected at each interval using the load soak pins. All results are reported as average ± standard deviation.

Pin Material	Disc Material	Wear Rate [mm^3/MC]
150 kGy 1020-E	CoCr	-0.03 ± 0.09
75 kGy 1020	CoCr	0.04 ± 0.24
75 kGy 1020-E	CoCr	1.3 ± 1.2
25 kGy 1020	CoCr	2.6 ± 0.4
PEEK	CoCr	18.6 ± 10.0

This testing was conducted using a contact stress of 2.0 MPa which would be a stress level consistent with low demand activity levels in the hip such has typical normal gait. While the current study does allow material combinations to be compared under these conditions, adverse loading and higher contact stress loading may result in different wear performance of the different bearing couples. These results suggest that the ADLC, TiN and TiNbN should continue to be explored as potential orthopedic bearing materials. This study only investigated these bearing materials under a single set of contact and lubrication conditions. Further investigation such as response to abrasive challenge and biological response to coating particulate is warranted if these materials are considered for other orthopedic bearing design indications and demands.

Acknowledgements

This research was sponsored by Enovis.

References

1. Sonntag, Reinders, J. Reinders, and J. P. Kretzer. "What's next? Alternative materials for articulation in total joint replacement." Acta biomaterialia 8.7 (2012): 2434-2441.
2. Bal, B. Sonny, and M. N. Rahaman. "Orthopedic applications of silicon nitride ceramics." Acta biomaterialia 8.8 (2012): 2889-2898.
3. Bock, Ryan M., et al. "Surface modulation of silicon nitride ceramics for orthopaedic applications." Acta biomaterialia 26 (2015): 318-330.
4. Dearnaley, Geoffrey, and James H. Arps. "Biomedical applications of diamond-like carbon (DLC) coatings: A review." Surface and Coatings Technology 200.7 (2005): 2518-2524.
5. Roy, Ritwik Kumar, and Kwang-Ryeol Lee. "Biomedical applications of diamond-like carbon coatings: A review." Journal of Biomedical Materials Research Part B: Applied Biomaterials 83.1 (2007): 72-84.
6. Saikko V. A multidirectional motion pin-on-disk wear test method for prosthetic joint materials, 1998.
7. Saikko, V., A hip wear simulator with 100 test stations. Proceedings of the Institution of Mechanical Engineers, Part H: Journal of Engineering in Medicine, 2005.
8. Saikko, V., Performance analysis of an orthopedic biomaterial 100-station wear test system. Proceedings of the Institution of Mechanical Engineers, Part C: Journal of Mechanical Engineering Science, 2010.
9. Baykal et al, Advances in tribological testing of artificial joint biomaterials using multidirectional pin-on-disk testers. Journal of the mechanical Behavior of Biomedical Materials, 2014.

Correlation of crosslinking measured with the trans-vinylene index and wear as measured by a pin-on-disc test of polyethylene liners from various manufacturers used in total hip arthroplasty

Peter Wahl[1,2], Roman Heuberger[3], Andrea Pascucci[3,4], Thomas Imwinkelried[3], Markus Fürstner[2,5], Niels Icken[1], Robin Pourzal[6], Emanuel Gautier[7], Emanuel Benninger[1]

1 Cantonal Hospital Winterthur, Winterthur, Switzerland, 2 University of Berne, Berne, Switzerland, 3 RMS Foundation, Bettlach, Switzerland, 4 Swiss Federal Institute of Technology Zurich, Zurich, Switzerland, 5 Berne University Hospital, Berne, Switzerland, 6 Rush Medical College, Chicago, Illinois, 7 HFR Fribourg – Cantonal Hospital, Fribourg, Switzerland

Introduction: Highly cross-linked polyethylene (XLPE) is an important progress in total hip arthroplasty (THA), greatly reducing requirements for revision due to wear or osteolysis, compared to conventional polyethylene (CPE). Crosslinking is achieved most commonly by irradiation. Irradiation dose and thermal treatment are the main material determinants of revision after THA with polyethylene (PE) bearings identified so far. How the degree of crosslinking varies between products and how this impacts wear resistance remains unclear so far. This study aims to compare the degree of crosslinking, respectively the absorbed irradiation dose of the material, and *in vitro* wear rates across a cohort of retrieved and unused PE cups/liners from various manufacturers.

Methods and Materials: Both new and retrieved PE acetabular cups/liners were collected from one centre from April 2021 to April 2022. Time *in situ* ranged from 0 up to 18 years. The material used for further tests was sampled at least 2 mm below the surface. Samples were analyzed for trans-vinylene index (TVI) and oxidation index (OI) using Fourier-transformed infrared spectrometry, following corresponding ASTM standards. The TVI was utilized to calculate absorbed irradiation doses, using a previously published calibration curve. Simulations of absorption of irradiation within PE were provided to illustrate potential manufacturing issues. Wear was measured using a pin-on-disc test with minor modifications to the ASTM F732-17 standard to accommodate smaller sample sizes. All measurements were performed in triplicate.

Results: Forty-seven PE specimens (3 CPE, 43 XLPE, 1 unknown) from eight manufacturers were included. No excessive oxidation interfered. TVI remained stable within each group and independent of time *in situ*. A linear correlation (r^2=0.995) was observed between the old and the current TVI standard, except for vitamin E infused PE. Absorbed irradiation doses calculated from the TVI corresponded to product specifications, except for two XLPE products. One XLPE exhibited significantly higher absorbed doses (mean 241% ± 18%), most likely explained by higher crosslinking from electron irradiation, compared to gamma irradiation. Another type of XLPE showed unexpectedly low (mean 41% ± 13%) doses. A one-sample t-test showed highly significant deviation from specifications for both ($p<0.001$) compared to specifications, while not significant for the other products. As illustrated by simulations, electron and gamma irradiation do have similarities, but also differences, which may well explain part of the observations regarding absorbed irradiation dose. Lower wear rates were observed in samples with higher TVI, but the relation was not linear and some exceptions were present. Notably, one type of XLPE with unexpectedly low TVI demonstrated wear rates more comparable to CPE ($p<0.0001$ *vs*. all other XLPE). Despite adequate TVI, another vitamin E infused XLPE showed slightly higher *in vitro* wear than the other ones ($p=0.033$). All other XLPE performed similarly, although further analysis was limited by small sample sizes. The one unknown PE may be classified as CPE with 30 kGy of irradiation used for sterilization.

Discussion: The TVI serves as a reliable measure of the absorbed dose of irradiation of PE and does not alter over time. Conversion from the old to the current standard is linear, except for vitamin E infused PE. Various products differ in manufacturing details and consequently material characteristics. Absorption and penetration of electron irradiation and gamma irradiation differ, potentially leading to different degrees of crosslinking. The unexpectedly high TVI measured in the samples from one XLPE may well be explained by a higher degree of crosslinking obtained through the electron beam irradiation used for this product. Unexpectedly low TVI, and consequently absorbed irradiation doses, were observed in another type of XLPE. This remains unexplained. Considering absorption of gamma irradiation within PE, issues with geometry of the material during the irradiation process may be a potential explanation. There is a non-linear, inverse correlation between TVI and *in vitro* wear. Irradiation doses calculated from the measured TVI deviated from specifications for one type of XLPE, which correlated with an inferior *in vitro* wear rate, comparable to CPE, rather than the other XLPE. Despite minor discrepancies among the results of the other products, vitamin E infusion alone does not guarantee reduced wear, as evidenced by slightly higher wear observed in one vitamin E infused XLPE brand. A comparison with various studies and reports from national arthroplasty registries shows that the XLPE with surprisingly low TVI and poor wear behavior appears to be associated with excessively high revision rates reported after THA from this manufacturer. Separating CPE and XLPE in studies and reports from national arthroplasty registries may not be sufficient to identify properly the performance of individual products. Surgeons should also be aware that relevant differences may be present among the various products available in THA.

Unveiling the Shocking Reality of Rampant UHMWPE Counterfeiting in Today's Supply Chain Management

Allen M.D (mallen@orthoplastics.com)
Orthoplastics Ltd, Unit A, Beech Ind. Estate, Bacup, Lancashire, OL13 9EL, UK.

Introduction
The Orthopedic world is a highly regulated industry, continuous product scrutiny and development are a critical focus of the regulator, but more importantly the recent European MDR was a born about from unscrupulous activity and the use of incorrect materials within implanted products.

The Orthopedic sector has never been a subject to discussion because of its unique position since 2000 with only one materials supplier and processors with extensive clinical history. However, we are all familiar with the changing world and daily evidence of unscrupulous companies and products in every market, it's only a matter of time before we as an industry will be a victim of this and patients are affected with life changing consequences.

History
Over the past 20 years we have evidence of processors using fraudulence regulatory certification and plagiarising of literature supplied by legitimate companies. ISO certification in certain geographic region can be purchased on the internet; certificates have been copied and in some cases device submissions have been completed with approved materials only to be substituted with industrial grades for production.

Such examples are rare and in many cases restricted to those geographies, however all OEMs tend to start local and expand their market, thus the possibility is that such materials may become a global problem.

Evidence
Orthoplastics were made aware of a new processor active in the Indian continent in Q4 2022, initial investigation showed that fraudulent documentation had been produced referencing;

- Orthoplastics internal work instruction
- Orthoplastics and resin supplier trademarks
- Resin supplier documentation
- Fake resin batch information

The processor in question was actively promoting the material within India and has since started to promote these in other geographic regions including Europe.

Materials
In May 2023 Orthoplastics obtained samples of the material through the cooperation of a European distributor, the following documentation pack was provided

- Materials certification
- ISO 13485 certification (URS holdings)
- Resin test data
- Irradiation certificates

Following contact with URS holdings ltd, they confirmed that the ISO 13485 certificate was **fraudulent**

Testing
Material samples obtained were tested against current materials in both standard and Crosslinked forms

The standards material were supplied as a Type I (GUR 1020) and certified to ISO5834 and ASTM F648

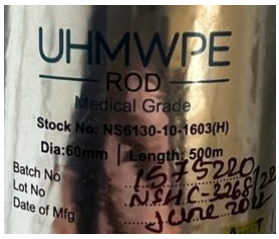

Results
Physical properties

Test Parameter	Certified Value	Tested Material	Typical GUR 1020
Density (kg/m³)	930	933.6	936
Morphology Index	0	FAIL	0
Izod Impact Strength (kJ/m²)	144	42.95	145
Ultimate Tensile Strength (MPa)	55.1	57.66	66
Tensile Yield Stress (MPa)	23.56	23.84	23
Tensile Elongation @ Break (%)	429.5	266.27	450
Peak Melting Temperature (°C)	135	139.73	138

FTIR evaluation

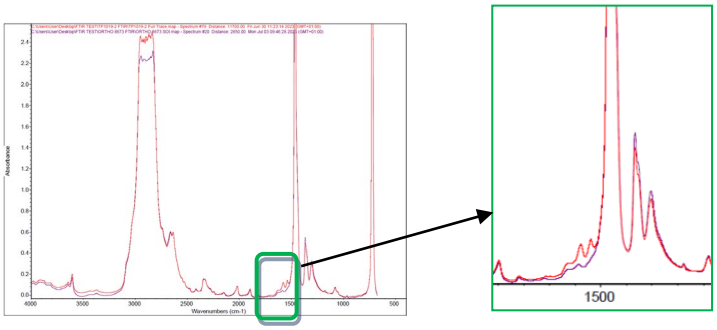

FTIR shows the presence of calcium stearate

Morphology
Testing revealed significant fusion defects within the materials

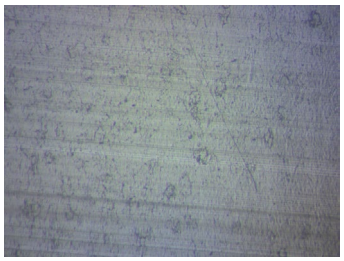

Conclusions

- Certification provided for regulatory compliance - FAKE
- Materials certification did not meet the international standards for implantable UHMWPE – FAKE
- Fusin defects clearly showed poor processing failure
- Impact strength was 70% lower than market GUR 1020
- Tensile strength was 13% lower than market GUR 1020
- Tensile elongation was 41% lower than market GUR 1020
- Materials tested contained 3000ppm Calcium stearate

Orthoplastics also tested highly Crosslinked and extruded materials from the company, all were found to have similar disturbing results.

As an industry, regulatory compliance states that the OEM shall be responsible for supply chain management; we all have to be aware of fraudulent and unscrupulous companies that could destroy the reputation of legitimate materials and processors with unsurpassed clinical history

Long-term revision risk for highly crosslinked versus conventional polyethylene in total knee arthroplasty

Prentice, HA[1]; Chan, PH[1]; Fasig BH[1]; Kelly MP[2]; Hinman AD[3]; Kurtz SM[4]; Paxton EW[1]
[1]Medical Device Surveillance & Assessment, Kaiser Permanente, San Diego, CA; [2]Department of Orthopedic Surgery, Southern California Permanente Medical Group, Harbor City, CA; [3]Department of Orthopedic Surgery, The Permanente Medical Group, San Leandro, CA; [4]Implant Research Core, School of Biomedical Science, Engineering, and Health Systems, Drexel University, Philadelphia, PA
Heather.Prentice@kp.org

Introduction: While studies have found highly crosslinked polyethylene (HXLPE) to be associated with a lower revision risk compared to conventional polyethylene (CPE) in total hip arthroplasty, evidence of any benefit in implant performance for total knee arthroplasty (TKA) is lacking. HXLPE was first introduced to in an effort to reduce wear and subsequent osteolysis. A 2015 study from a US-based integrated healthcare system found no differences in revision risks within 5-years follow-up when comparing HXLPE to CPE in TKA. The present study sought to build upon this prior study, the purpose was to evaluate revision risk out to 20-years follow-up for HXLPE versus CPE in primary TKA.

Methods and Materials: Data from a US-based healthcare system's Total Joint Replacement Registry was used to conduct a cohort study. Adult patients who underwent primary TKA involving the patella for osteoarthritis between 2001-2022 were included. To minimize confounding due to implant factors, the study sample was restricted to fixed bearing TKA using cobalt-chromium alloy on HXLPE (CoCr-HXLPE) and CoCr-CPE bearings; only posterior stabilized or minimally stabilized designs were included. The HXLPE group included all materials other than conventional polyethylene, include with and without antioxidants. The primary outcome was all-cause revision out to 20-years follow-up; septic revision and aseptic revision were secondary outcomes. Multivariable Cox proportional hazards regression was used to evaluate revision risk by treatment group. Age, body mass index (BMI), sex, race/ethnicity, ASA classification, bilateral procedure, cement utilization, implant stability, high flexion implant design, operative time, and average annual surgeon volume as covariates. Secondary analysis considered revision risk by treatment group for the two highest-volume implant systems used in the healthcare system: DePuy PFC Sigma and Zimmer Nexgen. Hazard ratios (HR) and 95% confidence intervals (CI) are presented. $p<0.05$ was considered statistically significant.

Results: The final study sample included 198,021 primary TKA: 47,370 CoCr-HXLPE and 150,651 CoCr-CPE. Mean age and BMI for the cohort was 68 years and 31.6 kg/m^2, respectively. Most patients were female (61.5%) and White race (68.8%). At 20-years follow-up, the crude cumulative incidence of all-cause revision for CoCr-HXLPE 6.3% was and 6.2% for CoCr-CPE (**Figure**). 20-year incidence of septic revision was 1.9% and 2.1% for CoCr-HXLPE and CoCr-CPE, respectively; aseptic revision incidence was 4.4% and 4.1% for CoCr-HXLPE and CoCr-CPE, respectively. In adjusted analyses, no differences were found in risk of all-cause revision (HR=0.94, 95% CI=0.88-1.01), septic (HR=0.95, 95% CI=0.85-1.05), or aseptic revision (HR=0.95, 95% CI=0.87-1.03) when comparing CoCr-HXLPE bearings with CoCr-CPE. Similarly, no differences were observed when comparing CoCr-HXLPE to CoCr-CPE for TKA with Nexgen systems: all-cause revision (HR=0.94, 95% CI=0.85-1.04), septic revision (HR=0.91, 95% CI=0.77-1.08), or aseptic revision (HR=0.96, 95% CI=0.84-1.09). While no differences were observed for CoCr-HXLPE compared to CoCr-CPE for TKA with PFC systems for all-cause revision (HR=0.89, 95% CI=0.79-1.01) and septic revision (HR=0.99, 95% CI=0.83-1.19), a lower aseptic revision risk was observed (HR=0.82, 95% CI=0.69-0.97).

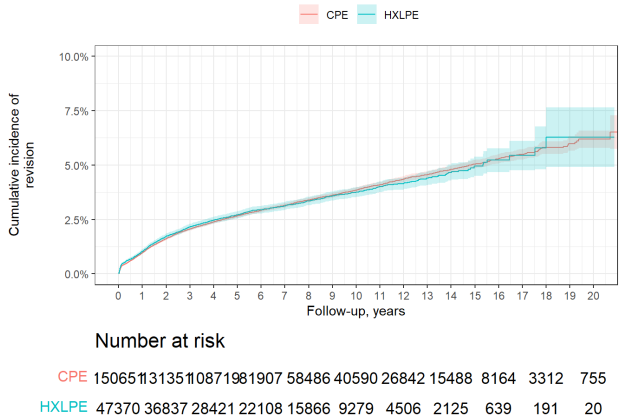

Figure. Cumulative all-cause revision probability following total knee arthroplasty (TKA) with highly crosslinked polyethylene (HXLPE) or conventional polyethylene (CPE). Table along the x-axis presents the number of TKA still at risk at every 2-years of follow-up.

Discussion: In this registry-based cohort study, we observed a lower aseptic revision out to 20-years follow-up for PFC CoCr-HXLPE compared with CoCr-CPE bearings in primary TKA. No differences were observed for Nexgen CoCr-HXLPE versus CoCr-CPE. Further study is needed to understand variations in HXLPE given the differences observed in performance across manufacturers.

Metrological assessment of tribological properties of a UHMWPE/Al_2O_3 contact pair relevant for biomedical applications

Pascual, F.J.[1,2], Albájez García, J.A.[2,3]
[1]*Centro Universitario de la Defensa de Zaragoza, CUD-AGM, Spain*
jpascual@unizar.es
[2]*Instituto Universitario de Investigación en Ingeniería de Aragón, I3A, Universidad de Zaragoza, Spain*
[3]*Departamento de Ingeniería de Diseño y Fabricación, Universidad de Zaragoza, Spain*

Introduction: The proper functioning of joint prostheses usually depends on the contact between two or more mobile elements. Inadequate friction properties will hinder the functioning of the joint, potentially leading to wear and subsequent associated clinical issues. In his publication of 1699, G. Amontons [1] established some of the fundamental principles of static friction between bodies. From these principles, the concept of the dimensionless coefficient of friction, denoted as μ, was derived and expressed as the ratio between the frictional force and the normal force on the contact surface. Therefore,

$$\mu = \frac{F_r}{N} \qquad (1)$$

In addition to friction, wear is another critical parameter in the design of joint prostheses, being essential its accurate determination. In both cases, the greatest difficulty in the numerical quantification of tribological properties lies in the complexity of determining the measurement uncertainty, conditioned by the destructive nature of the test, which prevents repetitive measurement through successive tests on the same sample. The general objective of this work is to propose a theoretical-practical procedure to estimate the measurement uncertainty of the tribological parameters of a sphere-flat contact pair of clinical interest.

Methods and Materials: Measurement of μ in our CSM TRB tribometer is performed using a pin-on-disk (POD) configuration, according to ASTM standard G99 [2], where the contact pair consists on a Ø6 mm hard sphere out of alumina (Al_2O_3) and a smooth ultra-high molecular weight polyethylene (UHMWPE) disk, Ø20 mm and 3 mm thick, acting as a semi-infinite plane. Experimentally, the applied force on the flat surface is kept constant by applying a dead load of 5 N. This load results in a Hertzian stress on the UHMWPE element close to 37 MPa, comparable to real-life stress levels. Figure 1 illustrates the basic scheme of the contact pair under study, with literature values for the coefficient of friction ranging around μ = 0.08-0.12 [3].

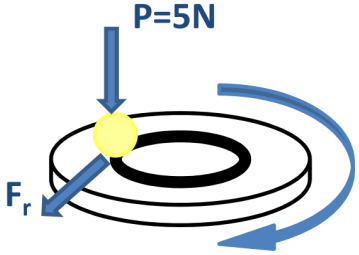

***Figure 1**. Scheme of the contact pair under study*

The contact pair described above is materialized in the studied tribometer, and the measurement of the friction force is carried out using two inductive displacement sensors mounted in opposition on the fork itself, measuring its deflection. The reading obtained will be exactly the average of the absolute value of the displacements recorded by each of the sensors. The chosen arrangement minimizes the influence of thermal gradients during the test while making the displacement measurement more robust, as it involves n=2 sensors. Additionally, to ensure that the displacement recorded by the sensors is representative of the friction (F_r) between the ball and the disk, the fork is designed to be sufficiently flexible in the sensing direction. Since the alumina ball undergoes no appreciable wear, the wear analysis is reduced to obtain the volume of polyethylene incoherent with the initial disk shape. This is performed through optical profilometry determining the "floodable" volume comparing the post-test shape against the original surface. These values include the effect of wear (understood as the removal or "cutting away" of material) and the plastic or permanent deformation that the polyethylene may experience.

Results: Metrological chains and subsequent mathematical expressions for the measurement uncertainty are proposed for both friction and worn volume determination. Additionally, by combining the aforementioned metrological chains, an appropriate estimation of the measurement uncertainty of the specific wear factor, W, is obtained.

Discussion: The present work proposes a first approach to the determination of the measurement uncertainties associated with the UHMWPE/Al_2O_3 contact pair, promoting more informed conclusions in further studies involving similar contact pairs. Nevertheless, the proposed theoretical calculation has several limitations attributable to two main causes: the difficulty in estimating some of the established uncertainties and the non-consideration of concurrent aspects during the conducted test.

References: [1] Amontons, G. De la resistance causée dans les machines. Mémoires de l'Académie Royale. 1699; 257-282. [2] ASTM G 99-17 Standard Test Method for Wear Testing with a Pin-on-Disk Apparatus, West Conshohocken, PA, USA: ASTM International, 2017. [3] Kurtz, S.M. UHMWPE Biomaterials Handbook, 3rd Edition, New York, USA: William Andrew (an imprint from Elsevier), 2015

High Demanding Activities Knee Wear Simulation of a PEEK-OPTIMA™ Femoral Component Articulating Against a UHMWPE Gliding Surface

Puente Reyna, AL[1]; Briscoe, A[2]; Schwiesau, J[1,3]; Revie, I[2]; Gerdesmeyer, L[4]; Mihalko, WM[5]; Grupp, TM J[1,3]
[1]Aesculap AG, R&D, Tuttlingen, Germany
[2]Invibio Ltd. Thornton Cleveleys, Lancashire FY5 4QD, UK
[3]Ludwig Maximilians University Munich, Department of Orthopaedic and Trauma Surgery, Musculoskeletal University Center Munich (MUM), Campus Grosshadern, Munich, Germany
[4]Orthopaedics and Trauma Surgery, Kiel Municipal Hospital & MedBaltic, Kiel, Germany
[5]Campbell Clinic Department of Orthopaedic Surgery & Biomedical Engineering, University of Tennessee Health Science Center, Tennesse, USA
ana_laura.puente_reyna@aesculap.de

Introduction: Total knee arthroplasty (TKA) is a well established treatment for degenerative joint disease. However, complications may occur due to a biological response to polyethylene wear particles, as well as systemic and allergic hypersensitivity reactions triggered by metal ions such as chromium, cobalt and molybdenum. PEEK (poly-ether-ether-ketone) has been investigated in recent years as an alternative material to CoCrMo, not only to avoid metal ion release, but also to improve patient satisfaction, as it is a material with a similar Young´s modulus to that of bone, which could reduce stress shielding and bone resorption. Furthermore, PEEK has a lighter weight than conventional metallic components (1).
Several studies have investigated the wear performance of PEEK materials articulating against UHMWPE in standardized and/or simplified test set-ups (ISO standards, pin-on-disc) (1, 2). However, there was a need for a more realistic and worst case wear testing in order to fully analyze the capabilities of PEEK as an appropriate TKA articulating material.
Therefore, the purpose of the following study was to compare the wear characteristics and performance of a PEEK femoral component against a clinically established knee implant made out of CoCrMo alloy under a highly demanding activities simulation.

Methods and Materials:
Four medium size femoral components based on the VEGA System® design (Aesculap AG, Tuttlingen, Germany) were manufactured out of PEEK-OPTIMA™ (PEEK group) (Invibio Ltd., Lancashire, UK). For the comparison group, four femurs from the clinically established cast CoCrMo alloy version of the femur implant (CoCrMo group) were selected. For both groups, UHMWPE gliding surfaces (VEGA System® PS+, size T3, high 10 mm) and CoCrMo VEGA System® tibial components were used.
Wear simulation was performed on a load controlled 4 station knee wear simulator (EndoLab GmbH, Thansau, Germany) capable of reproducing loads and movement of highly demanding activities measured in vivo on 8 patients (3) and normalized to a patient weight of 100 kg (4). The load profiles were applied for 5 million cycles in a combination of 40% stairs up, 40% stairs down, 10% level walking, 8% chair raising and 2% deep squatting.
The UHMWPE gliding surfaces were evaluated for gravimetric wear and wear patterns. A roughness analysis of the articulating surfaces (femoral components and gliding surfaces) was performed through the whole test.
An optical analysis of the femoral cam was performed in order to detect any cracks or deformation.

Results: An average wear rate of 2.6 ± 0.8 mg/million cycles was detected for the UHMWPE of the PEEK group, whereas in the CoCrMo group was 5.6 ± 1.2 mg/million cycles. The roughness of the UHMWPE gliding surface was similar for both groups through the whole test, showing similar wear patterns. The roughness of the PEEK femoral components showed a slight increase through the end of the wear test. Slight scratches were seen following the direction of the articulating surface. No cracks nor deformations were seen at the cam of the PEEK femoral component.

Discussion: The wear rate of the UHMWPE articulating against PEEK femoral components was below the one seen with the CoCrMo version of the femoral component design and was in the range of other wear rate results with CoCrMo implant designs (5, 6).
Furthermore, no cracks nor deformations were seen on the PEEK femoral cam, demonstrating to be a stable material during high flexion activities that involve post-cam interaction.
In conclusion, the PEEK femoral component shows promising results as an alterative for a future metal free TKA solution.

References:
(1) Cowie et al, Materials, 13, 1264, 2020.
(2) Cowie et al. J Mech Behav Biomed Mater, 89, 2019.
(3) Bergmann et al, PLoS ONE, 9(1): Article ID e86035, 2014.
(4) Schwiesau et al, BioMed Research International, 2014: Article ID 567374, 2014.
(5) Puente Reyna et al, Journal of Biomechanics, 79, 2018
(6) Schwiesau et al, J Mech Behav Biomed Mate, 2021.

Long term wear performance of first generation highly crosslinked polyethylene liners

Stuart Callary[1,2], Deepti Sharma[1,2], Taisha D'Apollonio[1], Bogdan Solomon[1,2] and David Campbell[1,3]

[1]Centre for Orthopaedic and Trauma Research, The University of Adelaide, Adelaide, SA, Australia
[2]Department of Orthopaedics and Trauma, Royal Adelaide Hospital, Adelaide, SA, Australia
[3]Wakefield Orthopaedic Clinic, Calvary Hospital, Adelaide, SA, Australia
email: *stuart.callary@adelaide.edu.au*

Introduction

Radiostereometric analysis (RSA) is the most accurate method to measure *in-vivo* wear of highly cross-linked polyethylene (XLPE) liners [1]. Less sensitive measurement methods from plain radiographs often report higher than expected wear rates and the variation within results inhibits correct clinical interpretation. RSA studies have confirmed the very low wear rate of XLPE liners at mid-term follow-up [2] however, there is a paucity of long-term (>10 years) studies. Previously used polyethylene implants wear rate has been affected by three factors including, manufacturing method, articulation size and patient age. Hence the aim of this study was to measure the long-term wear of different designs of XLPE liners against larger articulations and in patients of varying age groups.

Methods and Materials: 153 patients previously enrolled in six specific cohorts [3-4] underwent further RSA examinations at 7-, 10-, and 14-years follow-up (Table 1). Proximal femoral head penetration (FHP) was calculated between the day 2 RSA exam and latest follow-up. The proximal wear rate was calculated as the slope of the FHP between one year and latest follow-up.

Results: The mean proximal wear rate of one XLPE liner manufactured with a low irradiation dose (5Mrad) was significantly higher than two liners irradiated with 9- and 10-Mrad ($p<0.001$, Fig 1).
Non-inferiority of XLPE wear rates against larger articulations (36/40mm) was supported when compared to standard articulations (28/32mm, Figure 2). This supports the use of larger femoral heads to reduce the risk of dislocation. Non-inferiority of XLPE wear rates in younger patients (40-64years) was supported when compared to older patients (65-74years). This supports the use of these implants in young patients who have longer life expectancy and require implant longevity.

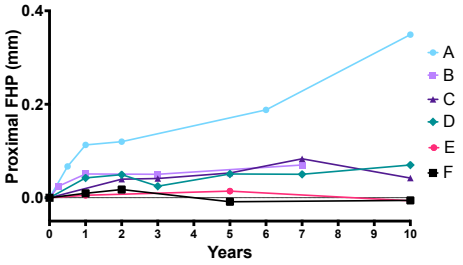

Figure 1. The median FHP for each cohort up to 10 years

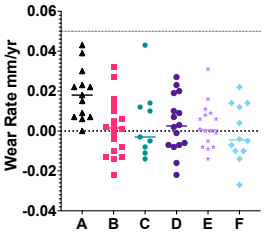

Figure 2. The median proximal wear rate of all cohorts. No individual was above the threshold associated with osteolysis (0.05mm/yr, dotted line)

Discussion: The low long-term wear rates (<0.02mm/year) are encouraging for the continued excellent survivorship of XLPE implants in their second decade of use. Companies introducing new designs of XLPE liners need to be aware that larger irradiation dose does result in a decreased long term *in vivo* wear rate.

Acknowledgements

Stuart Callary was supported by a Research Fellowship from The Hospital Research Foundation Group during this study.

References

1. Callary S, et al., *J Ortho Res.* 35:988-996, 2017.
2. Callary S, et al., *Acta Ortho.* 86:159-168, 2015.
3. Callary S, et al., *CORR Accepted Jan* 2024
4. Callary S, et al., *BJO.* 6:839-45, 2023.

Table 1: Patient and implant details for the six cohorts

Cohort	XLPE Type	Manufacturing Irradiation Dose	Age (yrs)	Head Size (mm)	M:F	Patients Recruited	Time Points
A	Marathon™	5 Mrad	55-80	28	10:16	29	1, 6 & 14yrs
B	Longevity™	10 Mrad	65-74	28	13:14	27	1, 2, 3, 5, 7 & 10 yrs
C	Longevity™	10 Mrad	65-74	36	15:14	29	1, 2, 3, 5, 7 & 10 yrs
D	Longevity™	10 Mrad	40-64	28	15:13	28	1, 2, 3, 5, 7 & 10 yrs
E	X3™	3 x 3 Mrad	47-76	32	11:10	21	1, 5 & 10 yrs
F	X3™	3 x 3 MRad	55-76	36/40	13:6	19	1, 5 & 10 yrs

An objective evaluation of the quality of UHMWPE in total hip replacements, which we implant in daily practice

Fulin P.[1], Slouf M.[2], Pokorny D.[1], Gajdosova V.[2]

[1]1st Orthopedics Clinic of the 1st Faculty of Medicine of Charles University and Motol University Hospital, Czech Republic
[2]Institute of Macromolecular Chemistry of the Czech Academy of Sciences, Czech Republic
petrfulin@gmail.com

Introduction: For an orthopedic surgeon it is difficult or even impossible to estimate the real quality of ultrahigh molecular weight polyethylene (UHMWPE) liners that are used in the total joint replacements (TJR) just on the basis of information given by the manufacturers. At the same time, the quality of the UHMWPE liner can impact strongly on the total lifespan of the implanted TJR.
This work aims at an independent, objective comparison of the properties of new UHMWPE inserts for total hip replacements (THR) before implantation and then after artificial ageing.

Methods and Materials: We analyzed seventeen most frequently implanted UHMWPE cups of different manufacturers after unpackaging and four control samples prepared by standard industrial-scale procedures according to our instructions, whose modification (crosslinking, thermal treatment, stabilization and sterilization) was known in detail. The UHMWPE polymer was characterized by four independent microscale methods, suitable for relatively small and irregular specimens such as THR cups: infrared microspectroscopy (IR), differential scanning calorimetry (DSC), microhardenss (MH) and thermogravimetric analysis (TGA). We tested the same characteristics also after arteficial aging.

Results: Oxidation index (OI) is a key indicator of oxidative damage of the UHMWPE. For new samples before implantation, the difference between individual samples is up to six times (in the range of 0.022 - 0.129). After artificial aging, the differences deepen up to almost fifty times (in the range of 0.059 - 2.902)! Trans-vinylene indices (VI, a measure of the absorbed dose of radiation during cross-linking and/or sterilization) give us information about polyethylene modifications that are often not reported by manufacturers. Crystallinity index (CI) and microhardness (MH) confirmed that the observed structure changes showed a real impact on mechanical properties. Significant correlations among oxidative damage (OI), crystallinity (CI) and microhardness (MH) were statistically proven. TGA experiments gave rough estimate of stabilization and, consequently, possible long-term oxidation resistance. Substitutes containing a stabilizer (vitamin E) clearly show the best oxidative stability. The highest oxidative degradation was usually observed in samples thermally treated by annealing and/or sterilized by gamma irradiation.

Discussion: The results confirmed our expectations that the UHMWPE liners from various manufacturers can be significantly different as far as their molecular structure, supermolecular structure, and mechanical properties are concerned. The differences among the various UHMWPE can be expected to increase after the implantation during in vivo up to fifty times!

Choosing an implant with objectively high-quality polyethylene can maximize the lifetime of the joint replacement several times over and thereby essentially improve the quality of life of our patients.

Towards a European database of explanted UHMWPE inserts: potential and challenges

Bracco P[1*], Righetti M[1], Bistolfi A[2], Mateo J[3], Panisello JJ[3], Canales V[4], Gómez-Vallejo J[5], Kruger J[6], Medel F[6], Gajdosova V[7], Dybal J[7], Fulin P[8], Pokorny D[8], Slouf, M[7]

[1] Chemistry Department and NIS Centre, University of Torino, Torino, Italy

[2] Cardinal Massaia Hospital, Department of Surgery, Orthopedics and Traumatology. Asti, Italy

[3] Department of Orthopaedic Surgery and Traumatology, Miguel Servet University Hospital, Zaragoza, Spain

[4]Department of Orthopaedic Surgery and Traumatology, Royo Villanova Hospital, Zaragoza, Spain

[5] Department of Orthopaedic Surgery and Traumatology, Lozano Blesa University Hospital, Zaragoza, Spain

[6] Department of Mechanical Engineering- Aragon Institute of Engineering Research (I3A), University of Zaragoza, Spain

[7] Institute of Macromolecular Chemistry of the Czech Academy of Sciences, Prague, Czech Republic

[8] 1st Orthopedics Clinic of the 1st Faculty of Medicine UK, Hospital Motol, Prague, Czech Republic

pierangiola.bracco@unito.it

Introduction: Monitoring the clinical performance of UHMWPE liners has proven to be an important tool to assess the reliability of UHMWPE formulations currently on the market and for developing future solutions.
This project was initiated in 2022, through the collaboration of researchers from the Czech Republic, Spain, and Italy, with the aim of creating a shared retrievals database to enable more comprehensive monitoring of UHMWPE liner performance across Europe.

Methods and Materials:
The explants included in the database come from the collections of the three research centers and were collected over a period of more than 15 years. At present, the database contains >500 retrievals. Each center has contributed only suitable portions of its database, based on the completeness and standardization of the data. However, additional data is being incorporated, following a review of past analyses. Each database is an independent XLS file, containing pre-defined columns with anonymized patient data, manufacturer data (irradiation, thermal treatment etc.), orthopedic evaluation (links to revision protocols), and material characterization (MicroFTIR and microindentation).
Each retrieval was analyzed by micro-FTIR and the maximum and average values of oxidation index (OI), trans-vinylene index (VI), and crystallinity index, (CI) were evaluated. All indexes were calculated in a standardized way by means of a freely available Python package [1]. The micromechanical properties of selected UHMWPE liners were also determined, by means of non-instrumented and instrumented microindentation hardness testing, from two locations (maximum oxidation area and central region of the sample). The final data analyses were performed with freeware Python scripts and libraries for data processing [2].

Results and discussion:
Our initial concern was to verify that standardized sample treatment, measurements, and data collection protocols from three independent research groups yielded reliable and consistent results. In fact, the aggregated results confirm some well-known trends in the literature [3], such as the correlation between the degree of oxidation and the crystallinity of the material, as well as the statistical significance of the difference in oxidative degradation of UHMWPEs with different sterilization. Furthermore, containing both manufacturer and clinical data, as well as systematically processed data from microFTIR and micromechanical measurements, the database offers an opportunity to correlate structural characterization of the failed materials with clinical evaluations (such as reasons of TJR failures), across three countries (Figure 1).

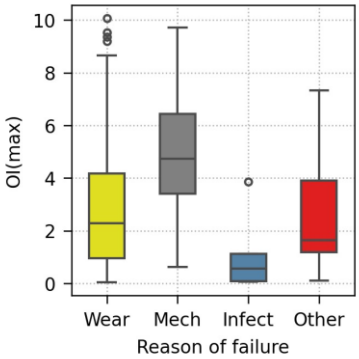

Figure 1 Oxidative degradation (max OI) versus causes of failures for UHMWPE hip liners

In summary, it has been demonstrated that our UHMWPE database contains enough information to show relevant results [4]. However, there are still significant limitations:
1) Different laboratories have varying data cataloging practices. Making the data compatible with the database requires extensive effort.
2) The current database still lacks comprehensive data on specific types of UHMWPE (HXLPE, Antioxidants containing), with the adoption of "modern" PEs progressing more slowly in Europe compared to the US.
3) Additionally, the database currently represents only three specific regions of Europe and specific areas within each country, limiting the generalizability of the results.
The project is still under active development [5] and partners from other countries are welcome.

References
[1] https://pypi.org/project/mpint
[2] https://pypi.org/project/mdbase
[3] UHMWPE Biomaterials Handbook, Elsevier, 2016
[4] Slouf M et al. Polymers 2023, 15, 568
[5] https://mirekslouf.webnode.cz/projects/uhmwpe

Determination of particle induced osteolysis in THA with highly crosslinked polyethylene liners

Songyun Liu[1], Deborah J. Hall[1], Corina Dommann-Scherrer[2], Robin Pourzal,[1] Peter Wahl[3,4]
[1]Rush University Medical Center, Chicago, Illinois
[2]Institute of Pathology, Cantonal Hospital Winterthur, Winterthur, Switzerland
[3]Division of Orthopaedics and Traumatology, Cantonal Hospital Winterthur, Winterthur, Switzerland
[4]Faculty of Medicine, University of Berne, Berne, Switzerland
peter.wahl@ksw.ch

Introduction: The use of highly crosslinked polyethylene (HXLPE) liners has resulted in much better wear behavior, lower incidence of particle induced osteolysis and increase implant longevity in total hip arthroplasty (THA). However, it is unclear if osteolysis is truly eliminated or only postponed. The problem is that late particle induced osteolysis is difficult to diagnose because pathologists can no longer see XLPE debris due to its smaller size, and certain periprosthetic tissue hallmarks of osteolysis, such as foreign body giant cells, are no longer obvious. Objective: to locate polyethylene debris within periprosthetic tissue of two THA cases with XLPE liners and obvious osteolysis.

Methods and Materials: Two THA cases (87- and 61-year-old, male) with implantation times of 7. 6 and 6.8 years and the same type of HXLPE liner were reviewed. Both were removed due to pain and implant loosening with obvious radiolucency visible along the femoral stem. The acetabular wear of both liners was assessed with an optical coordinate measuring machine and volumetric loss was calculated. Pseudo-capsule tissue was histopathologically analyzed. Two consecutive tissue sections were prepared for a) H&E staining and b) 5-µm unstained section was placed on a 25mm×2mm BaF_2 disc (IR transparent) for Fourier Transform Infrared Spectroscopic Imaging (FTIRI) analysis.

Results: Both acetabular liners exhibited prominent wear scars (Fig. 1) with wear volumes of 115.5 mm^3 and 208.28 mm^3 (wear rate: 15.2 mm^3/year and 30.6 mm^3/year), respectively. The maximum linear penetrations were 207.9 µm and 315.6 µm (linear wear rate: 0.0274 mm/year and 0.0464 mm/year), respectively. The macrophage infiltration of both cases exhibited no obvious presence of polyethylene debris. For instance, in Case one (Fig. 2D), under polarized light at most one birefringent particle could be detected per field of view. However, using the characteristic peak representing the absorbance of methylene group ($\nu_\delta(CH_2)$), centered at 2918 cm^{-1} and 2850 cm^{-1}, respectively, chemical images generated by FTIR-I clearly showed the prominent presence of polyethylene within the tissue (Fig. 2E). Aside from identifying the aggregation of PE debris, another finding was glycogen deposition within the hypertrophic synovial membrane of the neo-capsule (Fig. 2G). Using Case two as an example, the presence of polyethylene was co-localized with the presence of cells as indicated by characteristic IR signals, centered at 1081 cm^{-1}, associated with nucleic acid (Fig. 3B & C), whereas areas without either cells or polyethylene exhibited most dominantly the presence of Amide I, indicative of the collagenous tissue matrix (Fig. 3D).

Discussion: This study has shown that particle induced osteolysis can still occur THA with XLPE liners even under 10 years *in situ*. which is clearly below the average clinical expectation of THA with XLPE liners. Thus, further investigation is warranted to determine if the resulting wear of these components is specific to the implant design and/or material, or if other factors played an essential role in the wear process and subsequent inflammatory reactions observed. It has also demonstrated the difficulty of determining the presence of PE debris within periprosthetic tissue. FTIRI is an ideal tool to determine the presence of fine PE particle accumulations intracellularly. More retrieval analysis is needed to determine new histopathological hallmarks of osteolysis related to HXLPE liners and potential increased bioreactivity of these much finer sub-micron PE debris. The overall precedence of late osteolysis will be important to understand the longevity of current generation of HXLPE.

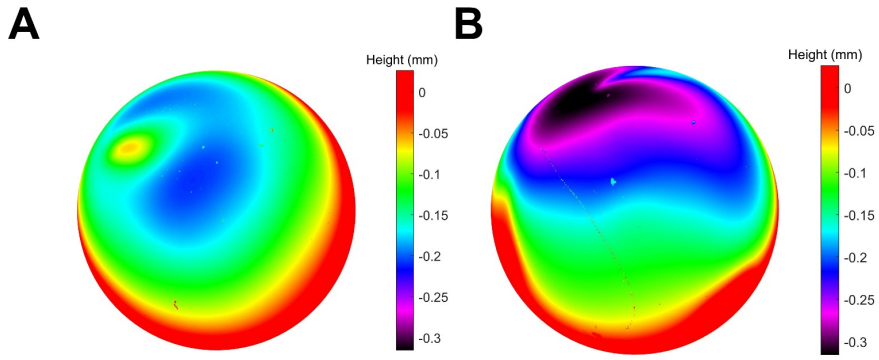

Figure 1 Heat maps of polyethylene wear of the liners of A) case1 and B) case 2.

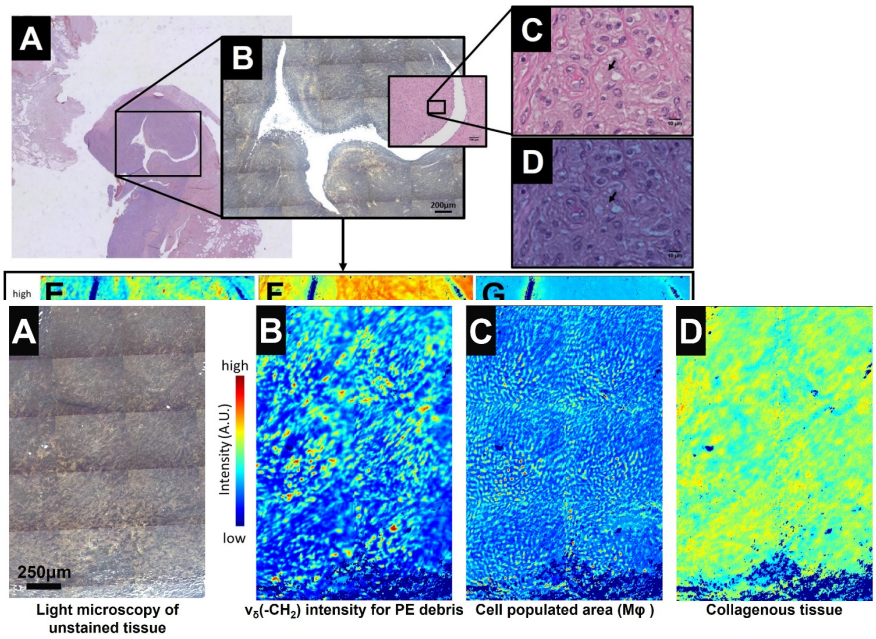

Figure 3 A) Unstained tissue section of case 2. B) Chemical FTIR imaging indicating the presence of PE debris, C) Chemical image at wavenumber 1101-994 cm^{-1}. This IR spectral region is characteristic for the presence of phosphorous-related functional groups including the nuclei of cells to highlight the overlaps intracellular accumulation of PE debris and actual inflammatory cell presence, i.e., macrophages (Mφ). D) chemical image indication the presence of the collagenous matrix.

In-Vivo Validation of the UHMWPE Creep Determination in Clinical Radiographs after TKA Using Artificial Intelligence

Puente Reyna, AL[1]; Lutter, C[2]; Mittelmeier, W[2]; Selig, M[1]; Bien, T[3]; Dreischarf, M[3]; Grupp, TM[1,4]
[1]Aesculap AG, Tuttlingen, Germany
[2]Rostock University Medical Center, Department of Orthopaedic and Trauma Surgery, Rostock, Germany
[3]Raylytics GmbH, Leipzig, Germany
[4]Ludwig Maximilians University Munich, Department of Orthopaedic and Trauma Surgery, Musculoskeletal University Center Munich (MUM), Campus Grosshadern, Munich, Germany
ana_laura.puente_reyna@aesculap.de

Introduction: Polyethylene wear represents a significant risk factor for the long-term success of knee arthroplasty [1]. As the wear rate of the polyethylene inserts is measured in vivo by analyzing clinical radiographs, accurate and precise methods are needed to perform reliable measurements. This work aimed to validate an automated algorithm for accurate and precise artificial intelligence (AI) based wear measurement in knee arthroplasty using clinical AP (anterior-posterior) radiographs for scientifically meaningful multi-center studies.

Methods and Materials: Twenty postoperative radiographs (knee joint AP in standing position) after knee arthroplasty (e.motion® Pro, Aesculap AG, Tuttlingen, Germany) were analysed using the novel algorithm. A convolutional neural network-based segmentation is used to localize the implant components on the X-Ray, and a 2D-3D registration of the CAD implant models precisely calculates the three-dimensional position and orientation of the implants in the joint at the time of acquisition. From this, the minimal distance between the involved implant components is determined, and its postoperative change over time enables the determination of wear in the radiographs. The measured minimum inlay height of 335 unloaded inlays excluding the weight-induced deformation, served as ground truth for validation and was compared to the algorithmically calculated component distances from 20 radiographs. Using early results from the clinical multi-center study creep of the polyethylene inlays after 3 months was compared to geometric creep results from a knee wear simulation study.
The creep simulation was performed on a load controlled 4 station knee wear simulator (EndoLab GmbH, Thansau, Germany) capable of reproducing loads of high demanding activities measured in vivo on 8 patients (3) and normalized to a patient weight of 100 kg (4). The load profiles were applied for 500,000 cycles in a combination of 40% stairs up, 40% stairs down, 10% level walking, 8% chair raising and 2% deep squatting.
The gliding surfaces (e.motion® PS Pro MXE, T5L, 10 mm height, Aesculap AG, Tuttlingen, Germany) were 3D scanned optically (ATOS 5; Carl Zeiss GOM Metrology GmbH, Braunschweig, Germany) before the test and after 500,000 cycles. The scans were superimposed, the geometrical changes calculated using an appropriate software and the results displayed in pseudo-colors in a transverse plane view. The deepest point at the medial and lateral proximal side of every gliding surface was measured.

Results: The average height of the as manufactured inlays was 6.242 mm. With an average weight of 94 kg in the studied TKA patient cohort, it was determined that an average inlay height of 6.160 mm was expected in the patient, giving an expected creep of 82 µm. Based on the radiographs, the algorithm calculated a minimum component distance of 6.158 mm, which deviated by 2 µm in comparison to the expected inlay height and resulted in an in vivo creep of 84 µm. The measured creep of the polyethylene inlays after in vitro axial loading during 500,000 cycles was between 70 µm and 90 µm, which falls in the range measured in vivo.

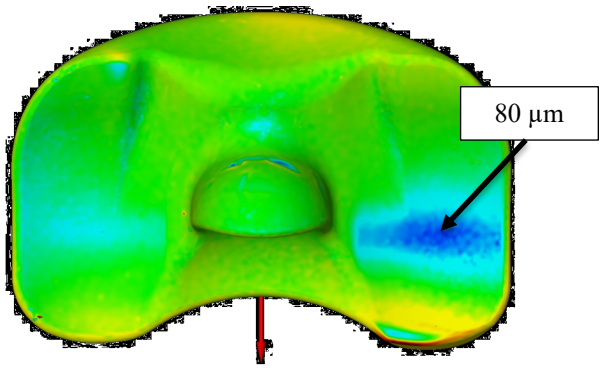

Discussion: An automated method was presented that allows accurate and precise determination of the inlay height and subsequently the creep and wear in knee arthroplasty based on a clinical radiograph and the CAD models. Precision and accuracy are comparable to the current gold standard Radio Stereometric Analysis (RSA) [2], but without relying on special radiographic setups. The developed method can therefore be used to objectively investigate novel implant materials with meaningful clinical cohorts, especially for larger multi-center post market clinical follow-up studies according to the new Medical Device Regulation in Europe [3,4] thus improving the quality of patient care.

References:

(1) AOA NJRR 2021
(2) Kaptein et al 2007
(3) Overgaard & Grupp 2023
(4) Jäger et al 2023

Antioxidant Performance in UHMWPE Knee Bearings: A Mid-Term Report

Solberg, PC[1], Currier, BH[1], Jevsevar KC[1], Van Citters, DW[1]
[1]Dartmouth College, Hanover, NH USA
peder.solberg.th@dartmouth.edu

Introduction: Materials used in joint replacement bearings must maintain a balance between wear resistance, toughness, and oxidation resistance. Antioxidant polyethylene has been introduced to stabilize free radicals resulting from the cross-linking process while avoiding mechanical property losses associated with some previous generations of highly cross-linked polyethylene, which use thermal processing to stabilize free radicals. Several forms of antioxidant are used in UHMWPE: blended vitamin E (VE-B), diffused vitamin E (VE-D), and a solid-state hindered phenol antioxidant pentaerythritol tetrakis [3-(3,5- di-tert-butyl-4-hydroxyphenyl)] propionate (PBHP). Retrieval studies published to date suggest that these antioxidants minimize in vivo oxidation as intended.[1,2] However, most studies have been limited by small sample size, short duration, and a stronger emphasis on VE devices than those with alternative antioxidants. This study seeks to address some of these limitations with a larger cohort of PBHP devices and longer in vivo durations. To investigate the performance of these materials to date, we examined several metrics related to oxidation: (1) ketone oxidation index (KOI), (2) polymer crystallinity, indicative of polymer chain scission, and (3) crosslink density (XLD), indicative of polymer crosslink degradation.

Methods and Materials: A total of 257 AO-HXLPE tibial bearings were received at revision by an IRB-approved retrieval laboratory from February 2016 to November 2023, with in vivo duration of 0 to 8.9 years (mean: 2.3). An additional six VE-D devices published in Currier et al. 2018 were included in this study to increase the size of that material cohort.[1] Thin sections (200 μm) were sliced from the center of the condylar region and scanned on a Thermo Scientific iN-10 FTIR microscope to obtain measures of oxidation and crystallinity. Maximum KOI was used to report oxidation using ketone peak height (1713-1718 cm^{-1}) normalized to the 1368 cm^{-1} peak height thickness proxy (1365-1371 cm^{-1}). A set of additional thin sections was taken from 86 PBHP samples in this dataset, assessed for KOI, then hexane extracted and scanned again to determine the effect of adsorbed content on KOI.[3] Crystallinity was measured via infrared crystallinity index (IRCI), defined as the quotient of the crystalline absorption peak height (1896 cm^{-1}) to one of the amorphous absorption peaks (1305 cm^{-1}).[4] For confirmation of crystalline behavior, dynamic scanning calorimetry (DSC) was performed on a subset of 139 PBHP samples. Articular XLD was measured in 65 of the implants using a gravimetric gel swell technique.[5,1] Statistical analyses used Spearman's correlations with $p<0.05$ considered significant.

Results: Maximum KOI remained far below the commonly-cited critical threshold of 1.0 to 1.5, but increased slightly with time in all materials (Fig. 1)[6]. Extracted samples indicated no increases to KOI with time. The contribution of adsorbed lipids to the ketone oxidation index was thus determined to be 0.0053 per year for the PBHP when excluding the one device with a subsurface KOI peak. Subsurface KOI peaks, typically indicative of polymer oxidation, were present in 5 of the devices in this study, including 4 VE-B and 1 PBHP. The maximum KOI associated with these subsurface peaks was generally low (KOI=0.24 for the highest VE, KOI<0.1 for the PBHP), especially considering the baseline KOI present in these materials. (Note the zero duration KOI of 0.08 in Fig. 1, due to the presence of a ketone group in the antioxidant). IRCI results (Fig. 2) showed no significant change in crystallinity with time for the two vitamin E materials ($p=0.86$, VE-B; $p=0.08$, VE-D). Slight but statistically significant increases in IRCI were observed with time for PBHP inserts ($p<0.001$). However, DSC crystallinity results for PBHP indicate a slight downward trend ($p=0.0015$). No correlation between XLD and either time in vivo or articular KOI was observed (Fig. 3).

Discussion:
Polymer oxidation as measured by maximum KOI typically increases exponentially with time, accompanied by the development of subsurface oxidation peaks, as well as increases in crystallinity and decreases in crosslink density at higher oxidation. Subsurface KOI peaks were observed in this study in only five of the retrieved bearings. An incidental finding in this study was that time in vivo led to small but predictable increases in KOI at the bearing surface due to lipid absorption. Oxidation, at the low KOI levels measured in most of these retrievals, would not be expected to yield detectable changes to the polymer microstructure, nor to pose a threat to mechanical properties. These results suggest that oxidation is hampered in these retrieved bearings by the presence of antioxidant, especially compared to previous generations of HXLPE. Long-term monitoring will be necessary to ensure this continues to be the case.

References:
[1] Currier BH, et al. JBMR-B 2018;106:353–9.
[2] Spece H et al. JOA 2019;34:3088–93.
[3] Currier BH, et al. CORR 2017;475:1356–65.
[4] Nagy E, Li S. "A FTIR Technique for the Evaluation of Polyethylene Orthopaedic Bearing Materials." SFB 16th Annual Meeting, 1990.
[5] Reinitz SD et al. JBMR-B 2017;105:39–45.
[6] Currier BH et al. JOA 2007;22:721–31.

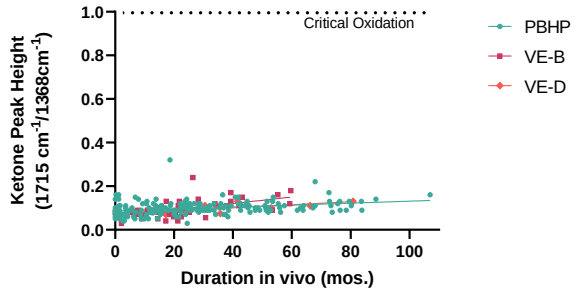

Fig 1: Oxidation over time in vivo demonstrates slight increases in KOI. These increases do not appear to exhibit exponential behavior as would be expected with polymer oxidation.

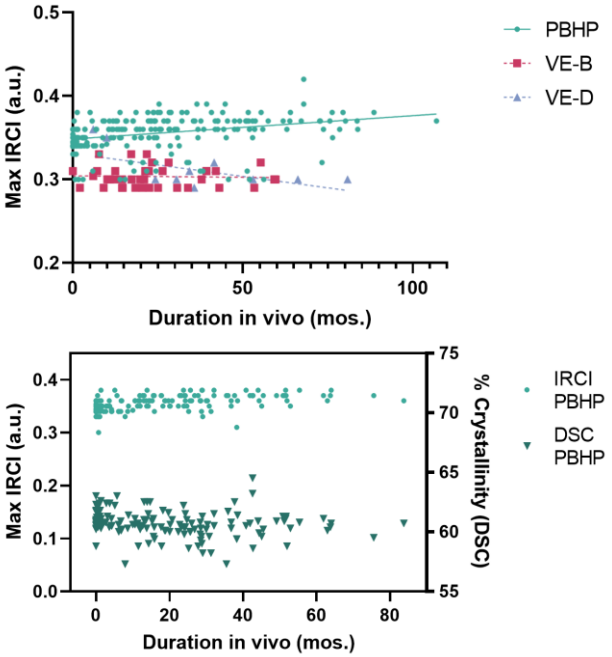

Fig. 2: (Top) infrared crystallinity index (IRCI) as a function of time in vivo, (bottom) DSC crystallinity observed for 139 PBHP inserts, along with the IRCI results for those same devices.

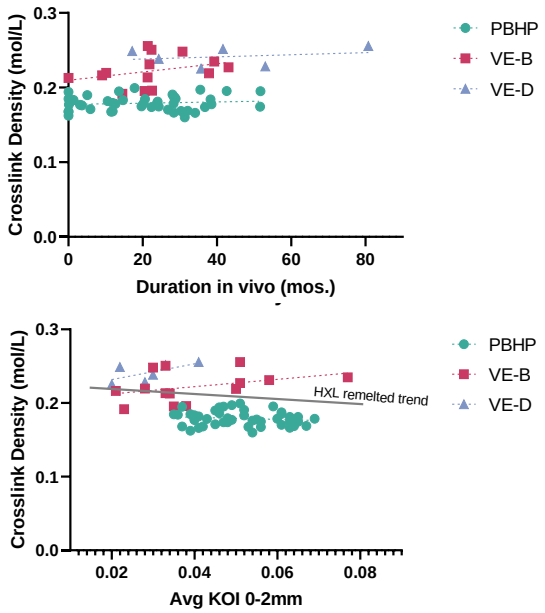

Fig. 3: Crosslink density is shown as a function of time in vivo (top) and KOI (bottom). The HXL remelted trendline represents the decreases in articular crosslink density noted in Currier et al. 2018[1] with increasing articular KOI, a trend dominated by non-AO devices with subsurface KOI peaks. No correlation of XLD was seen with either time in vivo or KOI for the AO retrievals in this study cohort.

Comparison of macro-, micro- and nanoscale creep behavior of UHMWPE, crosslinked UHMWPE, and PEEK

Slouf M[1*], Gajdosova V[1], Christofl P[2], Steinhart M[1], Rana L[1]
[1]Institute of Macromolecular Chemistry CAS, Praha, Czech Republic
[2]Polymer Competence Center Leoben, Leoben, Austria
* *slouf@imc.cas.cz*

Introduction: We compared macroscale tensile creep with microscale and nanoscale indentation creep of three polymers employed in orthopedic surgery: ultrahigh molecular weight polyethylene (PE), crosslinked ultrahigh molecular weight polyethylene (PE-XL), and polyether ether ketone (PEEK). Moreover, we compared additional properties of the three polymers, available from creep and indentation measurements. This is a continuation of our work focused on the correlations between tensile and indentation creep of polymer systems [1].

Materials and Methods: The ultrahigh molecular weight polyethylenes (PE; PE-XL) were bought from Beznoska Ltd., Czech Republic (PE: Chirulen 1020, non-modified; PE-XL: Chirulen 1020, γ-irradiation 75 kGy, remelting at 150 °C). PEEK polymer (Vestakeep®) was obtained from Evonik Operations GmbH. The creep behavior was determined from macroscale tensile measurements, non-instrumented and instrumented microindentation (MH and MHI) and instrumented nanoindentation (NHI) as described previously [1, 2]. The creep data were evaluated with software MCREEP [1, 3].

Results and discussion: The stiffness-related properties of PE, PE-XL and PEEK exhibited the same trends at all length scales. Figure 1 shows the initial, instantaneous, time-independent elastic moduli (E) of all polymers. The moduli were estimated from the fitting elasto-visco-plastic models to tensile and indentation creep data [1]. Their values agreed reasonably with the literature concerning UHMWPE (E ~1 GPa) and PEEK (E ~3 GPa).

The long-term macroscale tensile creep behavior of PE, PE-XL and PEEK (holding time 6000 s) could be estimated from the short-term microindentation and nanoindentation creep experiments, as documented in Figure 2. The creep constants, which were obtained from fitting empirical Power law model (PL model) to creep data (more details in ref. [1]) were similar for both macroscale and micro/nanoscale measurements.

The simple empirical PL model (Fig. 3, dashed curve) could predict the long-term creep behavior better than the more-sophisticated and multiparameter elasto-visco-plastic models (EVP models; Fig. 3, dotted curves). The EVP models combine springs (S), dashpots (D) and Kelvin-Voigt elements (KV), as described in our software MCREEP [3] and references therein. PL model yielded better predictions also in our previous study [1].

In summary, PEEK exhibited higher creep resistance and higher stiffness than both UHMWPE's. The creep of PE and PE-XL was quite similar. PE showed higher stiffness than PE-XL, which could be attributed to the lower crystallinity of the crosslinked and remelted polymer [2].

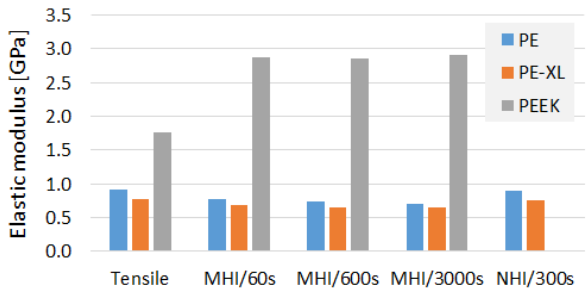

Figure 1: Initial compliance from tensile, microidnetation and nanoindentation creep measurements.

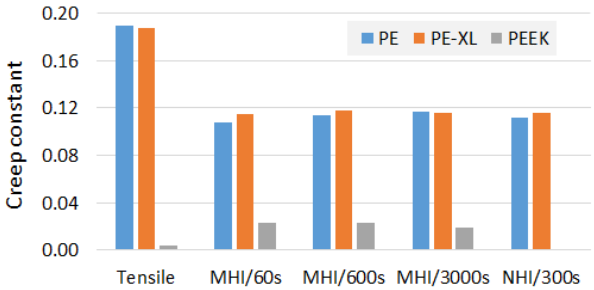

Figure 2: Creep constants from tensile, microidnetation and nanoindentation creep measurements.

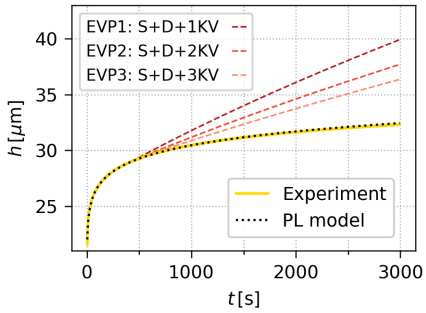

Figure 3: Fitting of EVP and PL models to microcreep data of PE-XL sample; fitting within range (0–500s).

Conclusion: All samples exhibited analogous behavior at all length scales. The micro- and nanoindentation are reliable techniques for characterization of polymers.

Acknowledgement: Projects NU21-06-00084 (AZV CR) and TN02000020 (TA CR).

References:

[1] *Materials* 16 (2023) 834.
[2] *Polymer Testing* 41 (2015) 191–197
[3] *https://pypi.org/project/mcreep*

Understanding Izod Impact strength variations as a function of different polymer resins and processing technologies

H. Smelt[1] , W. Cheng[1], T. Verspagen[1], R. Stepanyan[1,2]
[1]DSM Biomedical, Geleen, The Netherlands, [2]Avient Protective Materials, Geleen, The Netherlands
harold.smelt@dsm-firmenich.com

Introduction: There is a need for additional suppliers for medical grade type 1 and 2 UHMWPE powders as specified in ASTM F648 and ISO 5834-1. DSM Biomedical developed Ulteeva Purity™ powder grades MG001 and MG002 with similar molecular weights ('Mw') as currently used GUR 1020 and GUR1050 powders. After compression molding large sheets (>1 m^2) using usual recipe set points, it was noticed that especially the Izod Impact Strength kJ/m^2 ('Izod') was typically 10% lower for MG001 and MG002 materials as compared to GUR1020 and GUR1050. Post molding annealing step at 115°C reduced Izod by ±10 kJ/m^2, consistently for both MG and GUR materials. Once crosslinked at 50-100 kGy irradiation levels, the Izod for both materials reached similar levels again. In this study molecular and morphology properties were investigated to find the reason for the different magnitudes of Izod for non-crosslinked materials. High temperature molding and annealing was tested to improve Izod values [1].

Methods and Materials: MG001 (type 1) and MG002 (type 2) powder was produced in the UHMWPE plant in Geleen (NL) using a heterogeneous supported catalysts based on titanium compound (Ziegler Natta). Physical and mechanical properties were tested following ASTM F648-21. Materials were molded following ISO11542-1 at 10 MPa using temperatures from 210 up to 300°C at 1 up to 2 hours residence time. Powder and molded parts were characterized by linear solution rheology: UHMWPE samples (powder or grinded part) were dissolved at 10wt% in paraffin oil in presence of 2000 ppm of DBPC antioxidant and examined in a plate-plate geometry. SAXS and WAXS were used to measure the crystallinity and lamellar thickness.

Results: No significant difference in SAXS (long period L_p) and WAX (crystallinity) patterns is found, despite huge differences in Izod values.

sample	Cryst. wt.%	Lp (nm)	Izod (kJ/m^2)
MG001 (st. molding 210°C, 1 h)	61,8	49	130
MG002 (st. molding 210°C, 1 h)	57.8	52	80
MG002 (high T molding 300°C, 2h)	59.4	52	160

Table 1: Crystallinity (WAXS) and long period (SAXS) for UHMWPE molded materials with different Izod values.

The oxidation index (ASTM F2102) for the standard 210°C-1h molded versus 300°C-2h molded samples were in the same range of 0.007 – 0.015.

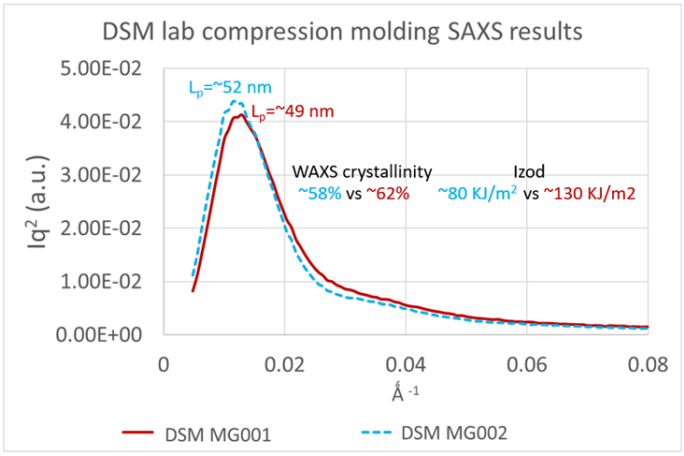

Figure 1; Semicrystalline morphology difference (e.g. crystallinity, crystal size and distribution) cannot explain the Izod difference between Type1 MG001 and Type 2 MG002.

Solution rheology showed that both chain scission and some branching took place during molding: phase angle of molded material as a function of oscillation frequency shifts to higher frequencies, signaling a reduction in Mw. But also shows early plateauing at lower frequencies, which is a sign of a fraction of very slowly relaxing (branched) material.

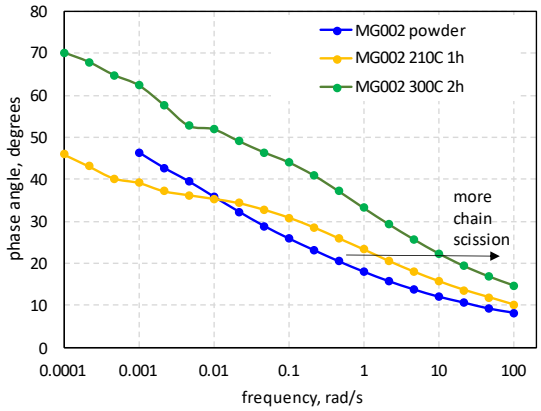

Figure 2; Solution rheology viscoelastic response expressed in phase angle showed the change in Mw between powder and molded materials for type 2 material MG002. Curve moving up at high frequency: sign of Mw reduction.

Discussion: WAXS and SAXS showed similar crystal dimensions and crystallinities, which indicates that these morphology parameters are not the main factors to explain the large differences in IZOD values between the materials. Solution rheology showed that Mw decreases during molding. It is also known that type 1 material with a lower Mw typically results in a significantly higher Izod value as compared to the higher Mw type 2 material. Major parameter to steer Izod is therefore the Mw after

molding. Mw of the molded part can be tuned by: 1) Initial Mw of the powder expressed in Elongations Stress (MPa) and Viscosity Number (ml/g), however limited space is available due to minimum ASTM F648 requirements for those properties. 2) Using UHMWPE chemistry which is more sensitive for chain scission, e.g., certain catalyst residues or branches in the high Mw PE fraction can be more sensitive for chain scission. 3) Use high temperature and/or longer exposure time during molding or annealing [1]. This last option was tested using 300°C molding plate temperatures and by a hot gas circulation oven under a nitrogen atmosphere at 270-300°C for 3 hours exposure time. When applying temperatures above 280°C during molding or post annealing/remelting, the Izod showed a significant increase. When the material is exposed too long the Izod will slowly decrease again due to further Mw reduction and potential mild crosslinking. Although type 2 MG002 material with a higher Mw needs a higher temperature (or longer exposure time), it eventually will reach the same level of Izod values around 160 kJ/m^2 as is achieved for type 1 MG001 material.

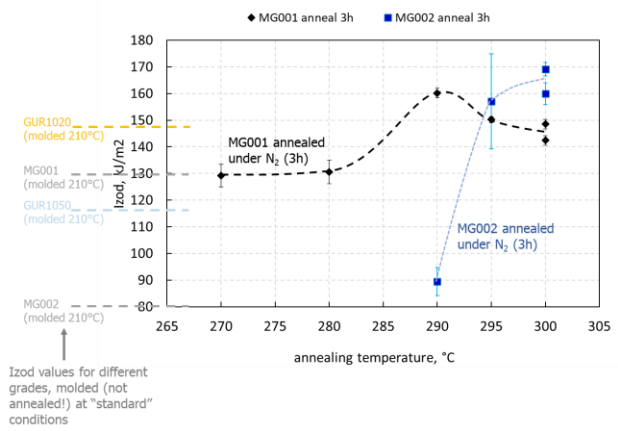

Figure 3: Izod values of MG001 and MG002 discs (160 mm diameter and 300 mm thick) as function of temperatures after 3 hours annealing at 300°C under nitrogen atmosphere.

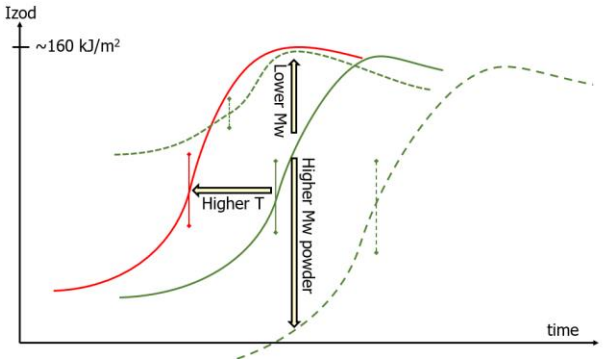

Figure 4: Lower Mw materials require less annealing time versus higher Mw materials. Additionally, higher temperature will accelerate the Mw reduction process.

A large sheet was molded using a standard type 1 recipe cycle and cut into 2,5" thick, 3" wide and 2-meter-long bars, applying both standard annealing at 115°C and high temperature annealing at a core temperature of ≥ 280°C for at least one hour. Tensile properties are not or less affected by high temperature annealing, the yield strength typically increases with 0.5-1 MPa.

Sample description	Yield (MPa)	UTS (MPa)	EAB (%)	Izod (kJ/m^2)
As molded	21.9	67.6	443	133
St. annealed (115°C)	22.0	65.8	452	128
High T annealed (280°C)	22.7	66.6	468	170
St. annealed + 75 kGy XL	22.9	59.7	292	72
High T annealed + 75 kGy XL	24.1	61.1	309	76

Table 2: Property data of as molded (standard type 1 cycle), standard annealed (115°C) & high temperature annealed (280°C) and crosslinked (75 kGy gamma nominal dose) MG001 material. Data are average values of a minimum of 3 samples.

The effect of 75 kGy gamma-crosslinking has been tested on both annealed bar series. Crosslinking will reduce the Izod and original large differences are converged to similar values. Both the effect of high temperature annealing or crosslinking indicates the high sensitivity of Izod for molecular connectivity changes via Mw reduction or crosslinks. Trans Vinylene Index and Swell ratio were respectively 0.024 versus 0.025 and 3.4% versus 3.5% for the standard versus high temperature annealed crosslinked samples.

To summarize: present work strongly suggests that Izod impact strength of UHMWPE molded parts is not only determined by the initial Mw (ES, VN) of the material (Type 1 vs Type 2) but is also quite sensitive to Mw shift taking place during molding. And there can be differences in sensitivity for chain scission between UHMWPE resins from different suppliers.

References:

[1] Fu J, Ghali W, Lozynsky AJ, Oral E, Muratoglu OK. Polymer 51 (2010) 2721-2731

Synergistic antibacterial UHMWPE-based materials: mechanical properties and morphology

Inverardi, N.[1,2], Serafim, M.F.[1], Ferreira, M[1], Marzouca, A.[1], Fujino, K.[1], Asik, M.D.[1,2], Sekar, A.,[1,2] Muratoglu, O.[1,2], Oral, E.[1,2]

[1]Harris Orthopaedics Laboratory, Massachusetts General Hospital, Boston, MA 02114

[2]Department of Orthopaedic Surgery, Harvard Medical School, Boston, MA 02114

ninverardi@mgh.harvard.edu

Introduction: Ultra-high molecular weight polyethylene (UHMWPE) is the material of choice for orthopaedic bearings for hip and knee replacement arthroplasty. Recently, UHMWPE has been proposed also as a polymeric matrix for incorporating various pharmaceuticals, including analgesic and antibiotic drugs. The achievement of a UHMWPE that can also act as a drug delivery device, in addition to its primary mechanical and structural function, could be of outmost importance for addressing some potential side effects of the surgery, such as postoperative pain and the occurrence of infections. To this end, UHMWPEs eluting a wide range of drugs were successfully obtained by mechanical blending/mixing of the drugs and the polymer powder before compression molding. However, this approach generally leads to a phase-separated material in which the poor interaction between the polymer matrix and the drug domains causes a decrease in the mechanical properties, in terms of strength, ductility and toughness. In this work, we investigated the mechanical properties under tensile, impact and fatigue conditions of dual drug loaded UHMWPEs, previously proved to be effective in eradicating *Staphylococcus aureus* in in vitro conditions.

Methods and Materials: The antibiotic gentamicin sulfate (GS) and the analgesic bupivacaine (BP) in its salt form, BP hydrochloride (BP HCl, melting point ~259°C) or its free-base form (BP base, melting point ~108°C), were selected for incorporation into 1020 UHMWPE resin. The powders were blended by using a mechanical mixer; selected compositions were previously sieved through a 75 μm mesh and dehydrated in a vacuum oven at 45 °C prior to blending. Compression molding was done at 170 °C under 20 MPa for 10-20 min (area: 85x55 mm^2), followed by at least 40 min of cooling under load. The compositions prepared were 5% GS loaded UHMWPE, 0.5%GS+4.5%BP HCl loaded UHMWPE, 0.5%GS+9.5%BP base loaded UHMWPE, along with virgin UHMWPE. Tensile testing was performed according to the ASTM D638-10 on samples (3.2 mm thick) die-cut from the molded blocks, at a crosshead speed of 10 mm/min (MTS Insight 2 equipped with a 2000N load cell and a laser extensometer). Izod impact testing was performed according to the ASTM F648-14 on pre-notched 6.35×12.7×63.5 mm^3 coupons (CEAST 9050 pendulum, Instron). Fatigue crack propagation resistance testing was performed for virgin UHMWPE and 0.5%GS+9.5%BP base loaded UHMWPE samples, on type A1 compact tension specimens (ASTM E647). A sinusoidal waveform was used for applying the force (load ratio R: 0.1, frequency: 3 Hz). Crack length was measured optically by using an automated measurement system (Cambridge Polymer Group). Thin cross-sections (3x5mm^2) obtained by microtome were observed with an optical microscope (Olympus STM6-F00-3, Olympus Corporation). Fracture morphology was observed with a field emission SEM (ZEISS GeminiSEM 560) at an accelerating voltage of 3 kV and using a secondary electron detector, after sputter coating the surfaces with a 5nm layer of Platinum-Palladium (80:20).

Results: The mechanical properties of drug-loaded UHMWPEs resulted to be dependent on the drug loading and drug choice (**Table 1**). Loading 5% GS in UHMWPE resulted in a decrease of about 26% in ultimate tensile strength (UTS) and of about 21% in elongation at break (EAB) compared to virgin UHMWPE. The resulting morphology is phase-separated with spherical drug domains embedded in the polymeric matrix. For dual drug loaded UHMWPE based on 0.5%GS, the use of the salt form of BP or its free base resulted in significantly different UTS and EAB: 0.5%GS+9.5%BP base loaded UHMWPE outperforms 0.5%GS+4.5%BP HCl. This behavior was confirmed also under impact conditions, as the Izod impact strength of the composition with BP base is similar to that of virgin UHMWPE, while the composition with BP HCl has an almost halved value. The morphology of the composition containing BP HCl is significantly phase-separated, whereas that of UHMWPE containing BP base is to a much lower extent, as the phase separation appears to be related only to the GS phase (0.5%). Concerning fatigue testing, the stress intensity factor at the crack inception (ΔK_{incep}) for 0.5%GS+9.5%BP base loaded UHMWPE resulted to be about 29% lower than that of virgin UHMWPE.

Discussion: The dual drug-loaded UHMWPEs based on GS and BP HCl or BP base here investigated have been previously found to provide synergistic drug elution and antibacterial activity, effective in eradicating *S. aureus* in in vitro conditions over a period of 7 days. In this work, we showed that the physico-chemical properties of the drugs (i.e., melting point, solubility) can play an important role in determining the morphology of the composite material and thus its mechanical properties. Supplementing GS with BP base instead of BP HCl, while still resulting in an effective antibacterial activity, provides higher strength, toughness, and good resistance to fatigue crack propagation.

Acknowledgements: This work was funded by the National Institutes of Health, grant R01AR077023.

	UTS (MPa)	**EAB (%)**	**Izod impact strength (kJ/m^2)**	**Stress intensity factor at crack inception, ΔK_{incep} ($MPa\ m^{1/2}$)**
Virgin UHMWPE	50.8 ± 2.5	448 ± 34	147.2 ± 3.3	1.965 ± 0.248
0.5%GS+4.5%BP HCl loaded UHMWPE	32.9 ± 0.5	333 ± 10	60.0 ± 8.4	n.t.*
0.5%GS+9.5%BP base loaded UHMWPE	37.7 ± 2.5	403 ± 22	140.9 ± 4.0	1.404 ± 0.160

Table 1. Mechanical properties under tensile (UTS and EAB), impact (Izod impact strength) and fatigue testing (ΔK_{incep}) conditions. *n.t.: not tested.

Toughness Study of Super Gradient Crosslinked UHMWPE

Zongtao Zhang[1], Imants Liepins
[1]b-ONE Ortho Corp, NJ
ZTZhang@b1.co

Introduction: Wear and toughness are usually compromised for bulk crosslinked UHMWPE. A super gradient crosslinked GUR1020-E (0.1wt% Vitamin E) has been made by UV assisted-chemical crosslinking [1]. It achieved super crosslinking (250 kGy) on bearing surface and low crosslinking (22 kGy) in the bulk material [2]. The material showed 3 times lower wear rate than 100 kGy crosslinked GUR1020-E in abrasive wear condition at 5 million cycles as well as high tensile strength 70 MPa and 422% elongation as conventional UHMWPE [3]. This study will further study the material toughness by tensile, Izod, and fatigue crack propagation (FCP).

Material and Method: The super gradient crosslinked GUR1020-E (0.1wt% Vitamin E) was made by B-ONE Ortho Corp using UV assisted-chemical crosslinking method [3]. The gradient crosslinking was measured by swell ratio and calibrated to equivalent crosslinking degree in gamma dose by small punch and tensile toughness [1-4,5]. Crosslinking density is the highest at 0.25 mol/dm^3 (~250 kGy) on the surface, gradually decreasing to 0.07 mol/dm^3 (~22 kGy) at 3.50-6.35 mm in bulk material. The tensile testing was performed layer-by-layer per ASTM D638-14 using TYPE V specimen with a thickness of 0.25 mm at depth of 0, 1, 2, and 4 mm, a speed of 25.4 mm/min. Five samples were tested for each data point. The layer-by-layer gradient impact toughness was calculated by tensile toughness using the formula of Tensile Toughness (MPa) = 1.09 Impact Toughness (kJ/m^2) [5]. IZOD testing was conducted per ASTM F648-21 with a geometry of 63.5mm×12.7mm×6.35 mm. Impact directions were perpendicular and parallel to crosslinking directions. Five samples were tested for each data point. FCP testing was conducted per ASTM E647-15 with a geometry of 40 mm ×40 mm ×10 mm, a pre-notched crack perpendicular to the gradient crosslinking direction. The test conditions were R-ratio 0.1, a sinusoidal load 80-800 N, frequency 3 Hz. Three samples were tested for each data point for Paris Equation ($da/dN=C\Delta K^m$).

Results: The layer-by-layer tensile and impact toughness gradually increase with an increase of depth (Fig.1). At the same crosslinking degree, the super gradient crosslinked GUR1020-E has higher tensile strength than gamma ray bulk crosslinked and remelted GUR1020 (Fig.2). The integrated IZOD toughness was 80-85 kJ/cm^2 at the impact direction perpendicular to crosslinking direction (Table 1). When the impact was parallel to the crosslinking direction, the test samples were not completely broken in the first impact, and finally fractured in the second impact as the pendulum swung back. Table 2 shows Super gradient crosslinked GUR1020-E has medium ΔK_i, but several orders of magnitude lower crack propagation rate da/dN as compared to 100 kGy GUR1020-E, and 30 kGy GUR1020.

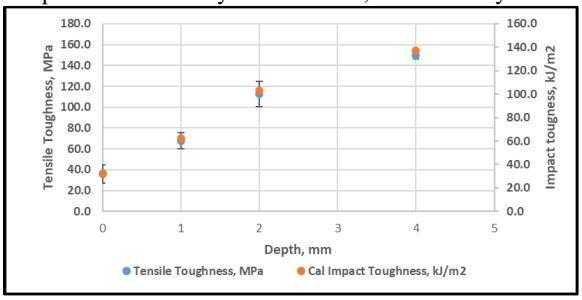

Fig.1. Super gradient crosslinked GUR1020-E tensile/impact toughness.

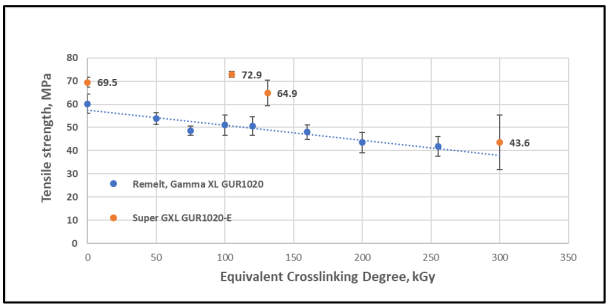

Fig.2. Super gradient crosslinked GUR1020-E tensile strength.

Table 1 IZOD test results of super gradient crosslinked GUR1020-E (Super-GXL UHMWPE).

	IZOD Impact strength (kJ/m^2)	Impact direction	Test Lab
Super-GXL UHMWPE	86.5 ± 2.4	Group I, ⊥ XL	China National Test Center
Super-GXL UHMWPE	80.0 ± 4.0	Group I, ⊥ XL	Cambridge Polymer Group
Super-GXL UHMWPE	No Broken	Group II, // XL	China National Test Center
100 kGy GUR1020-E	73.0 ±1.3	Group I, ⊥ XL	Cambridge Polymer Group
30 kGy GUR1020	102.4 ± 3.4	Group I, ⊥XL	Orthoplastics, Ltd.

Table 2 FCP test results of super gradient crosslinked GUR1020-E.

	DK_i	Coefficeint, C	Exponent, m
	MPa m$^{1/2}$	[(μm/cycle)]/MPa m$^{1/2}$	
Super GXL GUR1020-E	1.68 ± 0.05	$(4.04 \pm 3.5) \times 10^{-5}$	10.95 ± 0.78
100 kGy GUR1020-E	1.52 ± 0.02	$(3.48 \pm 1.88) \times 10^{-4}$	9.22 ± 0.84
30 kGy GUR1020	1.95 ± 0.21	$(8.89 \pm 8.45) \times 10^{-1}$	7.41 ± 0.85

Discussion: The super gradient crosslinked GUR1020-E has three crosslinking zones, super crosslinking, highly crosslinking, and low crosslinking [1-3]. The three zones account for 24%, 15%, and 61% area for IZOD test samples, and 15%, 13%, and 72% area for FCP test samples. Each zone contributes to total toughness proportionally to its percentage of area. The low crosslinked zone accounts for most of the total area of IZOD and FCP test samples, thus dominating the integrated toughness values. The average integrated IZOD and FCP values are higher than 100 kGy GUR1020-E, but lower than 30 kGy GUR1020. The higher tensile strength of the super gradient crosslinked GUR1020-E could contribute to its higher crystallinity (62-66%) than gamma ray crosslinked and remelted GUR1020 crystallinity 54% [6,7]. The super gradient crosslinked material is intrinsically non-homogenous. The application of toughness values must consider the thickness of device and the direction of applied force. A simple comparison of gradient crosslinked toughness to uniform crosslinked toughness is not valid.

References: [1] Zongtao Zhang, US patent application 2022/0002452 (2022). [2] Nolan Lacombe, 2023 ORS Paper No.1207. [3] Zongtao Zhang, 2023 ORS Paper No.1643. [4] Zongtao Zhang, 2023 ORS Paper No.1208. [5] Hout, J. Caitlin et al, J. Biomed. Mat. Res, Part B, Vol 97, 2 (2011):327-33. [6] Harry A. McKellop, et al, J. Orthopedic Res., Vol.17, No.2 (1999):157-167. [7] King, R et al, 55th ORS meeting, Paper No.19.

Bis-diazirine crosslinked UHMWPE

Carvalho, BL[1]; Bellare, A[1]
[1]Polymerix Technologies, Boston, MA, USA
anuj@alum.mit.edu

Introduction: Highly crosslinked ultra-high molecular weight polyethylene (UHMWPE) has been used for over two decades in total joint replacement prostheses due to their toughness and high resistance to wear. The most common method of crosslinking has been to irradiate bulk components using gamma radiation to a dose of 50-100 kGy. However, the short supply of these sources has recently led to alternative sources of crosslinking being employed, such as peroxides[1]. Like ionizing radiation, peroxides abstract a hydrogen from the C-H bonds on the UHMWPE chain, which leads to a free radical that recombines with another to form inter- or intra-chain crosslinking. However, with peroxides, residual small molecules remain in the polymer, which require cumbersome and lengthy processes to remove them from the bulk polymer, such as high temperature evacuation.

In this study, we investigated the use of bis-diazirine to crosslink UHMWPE. Equilibrium swelling, differential scanning calorimetry and tensile testing were employed to characterize the molecular structure, morphology and macroscopic properties of bis-diazirine crosslinked UHMWPE. Unlike the aforementioned crosslinking methods, bis-diazirines are versatile, biocompatible crosslinkers that insert themselves into C-H, N-H and O-H bonds and the by-product is nitrogen gas which can be easily removed[2,3]. Another advantage is that they can be used to adhere UHMWPE to other polymers, such as acrylic bone cement, as well as functionalized metals, ceramics and tissue, if needed. The general form for bis-diazirines is shown in Figure 1, where N represents nitrogen, R_1 and R_2 usually comprise, alkyl, aryl or perfluorinated moieties.

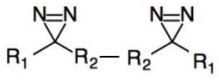

Figure 1. Schematic of the general form of a bis-diazirine.

Methods and Materials: GUR 1020 UHMWPE powder containing 0.1% Vitamin E (Celanese, Oberhausen, Germany) was blended with 0, 1.5, 3, 6 and 12 wt% bis-diazirine (BXW-202, Xlynx Materials Inc., Victoria, Canada) of 435 g/mol molecular weight dissolved in acetone. The dried blended powder was compression molded into 1.5 mm thick plaques at 180ºC and 10 MPa applied pressure using a Carver hydraulic press and slow cooled. ASTM 638-Type V specimens were punched from the molded sheet and subjected to tensile tests at a crosshead speed of 10 cm/min (n=8 per group) to measure the modulus (Mod), yield stress (YS), ultimate tensile stress (UTS) and maximum strain (MS). Differential scanning calorimeter (DSC) were used to measure the crystallinity using a heating rate of 10ºC/min and a heat of fusion of 293 J/g (n=3). Equilibrium swelling experiments were performed in O-xylene at 130ºC. Swell ratios, crosslink density and molecular weight between crosslinks (Mc) measured using the gravimetric method (n=6)[4].

Results: Equilibrium swelling showed a monotonic decrease in swell ratio, increase in crosslink density and a decreasing in molecular weight between crosslinks with increase in the weight % of the bis-diazirine, as shown in Figures 2 and 3. There was no statistically significant difference in the swell ratio of the UHMWPE with 6% and 12% bis-diazirine as well as the crosslink density of the UHMWPE containing 1.5 and 3 wt % bis-diazirine and the molecular weight between crosslinks for UHMWPE containing 6 and 12 wt% bis-diazirine ($p>0.05$, ANOVA). There was no statistically significant difference in the crystallinity (see Table 1) of the UHMWPE control and crosslinked groups ($p>0.05$), and their values were approximately 54-58%. The ultimate tensile properties generally decreased with an increase in the weight fraction of bis-diazirine while they did not affect the tensile modulus and yield stress substantially (see Table 1).

Discussion: This study showed that bis-diazirine can effectively crosslink UHMWPE but, as with other forms of crosslinking, there was a dose dependent decrease in the tensile properties. The bis-diazirine used in this study activates thermally at approximately, 110ºC, which is below the melting temperature of UHMWPE. A low activation temperature is not desirable since it would then segregate and crosslink the UHMWPE at the boundaries between powder particles to which they are coated, which is probably the reason for the significant decrease in tensile properties with increasing weight percent. Several approaches can be taken to minimize the effect of bis-diazirine crosslinking on the tensile properties of UHMWPE. The use of a bis-diazirine with a higher activation temperature, preferably at a temperature above the melting point of UHMWPE, will enable more uniform distribution of crosslinking by allowing them to diffuse into the powder and prevent segregation at powder boundaries. In addition, novel processing methods such as elevated temperature and pressure molding can be used to increase tensile properties. More comprehensive biocompatibility, wear, fatigue and other mechanical tests will be required prior to considering these crosslinkers for application in UHMWPE used in joint replacements.

References: (1) Muratoglu et al, J Orthop Res,2024, 42(2), 306 (2) de Zwart et al, Science, 2019, 366 ,6467 (3) Djordjevic et al, Macromol Rapid Comm, 2020, 41(21), e20035 (4) Abreu et al, J Mech Behav Biomed Mater, 2014, 32, 1.

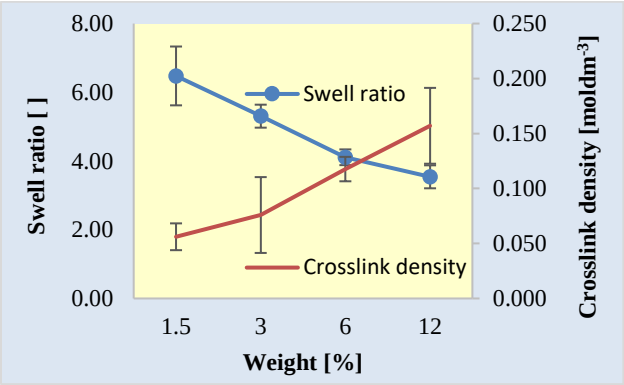

Figure 2 Swell ratio and crosslink density as a function of weight % of bis-diazirine crosslinker.

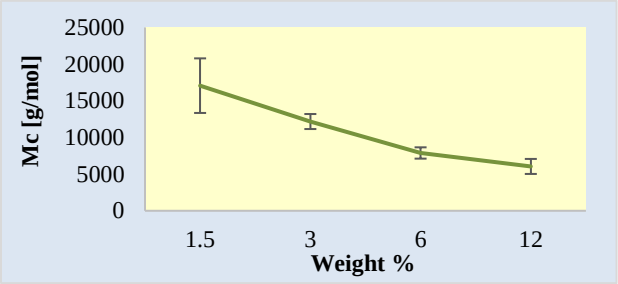

Figure 3. Molecular weight between crosslinks, Mc, as a function of weight % of bis-diazirine crosslinker.

Table 1. Crystallinity (X), modulus (Mod), yield stress (YS), ultimate tensile strength (UTS) and Maximum strain (MS) vs wt % of bis-diazirine crosslinker (mean ± stdev).

Wt %	X [%]	Mod [MPa]	YS [MPa]	UTS [MPa]	MS [ ]
0	57.0±2.5	163±35	22.3±0.6	48.4±5.3	11.1± 1.2
1.5	56.3±4.5	121±13	22.6±0.5	40.5±6.4	4.8±1.4
3	57.7±6.1	196±24	23.5±0.4	40.6±4.6	4.5±0.9
6	57.2±4.3	171±31	22.4±0.9	38.4±4.6	4.3±0.9
12	53.9±4.0	189±27	23.6±0.6	33.4±3.7	2.3±0.5

The synergistic role of beta-carotene in *in vivo* oxidation of contemporary UHMWPE tibial liner

Songyun Liu[1], Douglas W. Van Citters[2], Joshua J. Jacobs[1], Robin Pourzal[1]
[1]Department of Orthopedic Surgery, Rush University Medical Center, Chicago, Illinois, United States
[2]Thayer School of Engineering, Dartmouth College, Hanover, New Hampshire, United Stated
Songyun_Liu@rush.edu

Introduction: The use of highly cross-linked UHMWPE (HXLPE) has successfully combatted early total knee arthroplasty (TKA) failure due to particle induced osteolysis. Nonetheless, studies have shown that *in vivo* oxidation of HXLPE components is related to accelerated wear in TKA. Currently, there is no consensus on oxidation pathways. Studies have also shown that absorbed lipids play a role in the oxidation during accelerated aging. Various lipids are abundant within synovial fluid which varies in its complex composition between individuals. In this study, we are presenting a combined Fourier transform Infrared spectroscopic imaging (FTIRI) and Raman spectroscopic mapping approach to generated spatial maps of full-depth oxidation profiles and correlates the distribution of an identified absorbed organic constituent to better understand *in vivo* chemical alterations and its impact on wear and clinical outcomes.

Methods and Materials: 24 retrieved tibial liners, with a minimum postretrieval shelf time, from 6 designs and 4 manufactures were analysed. This balanced cohort covers conventional designs, various HXPESs, and 2nd generation antioxidant blended liners. The average time *in situ* was 110.4 months (28.4, 197.5). Liners were cut in the sagittal plane of the medial condyle to expose a vertical cross-section. Thin sections (~200 μm thick) were removed parallel to the exposed cross-section using a microtome for FTIRI/Raman analysis. For FTIRI, a large field of view was achieved via mosaic mode for a full-depth scans reaching from the articulating surface to the backside. All imaging data were collected using an Agilent Cary 670/620 system with 2 cm^{-1} spectral resolution (wavenumber range: 3750-900 cm^{-1}). Absorbed species were not extracted from the liners to capture their location within the material. The spatial distribution of the oxidation profile was calculated using the ester-insensitive ketone oxidation index (KOI), defined as the ketone peak intensity centring of around 1715 cm^{-1}, referenced against the peak at 1368 cm^{-1}. Data processing was done using CytoSpec software. Potential absorbed species and polymer crystallinity were assessed by Raman micro-spectroscopy (LabRAM Evolution, Horiba. NJ).

Results: 18 of 24 liners exhibited a strong subsurface oxidation band, a few hundred microns below the articulating surface. A zone of increased oxidation in the subsurface of the backside was also presented in some cases. The average maximum KOI was 0.64 ± 0.55, ranging from 0.05 to 2.3. For comparison with the ASTM oxidation index based on the carbonyl band (~1737 cm^{-1} *vs.* 1368 cm^{-1}), the corresponding chemical images of one liner are showcased in **Figure 1**. Our Raman data identified the presence of different concentration of β-carotene infiltrates within the surface of 23 tibial liners. β-carotene is an antioxidant, naturally occurring in human femoral bone, characterized by Raman shift at 1005 cm^{-1}, 1155 cm^{-1}, and 1514 cm^{-1}. The overall β-carotene presence is non-uniform both under the surface and backside surface of the liner. **Figure 2** showcased a comparison of β-carotene presence from a liner (>12 years *in situ)* and KOI_{max}=0.58. The subsurface oxidation band was evident in both areas at the center and edge/corner of the liner. Both showed a strong intensity of ether (*R1-C-O-C-R2*) group, a common linkage on lipids, characterized by peak integral of 1205-1145 cm^{-1}.

Discussion: This study highlights the heterogeneity of oxidation profiles of conventional and HXLPE liners across manufacturers, both first and second generation. Imaging revealed a complex oxidation progression scenario that likely results from a competitive interplay between the absorption of anti- and pro-oxidative species, which could ultimately affect the mechanical property of these liners. Interestingly, the two liners with only minimal oxidation—other than those doped with antioxidant—exhibited the strongest β-carotene signal at the surface. The cause of *in vivo* oxidation is multifactorial warranting further research. The chemical state of wear debris generated from chemically altered surfaces also needs to be considered with respect to its bio-reactivity. The presented study provided a universal approach in visualizing the oxidation profile in a full depth scale and demonstrated the importance of studying the polymer liner *in vivo* degradation for the sake of better long-term clinical outcome.

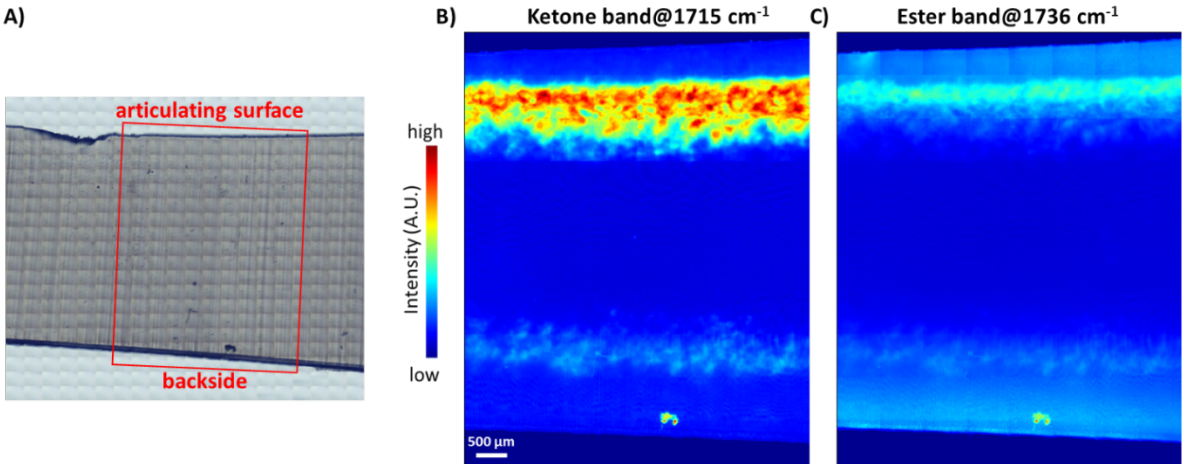

Figure 1 The FTIR spectroscopic characterization of a liner with time *in vivo* of 107.5 months and a maximum KOI of 0.88: A) The light microscopic image of the cross-section sample. FTIRI was performed on the red-boxed area. Chemical images of the B) Dartmouth oxidation index and C) ASTM method. A higher subsurface oxidation band was evident at both the articulating surface and the backside. By using the ketone band for imaging, the heterogenous nature of the subsurface oxidation can be appreciated, while the ester band-based image is more evenly distributed and narrower in width. It also has a transition zone from the surface and backside, whilst it is not the case for KOI band. It should be noted that the chemical map should not be compared directly with each other because the color scale is not global.

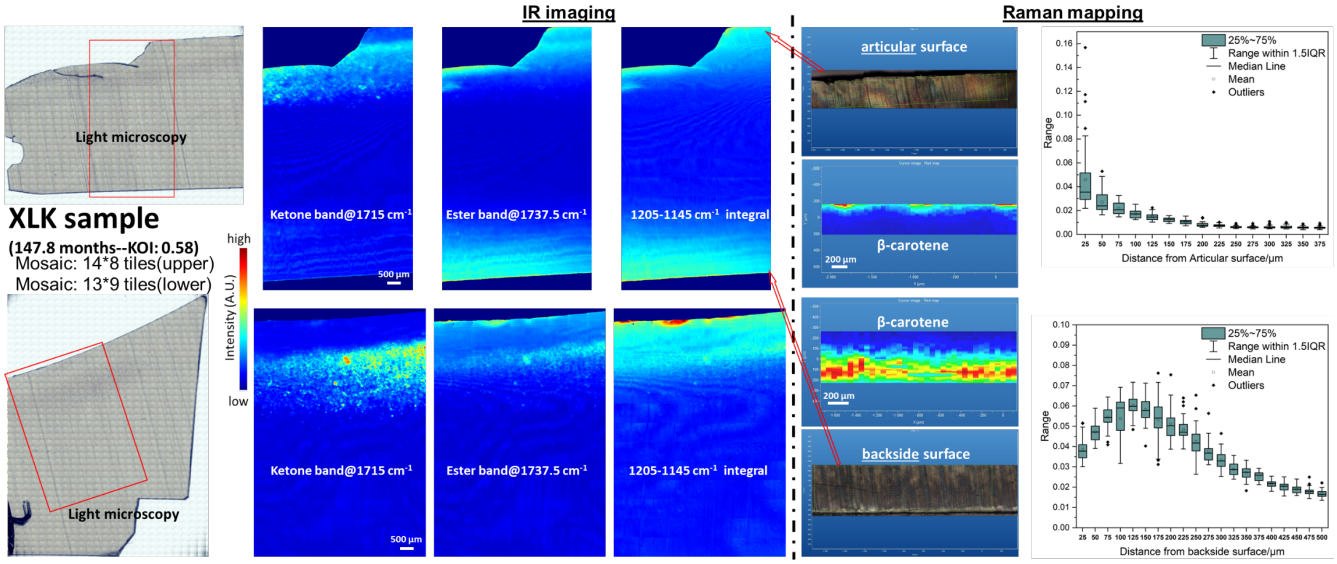

Figure 2 The FTIR spectroscopic characterization of a liner with time *in situ* of 147.8 months and a maximum KOI of 0.58: The light microscopic image of the cross-section sample showed some crack presence in the subsurface causing the detachment, and some discoloration in the subsurface, both at the center and corner. FTIRI was performed on the red-boxed areas from both the center and edge/corner of the sample. Chemical images of the ketone oxidation index and ASTM method were compared. A higher subsurface oxidation band was evident at the articulating surface. By using the ketone band for imaging, the heterogenous nature of the subsurface oxidation can be appreciated. The ester band-based image is more evenly distributed and located right below the surface. It also has a transition zone from the surface of the backside, whilst it is not the case for KOI band. The β-carotene characterization was done at both areas at surface and backside surface roughly located at the arrowed areas. The map has a step-size of 25 μm in Y-direction and 50 μm in X-direction. The heat maps were generated using β-carotene peak at 1155 cm^{-1} after the vector normalization in the peak centered at 1295 cm^{-1} raised from -CH_2- twisting mode of polyethylene. The overall trend with respect to the depth were plotted in box plot fashion. It should be noted that the chemical map should not be compared directly with each other because the color scale is not global.

4Degra®- A new surface eroding bioresorbable material for 3D printing medical devices.

Robinson, T, K. Wigdahl, E, A. Tortell-Milhano, A, A. Godbert, J, D. Naylor, A.
4D Biomaterials, Medicity, D6 Building, Thane Road, Nottingham, NG90 6BH, UK
info@4dbiomaterials.co.uk

Introduction: 3D printing implantable, bioresorbable medical devices in high resolution offers a range of advantages over current manufacturing methods. These include design freedoms afforded by additive manufacturing and the opportunity for patient specific treatments. To date, 3D printing such devices has not been possible due to the lack of materials available with the required properties of being photocurable, biocompatible and bioresorbable. Presented here is the development of a polycarbonate based fully bioresorbable, surface eroding photocurable material designed for 3D printing. The predictable degradation pathway provided by surface erosion enables the geometry of a device to have built in characteristics which can be designed to prolong or decrease the time until full resorption. Altering the formulation allows the mechanical proeprties of 4Degra® to be tuned across a wide range. Together with the design freedoms offered by additive manufacturing enables its use in a vast array of clinical applications including; soft tissue, drug delivery and orthopaedics. Previous work detailed the synthesis an preparation of resin components[(1)]. Work undertaken here demonstrates the material's utility, biocompatibility and functionality through the production of an interference screw and subsequent *in vivo* testing.

Methods and Materials: 4Degra® formulations were produced in-house from polycarbonate oligomers with additional reactive diluents containing both allyl and thiol groups. Photo initiators were added, which upon UV irradiation initiated a thiol-ene click reaction building a crosslinked network.
An interference screw designed for repair of the Anterior Cruciate Ligament (ACL) was used as test article for investigation. Screws were designed using Solidworks CAD software (Dasault Systems) to generate 3D shapes. These were converted into printable files using Netfabb (Autodesk).
3D printing was performed using UV Digital Light Processing (DLP) on a RapidShape (Heimsheim, Germany) D20+ printer. Parts were post cured using a RapidShape UV post cure unit.
Sterility was achieved by terminal sterilization using electron beam irradiation at 25 kGys (STERIS, Tullamore, Ireland).
Interference screws were evaluated following implantation in an ovine model. Screws were inserted line-to-line in distal femur and proximal tibial sites. Timepoints were at 4 week, 12 week and 26 weeks, with µCT and histology with H&E staining at each.

Discussion: It has been shown that the formulation of liquid resin can be tuned to give different mechanical properties to the post processed printed parts. The accessible Young's Modulus range is from 5 MPa to 2500 MPa dependent upon the resin composition. This can be used to enable the properties to be tuned across a range of regenerative medical device applications from soft tissue to orthopedic. During this work a range of 3D printers were tested demonstrating the versatility of the material on a range of platforms. 3D printing of interference screws was undertaken successfully using a high modulus formulation of 4Degra® best suited to this application, with final properties being obtained after post curing (**Figure 1**). Test articles for *in vivo* use were sterilized by electron beam irradiation. No adverse impact of the sterilization process on the material was observed.

Figure 1: a) CAD rendered image of a screw design, b) Build plate immediately after 3D printing step, c) Fully cured 4Degra® interference screw.

Following implantation in the ovine model no adverse implant site reactions were noted. Tissue was observed growing tight up to the surface of implanted material, and indeed also up the cannulation of the screw (**Figure 2**). Good bone to implant contact was seen across the entire surface with no evidence of osteolysis. The test article's originally smooth edge was found to be jagged in shape, strongly indicative that degradation is beginning to occur at the surface. It was also found the interior of the screw remains intact, indicating that the screw is likely still capable of performing mechanical fixation at 26 weeks.

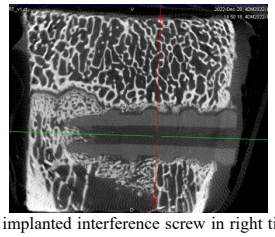

Figure 2: µCT image of implanted interference screw in right tibia of ovine model at 4-week timepoint.

Minimal inflammatory responses were observed in histology imaging at 4, 12 and 26 weeks (**Figure 3**), with all three timepoints showing cells and bone formation at the surface if the implant. New bone formation on the surface of the material is evidence of the osteostimulatory properties of the 4Degra® material.

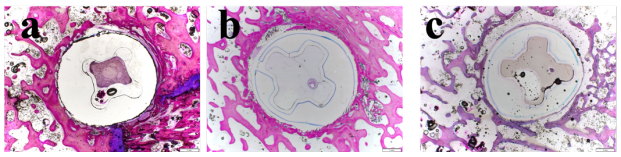

Figure 3: Histological images taken at a) 4 weeks, b) 12 weeks, c) 26 weeks. Evidence of surface erosion shown by change in geometry of the tool cannulation.

Conclusion: Herein is presented a novel photocurable polycarbonate based material, with a demonstrated biocompatibility. 3D printed interference screws were produced and sterilized by terminal sterilization. When implanted into bone in an ovine model, the screws were found to be biocompatible and osteostimulatory. Degradation was observed through surface changes. As a 3D printable, surface eroding material it has the potential to unlock the next generation of resorbable medical devices. Ongoing large animal studies aim to further validate the material for use in human medical devices.

References:

1) Weems, A.C., Arno, M.C., Yu, W. *et al.* 4D polycarbonates via stereolithography as scaffolds for soft tissue repair. *Nat Commun* **12**, 3771 (2021).

Investigating the Feasibility and Performance of Hybrid Overmolded UHMWPE 3D-Printed PEEK Structural Composites for Orthopedic Implant Applications: A Pilot Study

James A. Smith [1,*], Cemile Basgul [1], Bita S Mohammadlou [2], Mark Allen [3] and Steven M. Kurtz [1]

[1] Implant Research Core, Drexel University School of Biomedical Engineering, Science, and Health Systems, Philadelphia, PA, U.S.A
[2] Department of Mechanical Engineering, Drexel University, Philadelphia, PA, U.S.A.
[3] Orthoplastics, Bacup, U.K.

* Correspondence: jas997@drexel.com

Ultra-high-molecular-weight polyethylene (UHMWPE) components for orthopedic implants have historically been integrated into metal backings by direct-compression molding (DCM). However, metal backings are costly, stiffer than cortical bone, and may be associated with medical imaging distortion and metal release. Hybrid-manufactured DCM UHMWPE overmolded additively manufactured polyetheretherketone (PEEK) structural components could offer an alternative solution, but are yet to be explored. In this study, five different porous topologies (grid, triangular, honeycomb, octahedral, and gyroid) and three surface feature sizes (low, medium, and high) were implemented into the top surface of digital cylindrical specimens prior to being 3D printed in PEEK and then overmolded with UHMWPE. Separation forces were recorded as 1.97–3.86 kN, therefore matching and bettering the historical industry values (2–3 kN) recorded for DCM UHMWPE metal components. Infill topology affected failure mechanism (Type 1 or 2) and obtained separation forces, with shapes having greater sidewall numbers (honeycomb-60%) and interconnectivity (gyroid-30%) through their builds, tolerating higher transmitted forces. Surface feature size also had an impact on applied load, whereby those with low infill-%s generally recorded lower levels of performance vs. medium and high infill strategies. These preliminary findings suggest that hybrid-manufactured structural composites could replace metal backings and produce orthopedic implants with high-performing polymer–polymer interfaces.

Development of Press-Fit Polyether-Ether-Ketone (PEEK) Hip Prosthesis for Reducing Stress-Shielding and Bone Resorption

Seyed Ataollah Naghavi [1], Changning Sun[1], Dongmei Yu [1], Chaozong Liu[1*]
[1] University College London, London, UK
Chaozong.Liu@ucl.ac.uk

Introduction: Total hip arthroplasty (THA) is referred to replacement of the diseased hip joint with an artificial hip prosthesis to restore the patient's mobility and improve the quality of life. One of the major post-surgery complications is aseptic loosening. Noticeably, stress shielding is the main cause of aseptic loosening in long-term service, which is commonly revealed in clinical cases. It is caused by insufficient load transfer between bone and the implants. In post-surgery conditions, only part of the load is transferred to the bone while most of the load is carried by the implant. This altered stress profile is expected to cause mineral bone lost in the interface of bone and implants, and thus, cause loosening due to the lack of contact in the interface.

Previous research tackled stress shielding either by geometric design or applications of novel materials. Apart from geometric design, several works tried to reduce the stress shielding effect by utilising biomimetic materials. Polyether-ether-ketone (PEEK) is a high-performance thermoplastic from the polyaryl-ether-ketone (PAEK) polymer family. PEEK biomaterials can exhibit an elastic modulus ranging between 3 and 4 GPa, the modulus can be tailored to closely match femur (1- 10 GPa) and cortical bone (18 GPa) through various processes. This unique feature makes PEEK a promising low-stiffness biomaterial for orthopaedic implants to reduce stress shielding.

This study reported a surface porous hip implant using PEEK biomaterial for the entire femoral stem. The feasibility of PEEK implants in reducing stress shielding is validated through experimental tests and FE simulation by comparison with a generic Ti6Al4V implant manufactured with the same geometry mounted in the Sawbone.

Methods and Materials: A customized porous hip stem was designed by based on the geometry of a large, left, fourth-generation artificial composite femoral bone (Model 3406, Sawbones). The hip stem was made to fit as firmly as possible against the cortical bone that surrounds it. The orthogonal rectilinear structure, with unit cell sizes of 0.8 mm, pore sizes of 0.4 mm, and strut sizes of 0.4 mm, was used to construct both the anterior and posterior lattice structures, ensuring the porous part of the scaffolds to have a nominal porosity of 50%. A PEEK hip stem was produced utilizing a fused deposition modelling (FDM) technique, as shown in Fig 1.

The resultant hip stem was fixed in Sawbone model with strain gauges attached to the surfaces to measure the strain distribution. A dynamic load was applied to the hip stem to evaluate the fatigue properties of the hip stem and the strain distribution within the cortical bone. A FE model was created to evaluate the reduction of stress shielding and bone resorption compared to a solid titanium hip stem.

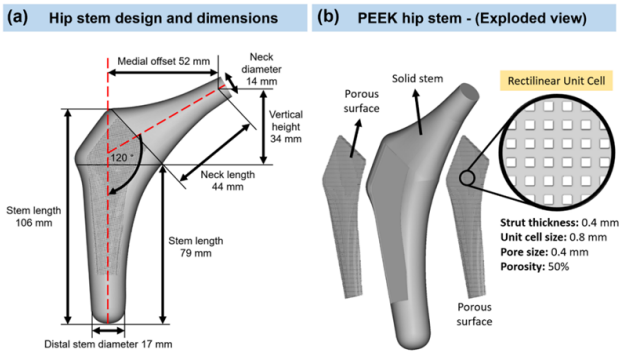

Figure 1. (a) Design and dimensions of the hip stem. (b) Isometric exploded view of the PEEK hip stem

Result: The von Mises stress ratio calculation suggests the change of stress in each point of interest after implantation with Ti6Al4V and PEEK stems. From the experimental data, we can see that for most sites, the femur with the PEEK stem has a higher stress ratio compared to the femur with the Ti6Al4V stem, which indicates that the femur with the PEEK stem would undergo more load compared to its counterpart in loading condition, and thus, mitigates the stress shielding effect. A relatively low stiffness at 0.276 kN/mm is obtained for the PEEK stem, which is below the range of stiffness for the intact femur. It is remarkable that the bone loss reduction with PEEK stem almost reaches 100% for Gruen zone 5 and 6, which suggests that the bone loss in the medial side of the femur with Ti6Al4V stem can be effectively minimised by using PEEK stem. The combined FE and experimental results demonstrated a 72% reduction in bone loss secondary to stress shielding for the PEEK stem.

Discussion: In static analysis, the PEEK implant is proved to be safe at a load equivalent to walking status, but likely to fail with a larger load at the neck in more intensive activities, e.g., jog-ging. In dynamic analysis, 0.05% volume of the PEEK implant, which is distributed in the near-surface region of both medial and lateral sides of the neck, is expected to fatigue in the required lifespan. For consideration of future work, tailoring in mechanical properties in terms of yield strength and endurance limit of the PEEK material is required for such load-bearing application. Possible strengthen method refers to heat-treatment, and incorporation of reinforcing fibres.

Carbon-fibre-reinforced PEEK as biomaterial in a rotating hinge knee design – biotribological testing, retrieval findings & clinical results

T.M. Grupp[1,2], R.A. Schierjott[1,2], A. Pfaff[1], G. Tozzi[3], J. Schwiesau[1], K. Vertesich[4], A. Giurea[4]

[1] Aesculap AG Research & Development, Tuttlingen, Germany
[2] Ludwig Maximilians University Munich, Department of Orthopaedic and Trauma Surgery, Musculoskeletal University Center Munich (MUM), Campus Grosshadern, Munich, Germany
[3] School of Engineering, University of Portsmouth, United Kingdom
[4] AKH Department of Orthopaedics, Medical College University of Vienna, Austria
thomas.grupp@aesculap.de

Introduction: Total knee arthroplasty with a rotating hinge knee with carbon-fibre-reinforced (CFR)-PEEK as an alternative bushing material with enhanced creep, wear and fatigue behaviour has been clinically introduced in 2009 [1-4]. The objective of our study was to compare results from in vitro biotribological characterisation to ex vivo findings on retrievals and to give an overview about 7 to 11 years follow-up clinical results.

Methods and Materials: A modified in vitro wear simulation based on ISO 14243-1 was performed for 5 million cycles on rotating hinge knee (RHK) designs (EnduRo®) out of cobalt-chromium and ZrN-multilayer ceramic coating. The rotational & flexion axles-bushings and the flanges are made of CFR-PEEK with 30% polyacrylonitrile fibre content.
Analysis of 12 retrieved EnduRo® RHK systems in cobalt-chromium and ZrN-multilayer in regard to loosening torques, microscopic surface analysis, distinction between different wear modes and classification with a modified HOOD-score has been performed. The use of RHK prostheses for severe primary as well as revision arthroplasty is widely established and the aim was to investigate long-term results of a new RHK prosthesis with CFR-PEEK components. Fifty-six consecutive patients, who received the EnduRo® modular RHK prosthesis were included in this prospective study: 21 patients (37.5%) received the prosthesis as a primary total knee arthroplasty (TKA) and 35 patients (62.5%) underwent revision total knee arthroplasties (rTKA). Clinical and radiographic examinations were performed pre-operatively as well as post-operatively after 3 and 12 months and annually thereafter. Minimal follow up was 7 and mean follow up 9.3 years. Clinical examination included Knee Society Score (KSS), Western Ontario and McMaster Osteoarthritis Index (WOMAC), Oxford Knee Score (OKS), and range of motion (ROM). Competing risk analysis was assessed for survival with respect to indication and failure mode.

Results: For the RHK design with the polyethylene gliding surface and bushings and flanges made out of CFR-PEEK, a cumulative volumetric wear was measured to be 12.9±3.95 mm^3 in articulation to cobalt-chromium and 1.3±0.21 mm^3 to ZrN-multilayer coating - a significant 9.9-fold decrease (p=0.0072).
For the CFR-PEEK flexion bushing and flanges the volumetric wear rates were 2.3±0.48 mm^3/million cycles (cobalt-chromium) and 0.21±0.02 mm^3/million cycles (ZrN-multilayer) (p=0.0016). The 5 million cycles of in vitro wear testing reflect a mean in vivo service life of 2.9 years, which is in accordance to the time in vivo of 12-60 months of the retrieved RHK components [5]. The main wear modes were comparable between retrievals and in vitro specimens, whereby the size of affected area on the retrieved components showed a higher variation.
Within the clinical cohort study KSS, WOMAC, OKS, and ROM significantly improved from the pre-operative to the follow up investigations ($p < 0.0001$). There was no difference in clinical outcome between the primary and the revision group. The overall cumulative incidence for revision for any reason was 23.6% and the cumulative incidence for complications associated with failure of the prothesis was 5.6% at 7 years respectively. Complications occurred more frequently in the revision group ($p = 0.002$). There was no failure mode related to the CFR-PEEK components.

Discussion: For the EnduRo® RHK design the findings on retrieved implants demonstrate the high suitability of CFR-PEEK as a biomaterial for highly loaded bearings, such as RHK bushings and flanges in articulation to cobalt-chromium and to a ZrN-multilayer coating.
The evaluated RHK prosthesis provided reliable and durable results with a follow-up of 7 to 11 years. Prosthesis survival was successful considering the complexity of cases. The use of this RHK system in primary patients showed high survival rates. Long-term functional and clinical results proved to be satisfying in both revision and primary cases. No adverse events were associated with the new bearing material CFR-PEEK.

References:

[1] Giurea et al. Biomed Research Int. 2014
[2] Grupp et al. Acta Biomaterialia 2013
[3] Boehler et al. 2017 Biomed Research Int. 2017
[4] EPRD Annual Report 2021
[5] Schierjott et al. Biomed Research Int. 2016

Population-based FE study on the primary fixation of a cementless PEEK femoral component

Corine Post[1], Thom Bitter[1], Adam Briscoe[2], Nico Verdonschot[1,3], Dennis Janssen[1]
[1]Radboud University Medical Center, Orthopaedic Research Laboratory, Nijmegen, The Netherlands, [2]Invibio Ltd., Thornton Cleveleys, Lancashire, United Kingdom. [3]University of Twente, Laboratory for Biomechanical Engineering, Enschede, The Netherlands.
Corine.Post@radboudumc.nl

Introduction: While cobalt-chrome (CoCr) alloy currently is the default material for femoral total knee arthroplasty (TKA) components, polyetheretherketone (PEEK-OPTIMA^{TM}) is of interest as alternative implant material in patients with metal hypersensitivity. As an additional benefit, PEEK has a stiffness that is similar to the stiffness of human bone, which may contribute to reducing peri-prosthetic stress-shielding. However, this difference in stiffness may also influence the primary fixation. In cementless fixation, adequate primary fixation is required to ensure for the long-term fixation through bone ingrowth. Primary fixation can be evaluated by studying micromotions between the femur and implant.
Previous finite element (FE) studies typically focused on parametric variations in a single model, while the outcome may depend on patient factors such as age, gender and BMI, which requires a population-based approach. The research question of this study is twofold: 1) What is the effect of implant material on femoral micromotions? 2) Are femoral micromotions sensitive to patient characteristics (gender, age and BMI)?

Methods and Materials: A CT database was created including 35 patients (70 femora) with known information on gender, age, weight and height. The CT data was used to create FE models of femoral TKA reconstructions, in which the femoral component was assigned with the material properties of either PEEK (3.7 GPa) or CoCr (210 GPa). Bone was assigned with elastic-plastic material properties to account for bone deformations that exceeded the yield limit during implant insertion or during the loading phase. Implant-specific tibiofemoral and patellofemoral contact forces and centers of pressure of gait and squat activities were derived from a musculoskeletal model. The contact forces were scaled based on the patient's bodyweight and applied during four loading cycles to allow for (numerical) settling of the implant. As an outcome measure, the resulting micromotions were analyzed visually via the distributions at the interface of the femoral component and quantitively using violin plots depicting the 95th percentile of the maximum micromotions for all models. The 95th percentile was taken to exclude the nodes with potential (numerical) outliers. A multivariate linear regression analysis was used to determine significant factors affecting implant-bone interface micromotions.

Results: The largest resulting micromotions were located at the anterior flange of both PEEK and CoCr models and additionally on the lateral distal side of the PEEK models (Figure 1). The PEEK models generated larger peak micromotions than the CoCr models (63 vs. 48 μm on average). Micromotions of both the PEEK and CoCr femoral models significantly increased with BMI (Figure 2). Neither gender nor age of the patients had a significant effect on the micromotions of the PEEK and CoCr models.

Discussion: The results of this FE study indicate that the peak femoral micromotions were larger for PEEK implants compared to CoCr implants. However, in the larger part of the femoral component micromotions were below the threshold for bone ingrowth (40 μm) [1], for both implant materials. Further research is required to further elucidate the relation between implant stiffness and primary fixation, and whether there is an optimal stiffness that provides a good balance between primary fixation and long term effects such as stress shielding. This study furthermore demonstrated that the micromotions increased with BMI. Future work will focus on a more in-depth multivariate analysis to investigate underlying mechanisms and interactions. Moreover, an outlier analysis will be performed to investigate the potential high-risk factors of patients.

References: [1] Engh, et al. Quantification of implant micromotion, strain shielding, and bone resorption with porous-coated anatomic medullary locking femoral prostheses. Clin. Orthop. Relat. Res., 285, 13 – 29 (1992).

Acknowledgements: PEEK-OPTIMA^{TM} is a trademark of Invibio Ltd. Implant geometry was supplied by Maxx Orthopaedics Inc.

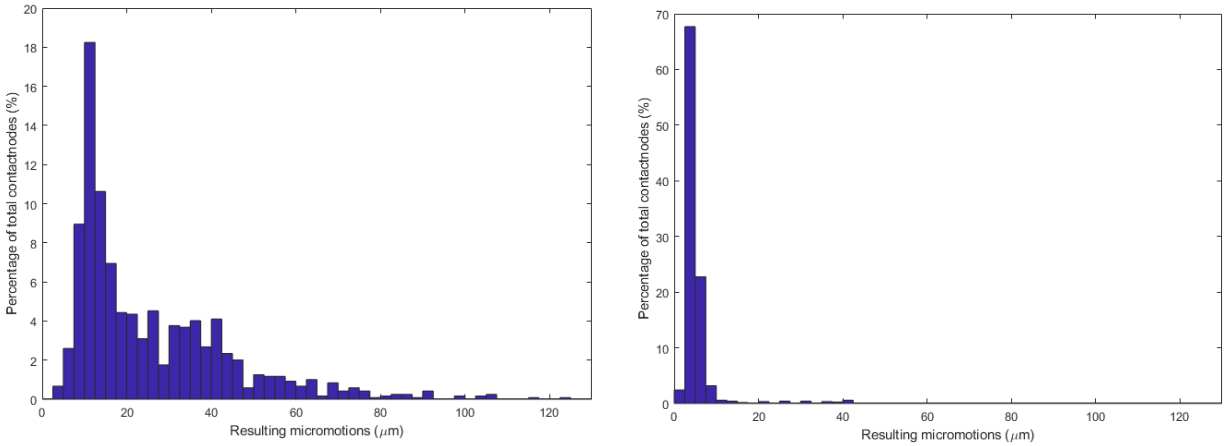

PEEK **CoCr**

Figure 1. Resulting micromotion distribution (μm) at right femoral component interface after 4th squat cycle.

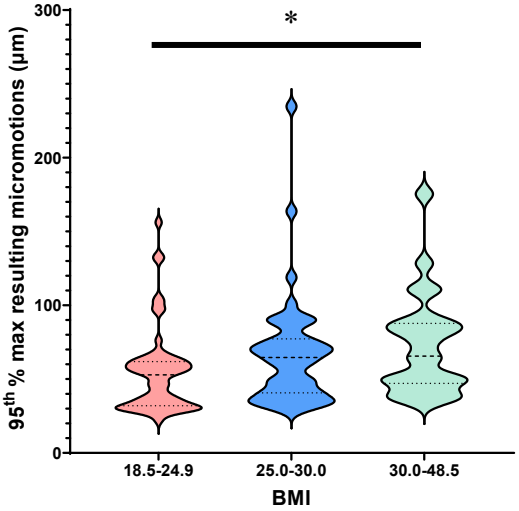

Figure 2. Violin plots of all PEEK models per BMI classification.

Population-based FE study on the primary fixation of a cementless PEEK tibial component

Corine Post[1], Thom Bitter[1], Adam Briscoe[2], Nico Verdonschot[1,3], Dennis Janssen[1]
[1]Radboud University Medical Center, Orthopaedic Research Laboratory, Nijmegen, The Netherlands, [2]Invibio Ltd., Thornton Cleveleys, Lancashire, United Kingdom. [3]University of Twente, Laboratory for Biomechanical Engineering, Enschede, The Netherlands.
Corine.Post@radboudumc.nl

Introduction: While titanium alloy currently is the default material for tibial total knee arthroplasty (TKA) components, polyetheretherketone (PEEK-OPTIMA™) is of interest as alternative implant material in patients with metal hypersensitivity. As an additional benefit, PEEK has a stiffness that is similar to the stiffness of human bone, which may contribute to reducing peri-prosthetic stress-shielding. However, this difference in stiffness may also influence the primary fixation. In cementless fixation, adequate primary fixation is required to ensure for the long-term fixation through bone ingrowth. Primary fixation can be evaluated by studying micromotions between the tibia and tibial tray.
Previous finite element (FE) studies typically focused on parametric variations in a single tibial model, while the outcome may depend on patient factors such as age, gender and BMI, which requires a population-based approach. The research question of this study is twofold: 1) What is the effect of implant material on tibial micromotions? 2) Are tibial micromotions sensitive to patient characteristics (gender, age and BMI)?

Methods and Materials: A CT database consisting of 74 healthy knees including the patient information on gender, age and BMI was created. An automated workflow was used to build FE models of tibial reconstructions, including a tibial tray and a polyethylene insert. The tibial tray was assigned with a Young's modulus of either PEEK (3.7 GPa) or titanium (109 GPa). Bone was assigned with elastic-plastic material properties to account for bone deformations that exceeded the yield limit during implant insertion or during the loading cycles. The implant-specific tibiofemoral contact forces and centers of pressure of a gait and squat movement were derived from a musculoskeletal model. The contact forces were scaled based on the patient's bodyweight and applied during four loading cycles to allow the implant to (numerically) settle. As an outcome measure, the resulting micromotions were analyzed visually via the distributions at the interface of the femoral component and quantitively using violin plots depicting the 95th percentile of the maximum micromotions for all models. The 95th percentile was taken to exclude the nodes with potential (numerical) outliers. A multiple regression analysis was used to determine significant factors affecting implant-bone interface micromotions.

Results: The largest resulting micromotions were typically located at the anterior and posterior lateral regions of the tibial tray, with similar distributions for the PEEK and titanium tibial trays (Figure 1). The PEEK models generated larger peak resulting micromotions than the titanium models (68 vs. 39 μm on average). BMI significantly influenced micromotions for both the PEEK and titanium models, with higher micromotions with increasing BMI (Figure 2). Gender and age did not have a statistically significant effect on the micromotions.

Discussion: The results of this FE study indicate that the peak tibial micromotions were larger for PEEK implants compared to titanium trays. However, in the larger part of the tray micromotions were below the threshold for bone ingrowth (40 μm) [1] for both implant materials. Further research is required to further elucidate the relation between implant stiffness and primary fixation, and whether there is an optimal stiffness that provides a good balance between primary fixation and long term effects such as stress shielding. This study furthermore demonstrated that the micromotions increased with BMI. Future work will focus on a more in-depth multivariate analysis to investigate underlying mechanisms and interactions. Moreover, an outlier analysis will be performed to investigate the potential high-risk factors of patients.

References: [1] Engh, et al. Quantification of implant micromotion, strain shielding, and bone resorption with porous-coated anatomic medullary locking femoral prostheses. Clin. Orthop. Relat. Res., 285, 13 – 29 (1992).

Acknowledgements: PEEK-OPTIMA™ is a trademark of Invibio Ltd. Implant geometry was supplied by Maxx Orthopaedics Inc.

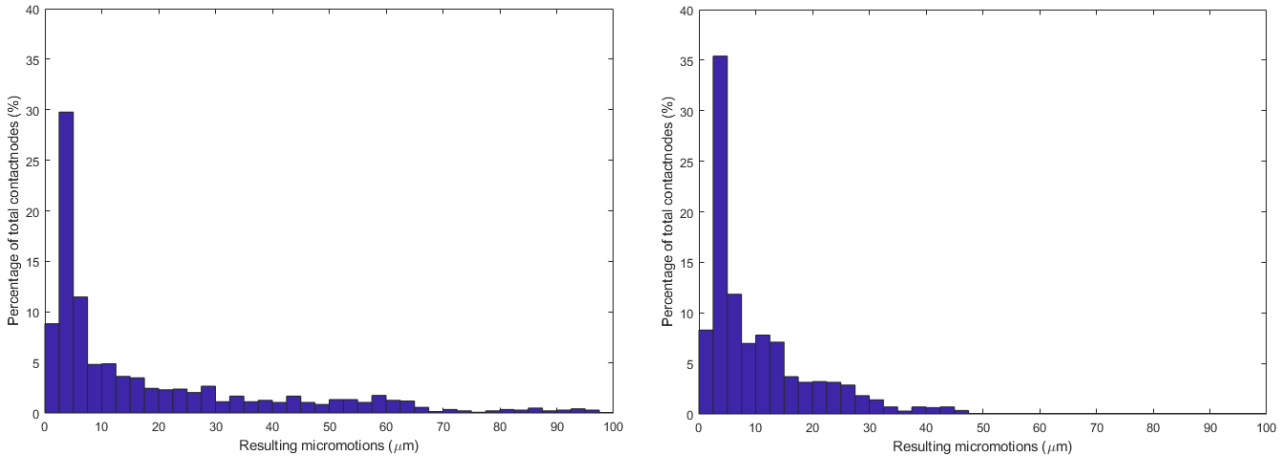

PEEK **Titanium**

Figure 1. Resulting micromotion distribution (μm) at tibial tray interface after 4th squat cycle.

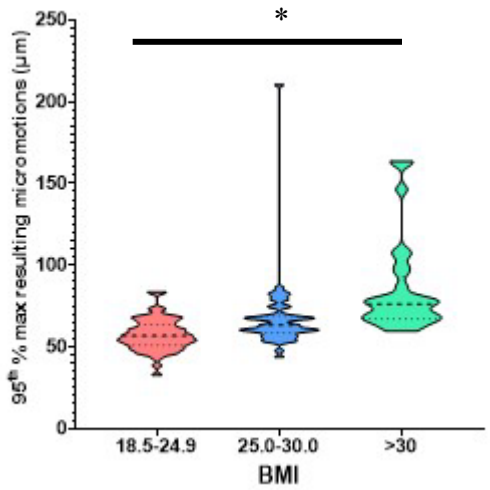

Figure 2. Violin plots of all PEEK models per BMI classification.

PEEK spinal Implants: Design and Manufacturing Considerations

R. Davies[1], Y. Chen[1], O. Ghita[1]
[1] Faculty of Environment, Science and Economy, University of Exeter, North Park Road, Exeter, EX4 4QF, UK
o.ghita@exeter.ac.uk

Introduction: Spinal cages, also known as intervertebral cages or interbody cages, were developed in the late 1980s and early 1990s. The first cage consisted of a stainless-steel cylinder packed with horse autograft, known as the "Bagby basket" [1]. To adapt the Bagby basket for human use, Kuslich *et al*. [2] changed the cage design, by including the use of a threaded hollow titanium cylinder with thick perforated walls. In this way, the cage was screwed onto the adjacent vertebrae, promoting stabilization and fusion [2]. The first FDA-approved interbody fusion device, the Bagby and Kuslich (BAK) cage, was introduced in 1992.

Figure 1. First FDA approved cage design - Bagby and Kuslich (BAK) cage [3].

Since then, various types of spinal cages have been developed and used in spinal surgeries to help treat conditions such as degenerative disc disease and spinal instability.

The adoption of titanium and its alloys became widespread in the spinal cage industry, primarily due to their biocompatibility and low density, making them the preferred materials. However, the use of titanium also introduced certain challenges. The mismatch in the elastic modulus of titanium (110 GPa) and that of vertebrae trabecular bone (2.1 GPa) and cortical bone (2.4 GPa) resulted in reduced stress shielding which led to local inflammation [2]. Also, the high radiodensity of titanium led to imaging artefacts hindering accurate assessment of fusion. This led to use of PEEK and carbon fibre reinforced PEEK as an alternative material to titanium.

A wide range of designs had been developed depending on the intended surgical application and patient needs in either titanium, PEEK or a combination of PEEK and titanium.

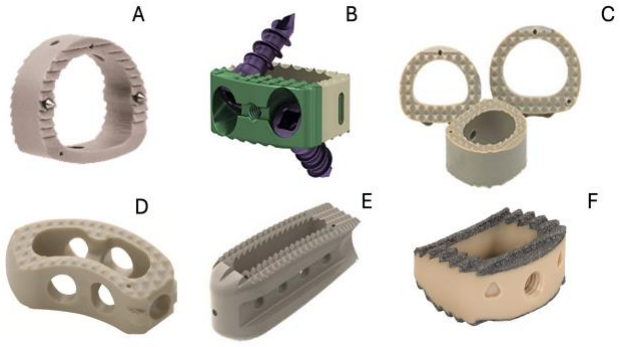

Figure 2. PEEK machined spinal cages (A) Stryker Solis – PEEK spacer - Anterior cervical PEEK spacer with a large graft chamber [4], B) Stryker AVS Anchor-C Cervical Standalone Cage System - A hollow PEEK cage with a titanium screw locking mechanism [4], C) Stryker IBD PEEK - Anterior Cervical Spacer System - Anterior cervical spacer [4], D) Stryker AVS TL PEEK Spacer - Curved posterior lumbar PEEK spacer with a large bone graft chamber [4], E) Stryker Aleutian Anatomically-Narrow Lordotic Interbody System - The Interbody System has a full range of anatomically-designed PEEK interbodies for multiple spinal applications [4], F) Medtronic - Pure Titanium Coating (PTC) of interbody fusion devices [5].

An ASTM design for titanium cages was also developed including a hollow interior to allow incorporation of autograft or allograft material and serrated exterior surfaces [6]. The serrations, the tooth-like features incorporated within cage, are prevalent in a significant number of designs. They offer several advantages: i) improved stability within the intervertebral space, preventing migration or displacement of the cage post implantation, ii) improved fusion by creating a rough surface and promoting bone ingrowth; iii) reduced migration; iv) anti-backout mechanism and v) distribution of the load accommodating the uneven implant - host interface and reducing stress concentrations. However, smooth-surfaced implants without teeth or serrations are sometimes available. These smooth cages rely on other mechanisms, such as the insertion technique, graft material, and supplemental fixation (such as screws or plates), to achieve stability and prevent migration.

The uptake of additive manufacturing (AM) by the medical industry, led to an increased interest in using various AM processes for customized and more complex spinal cage designs. However, majority of the developments in AM are in titanium possibly due to the ability of the powder bed melting technology to deliver fine meshes and fine surface features.

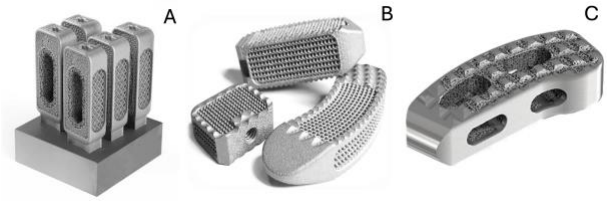

Figure 3. 3D printed Titanium spinal cages: (A) 3D Systems spinal cage combined with high precision GF Machining for optimized workflow [7], (B) Nexxt Matrixx Vertebral Body Replacement 3D printed implants [8], (C) Tritanium TL Curved Posterior Lumbar Cage - A hollow implant with both solid and porous structures [4].

When it comes to PEEK cage manufacturing, two AM technologies are obvious contestants: powder bed fusion and material extrusion. However, the manufacture of 3D printed PEEK spinal cages has been less explored than titanium, to date only one manufacturer (Bond3D)

commercially provides PEEK spinal cages using material extrusion.

The use of PEEK AM comes with a set of constrains which in certain instances can challenge the economics of printing vs standard machining methods. These constrains are: i) build orientation combined with the need of support structure and mechanical performance as well as accuracy of the external features. These aspects will be assessed here focusing on differences in the two AM technologies, the powder bed and the material extrusion.

Methods and Materials:

Powder Bed Fusion: (PBF)

The material used for the manufacture of PEEK components is VICTREX® PEEK 450PF. The material presents a glass transition temperature of 143 ˚C and a melting temperature of 343 ˚C. The powder was thermally treated for 24 hours before use in the EOSINT P800. The PEEK powder is not a laser sintering grade. Three build orientations were chosen to manufacture the cages: i) vertical, ii) oblique; iii) horizontal. The parts were manufactured in a reduced chamber configuration mode with laser power of 15 W, a laser speed for 2550 mm s^{-1} and scan spacing of 0.2 mm.

Material Extrusion: (MEX):

The filament material used for MEX was VICTREX AM™ 450 FIL provided by VICTREX plc. Due to the limitations of the MEX process, two modified designs were created, one in a vertical orientation and one in a flat orientation. Ten spinal cages were printed using a Minifactory 3D Printer equipped with a 0.4 mm nozzle in both flat and vertical orientations. For prints in flat orientation, the infill density was set as 50% and the infill angle of 0/90°, whilst for prints in vertical orientation, the infill density was set as 100% and the infill angle of ±45°. The layer thickness was 0.25 mm. No cooling was applied during printing. The printing speed was 30 mm s^{-1} except for the first layer, which was 10 mm s^{-1}. During printing, the nozzle temperature, the build platform temperature, and the chamber temperature were set at 450 °C, 200 °C, and 180 °C, respectively.

Dimensional measurements:

The geometrical accuracy of the prints was measured using using an LK Metrology Altera-S 7.5.5 Coordinate Measuring Machine (CMM) fitted with a Renishaw PH10M Plus motorised head and a Nikon LC15Dx non-contact laser scanning probe. The parts were placed on a common fixture for repeatable measuring, and a programme was created to automate the measuring sequence within the LK Camio software.

The collection of five directional scans per part were joined using the Fuse function within Camio, and the final meshes cleaned to remove any noise created by reflections of the laser. The final meshes (measured) were loaded into Nikon Focus inspection software alongside the original CAD model (nominal) and the measured was aligned with the nominal using the Global Best Fit function. After alignment, the global comparison function was used to compare the deviation of each point of the measured to the nominal, and a report created for each part.

Results:

The aim of the study is to print the spinal cage design used in the ASTM interlaboratory studies for spinal cage testing [6]. This cage will be referred to as the ASTM spinal cage. The powder bed process allowed the use of the original ASTM design without any design modifications, printing being possible in any orientation as shown in Figure 4. No internal or external support structures were needed, this resulting in increased cost-effectiveness at post-processing stages.

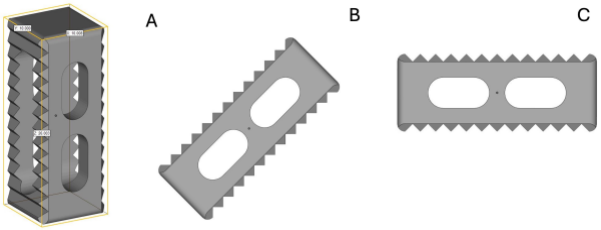

Figure 4. Spinal cage design and print orientation in powder bed fusion: A) Vertical (V); B) Oblique (O); C) Flat (F).

In comparison with the powder bed fusion, the material extrusion process required significant consideration in design, support structures and modifications.

For example, a previous study [9] used support structures within the holes of both sides of the cages to ensure that the horizontal cage struts did not collapse during printing. The design orientation allowed preservation of the serrations present on two of the cage sides, although their accuracy was not discussed. Also, to improve adhesion to the print bed and avoid warpage, a contour was added to the base of the cage. A replica of the cage with support structure and support base is shown in Figure 5A. Figure 5B presents an alternative build orientation, however, the quality of serrated teeth is sacrificed.

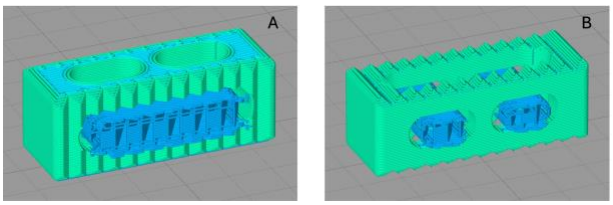

Figure 5. Cage design orientations (green) and support structures (blue): A) as shown in a previous study [9]; B) alternative orientation.

Removal of internal support structures is not straightforward; it requires additional machining, which starts to question the entire premise of AM. In certain instances, the support structures may be left inside to avoid the need for extra post-processing steps and additional manufacturing costs. The use of soluble support material compatible with high temperature PEEK MEX is now

possible with recent material advances, yet dual material printing at this scale is challenging and further increases printing time due to excessive purging requirements.
To avoid the use of support structures, printing in a different orientation with a slight modification of the original design was also proposed as shown in Figure 6. The serrated sides were hollowed and the plain sides which originally had two oval cavities, were converted to a solid wall. Although the design is easier to print, the proposed orientation could result in a weaker mechanical performance.

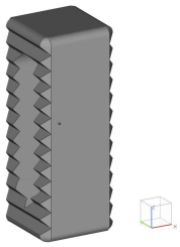

Figure 6. Vertical orientation with a slightly modified cage design (MEX cage 1).
An adapted design tailored for printing flat was also proposed, maintaining the serrated surfaces but replacing the internal cavity with a mesh structure as presented in Figure 7.

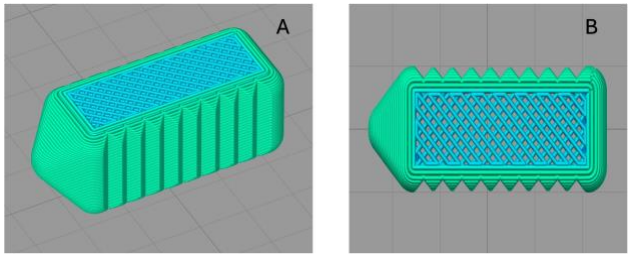

Figure 7. A fully adapted PEEK AM cage (MEX cage 2): A) side view; B) top view.
One of the primary hurdles in the design and printing of the original ASTM cage was preserving the quality of the serrations, a factor influenced by the chosen orientation, the nozzle diameter and the printing speed. A smaller nozzle diameter enables the printing of finer, more precise features, albeit at the expense of increased manufacturing time. For instance, reducing the layer thickness from the current print layer thickness of 0.25mm to 0.1mm, the printing time for MEX cage 1 changes from 12min to 30min. If in addition to the layer thickness, the speed time is also decreased from current setting of 30mm/s to 10mm/s, the time changes significantly from 30min to 67min.
Related to this, an interesting observation is the limited availability of alternative nozzle diameters for commercial systems, most 3D printers operate with 0.4mm nozzle and require modifications to accommodate smaller diameters.

In addition to the above discussed design issues, layer to layer bonding linked to materials crystallization kinetics, layer time and part nesting across the bed has to be considered as well, in a real manufacturing scenario.

The average minimum and maximum deviation from the original CAD design for each set of cages is presented in Table 1 and Figure 8.

Deviation	PBF cage			MEX Cage 1	MEX Cage 2
	V	O	F		
Max	0.6	0.6	0.8	1.2	0.9
Min	-0.5	-0.5	-0.5	-1.2	-1.8

Table 1 Average min and max deviation values for each set of 10 cages printed using the powder bed fusion process in different orientations (V- vertical, O – oblique, F – flat) and using material extrusion process for two designs (cage 1 and cage 2).

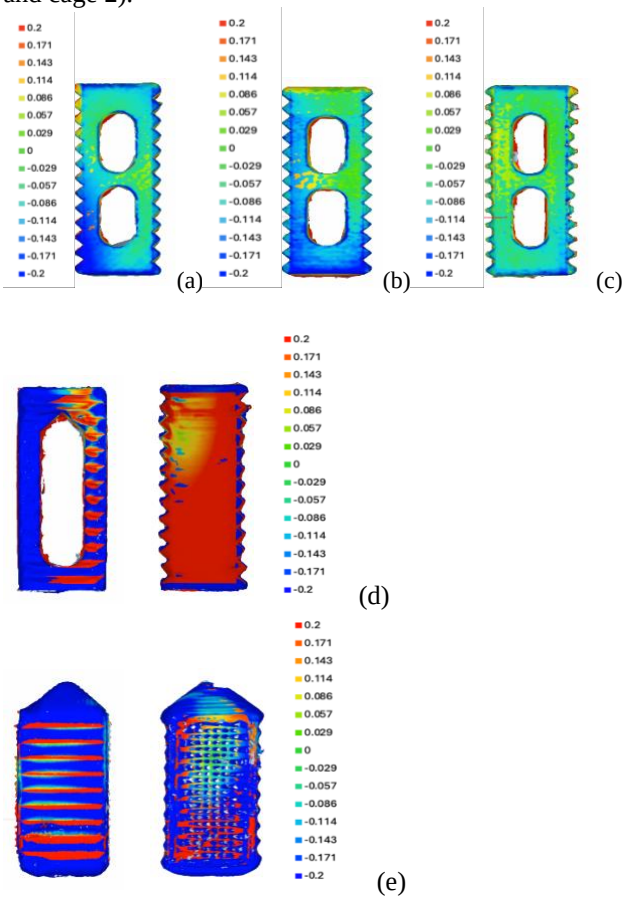

Figure 8. Distribution of the deviation across all printed cages: (a) PBF vertical, (b) PBF oblique, (c) PBF flat, (d) MEX cage 1, (e) MEX cage 2.

Discussion:
The design analysis for spinal cages, carried out using powder bed fusion and material extrusion highlighted limitations and significant design issues when using material extrusion technology especially on the serrated

surfaces. An alternative is to remove entirely the anchoring features provided by the teeth such as the cage design recently released by Bond3D.

Figure 9. Bond3D spinal cage [10].

Although capital equipment costs are significantly lower for MEX than PBF, making it more attractive, the additional post machining costs required to bring the part within specs can make the material extrusion process equally costly. From a technology cost perspective, in addition to the design consideration, other aspects such of number of parts per build should also be taken into account. A simulation of a full build in each technology showed that PBF could print 27379 spinal cages in an EOS P800 system where MEX could build 325 spinal cages (MEX cage 1) in a Minifactory system (see Figure 10).

From a technical point of view, mechanical performance, crystallinity homogeneity in parts, fracture behaviour combined with the design and dimensional stability during and after the build are key areas which need considering as well.

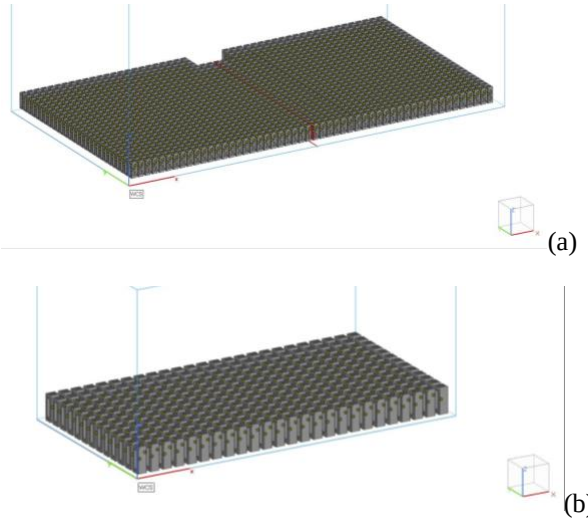

(a)

(b)

Figure 10. Parts nesting and full build simulation for (a) PBF process (EOS P800 -1441 parts in a single layer, 27379 parts in total) and (b) MEX process (Minifactory).

References:

[1] DeBowes RM, Grant BD, Bagby GW, Gallina AM, Sande RD, Ratzlaff MH. Cervical vertebral interbody fusion in the horse: a comparative study of bovine xenografts and autografts supported by stainless steel baskets. Am J Vet Res. 1984 Jan;45(1):191-9.

[2] Kuslich SD, Ulstrom CL, Griffith SL, Ahern JW, Dowdle JD. The Bagby and Kuslich method of lumbar interbody fusion. History, techniques, and 2-year followup results of a United States prospective, multicenter trial. Spine (Phila Pa 1976), 1998, 23: 1267–1278.

[3] Williams AL, Gornet MF, Burkus JK. CT evaluation of lumbar interbody fusion: current concepts. AJNR Am J Neuroradiol. 2005 Sep;26(8):2057-66.

[4]https://www.stryker.com/us/en/portfolios/orthopaedics/spine--ortho-/interbody-devices.html

[5] https://www.opnews.com/2015/02/peek/9398

[6] ASTM 2077- 2014

[7] https://www.tctmagazine.com/additive-manufacturing-3d-printing-news/3d-systems-gf-machining-3d-printed-spinal-cages/

[8] https://3dprintingindustry.com/news/nexxt-spine-to-use-mts-testing-systems-for-3d-printed-spinal-implants-150134/

[9] Basgul C, Yu T, MacDonald DW, Siskey R, Marcolongo M, Kurtz SM. Structure-Property Relationships for 3D printed PEEK Intervertebral Lumbar Cages Produced using Fused Filament Fabrication. J Mater Res. 2018 Jul 27;33(14):2040-2051. doi: 10.1557/jmr.2018.178.

[10] https://www.bond3d.com/parts/spinal-cage/

Evaluating All-Polymer PEEK Knee Prostheses: A Comparative Imaging Study

Bohyn. Cedric[1], Zaribaf. Fedra[2]-Briscoe. Adam[2], Janssen. Dennis[3]
[1]AZ Monica Hospital, Antwerp, Belgium
[2] Invibio Biomaterials Solution, Thornton-Cleveleys, UK
[3] Radboud University Medical Center, Nijmegen, The Netherlands.
cedric_bohyn@hotmail.com

Introduction: Radiographic examinations and subsequent follow-up of joint replacements often encounter challenges due to the limitations caused by metal artifacts. These artifacts can overshadow nearby areas, leading to potential oversight of complications like cement fracture or implant loosening, particularly during the early postoperative period. The PEEK-OPTIMA™ (Polyether Ether Ketone) Knee represents an innovative approach in joint replacement, employing a novel all-polymer prosthesis that is yet to be evaluated by radiologists specifically for use within the knee joint. Although the radiological profile of PEEK material has been documented in spinal applications, its performance within the intra-articular environment remains to be assessed. The intrinsic radiolucency of the PEEK knee replacement system and its absence of metallic components are likely to lead to a timely and more precise diagnosis of postoperative complications through radiologic follow-up (Fig. 1). The objective of this study is to ascertain the radiologic properties of the PEEK knee when examined under standard imaging protocols.

Methods and Materials: In this investigation, four cadaveric lower-limb specimens were surgically fitted with the all-polymer PEEK knee prosthesis (Maxx Orthopaedics, Pennsylvania, USA). These implanted prostheses were then subject to diagnostic imaging, utilising standard protocols across radiography (X-ray), computed tomography (CT), and magnetic resonance imaging (MRI).

To simulate postoperative complications, the PEEK implants underwent intentional alteration to replicate a series of common clinical issues: loosening of the implant, fractures within the cement, migration of the implant, and fractures of the prosthesis itself.

Post-intervention, each specimen was sealed and infused with saline via a catheter. During the filling process, the knee was flexed several times and compressed manually to minimise entrapped air in the joint. Imaging (X-Rays, CT, and MRI scans) was performed after the induction of each complication, using the same imaging protocol previously applied.

A specialist musculoskeletal radiologist evaluated all imaging outputs, including X-Rays, CT scans, and MRIs. The goal was to evaluate the imaging profiles of a normal PEEK knee against those displaying simulated complications, thereby assessing the diagnostic efficacy of each imaging modality.

Results: Using the three principal diagnostic imaging techniques, X-Ray, CT, and MRI, this investigation offered a distinct visual representation of the PEEK knee prosthesis and its position. These modalities (especially CT) facilitated comprehensive evaluations of the prosthesis and its interaction with the cement interface, typically obscured in metallic counterparts, the bone-cement interface of the prostheses, which is generally only partially visible in metallic implants, was clearly visible.

Imaging clearly pinpointed cement fractures via CT and X-ray. Nevertheless, the detection of subtle cement fractures was difficult and required comparison with initial studies. Conversely, the cement fracture was undetectable on MRI, due to the hypo-intense nature of the cement material, similar to the adjacent bone.

MRI was demonstrated to be more effective than X-rays or CT scans at identifying fractures and implant migration. Given MRI's superior demonstration of fluid in the widened bone-cement interface.

In this cadaveric study, the incidental observation of implant fractures and migration on radiographs was detectable due to the presence of gas. It should be noted that such gas, an artefact of the cadaveric model, is not present in a clinical setting and, as such these complications may be more difficult to spot.

Discussion: The investigation concludes that the all-polymer PEEK knee prosthesis markedly improves the visibility of post-operative complications in radiographic follow-ups, which are often obscured or undetectable in conventional metal-based knee replacements.

Acknowledgements- Authors would like to thank Richard van Swam for his assistance with the experimental work, and Maxx Orthopaedics and Invibio for providing materials used in this study.

Additional statement: All study work was conducted on cadaveric samples, as detailed in the methods section. Any additional illustrations in the presentation were used solely for exemplary purposes.

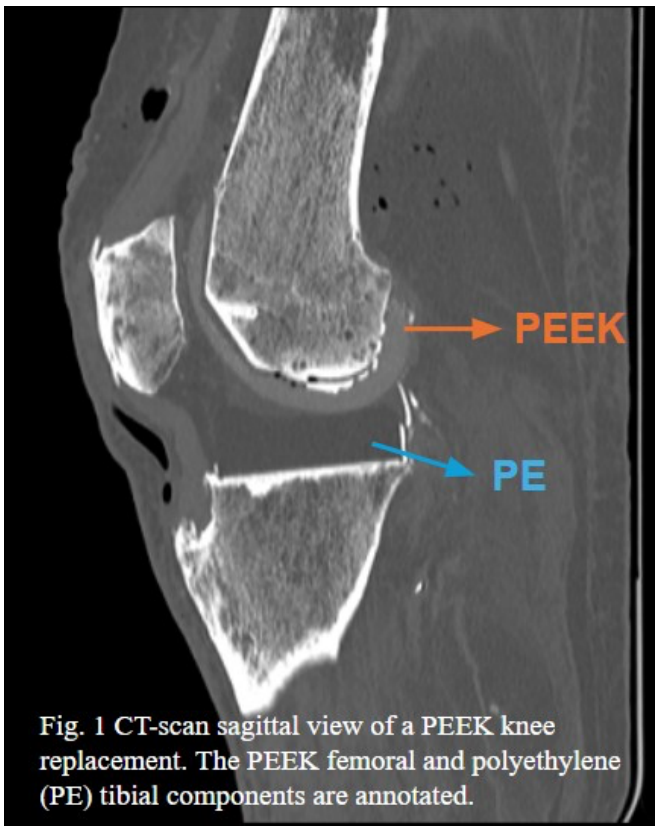

Fig. 1 CT-scan sagittal view of a PEEK knee replacement. The PEEK femoral and polyethylene (PE) tibial components are annotated.

Update on Implant Grade PEKK: Biocompatibility and Case Studies for 3D Printing

Gaillard, B
SEQENS-Innovative Drug Delivery Solutions department, Ecully, FR
boris.gaillard@seqens.com

Introduction: Semi-crystalline PolyArylEtherKetone polymers (PAEKs) are widely used in orthopedic, trauma, spine and dental implants as biomaterials. They are suitable for all conventional thermoplastic processing technologies, such as injection or compression moulding, extrusion, powder coating, but also for additive manufacturing, especially in SLS and FDM/FFF processes. This versatility not only means customized implantable devices, but also a more direct access for the patients and a significant time reduction. In medical implants manufacturing, PEEK is the widely recognized and used biomaterial (Invibio, Evonik, Solvay), benefiting from a solid history and an advanced ecosystem. Although PEKK is more recent (Oxford Performances Materials, Seqens), it is actually the first polymer used in implants manufactured by SLS technology, OsteoFab® from OPM[1] and well adapted to FFF technologies. In addition to the excellent properties (thermomechanical, chemical resistance and tribological) of others PAEKs, PEKK has a better temperature resistance (higher Tg), a better tensile strength and in particular case a better compressive strength. As PEKK is a copolymer comprising both Terephthaloyl and Isophthaloyl units, modularity allows fine tuning of the crystallization rate to be suitable for different technologies, with corresponding IMPE**KK**® Series (IMplantable PEKK), produced by Seqens. The addition of Isophthaloyl groups lowers the melting temperature without impacting the glass transition, so going from the semi-crystalline IMPE**KK 1**, which behaves in a very similar way to PEEK, to the pseudo-amorphous IMPE**KK 3D**, which can be printed both in its amorphous form (very limited crystallization and high ductility) or in its crystalline form.
[1] see OsteoFab https://www.oxfordpm.com/biomedical-3dp

	Norm	IMPE**KK 1**	IMPE**KK 3D**
Apparence	/	Beige pellet	Golden Yellow pellet/filament
Polymer type	/	Semi-crystalline	Pseudo-amorphous
% Tere/Iso	/	80/20	60/40
Melting point	ISO11357	350 – 360 °C	285 – 315 °C
Glass transition	ISO11357	160-170 °C	155-165 °C

Figure 1: Series of IMPE**KK** materials, produced by Seqens.

Methods, Materials: Biocompatibility tests were conducted with granule forms of both **1** and **3D** IMPE**KK** Series, as intended to be used into medical device manufacturing. A GLP-accredited laboratory followed ISO 10993-1:2018_Evaluation and testing within a risk management process, as a guidance for this raw material. Preparation of samples and references was performed according to ISO 10993-12:2021. *In-vitro* Cytotoxicity was investigated following ISO10993_5, *in-vivo* biological reactivity following USP88 and chemical characterization following ISO10993-18, by multiple analytical methods and on several extraction media (polar, semi-polar and non-polar systems). Additional analyses were performed to evaluate the heavy metal content with IMPE**KK 1** and **3D** granules (**1-**G and **3D-**G) and on IMPE**KK 3D** filament (**3D-**F). This study followed ASTM2820 recommendations considering the ongoing analytical method changes (from old colorimetric to expected ICP method). In parallel, mechanical properties were evaluated with specimen obtained by different manufacturing procedures with corresponding IMPE**KK** Series materials.

Results: Literature review revealed existing preliminary data regarding PEKK material evaluated in *in-vitro*, *in-vivo* and *in-human* studies. Indeed, PEKK is part of an FDA-established list (ISO10993-1_Attachment G) for intact skin contacting materials, considered as having a very low biocompatibility risk. For long-term implants, PEKK benefits from a track record by OPM's FDA-Master File (including extensive ISO10993 testing). Dedicated investigations performed with Seqens' IMPE**KK** materials confirmed existing data, without any biological reactivity or toxic effects. Chemical characterization didn't reveal any extractable volatile, semi volatile, non-volatile and inorganic substance, equal or above the corresponding reporting limits (respectively established at 0.98ppm, 0.05ppm, 0.25ppm and according to investigated 42 inorganic elements). Among a list of 11 selected heavy metals (from ASTM2026-23 list for PEEK), measurements were respectively under the element-reporting limit (established at 1ppm).

	Norm	IMPE**KK 1**	IMPE**KK 3D**
Cytotoxicity	ISO10993-5	Not cytotoxic	
	USP<87>	Grade 0	
Systemic Toxicity	USP<88>	Pass	
Irritation	USP<88>	Pass	
Implantation	USP<88>	Pass	
Chemical characterization	ISO10993-18 Headspace-MS	No extractable volatile above 0.98µg/g of material	
	ISO10993-18 GC-MS	No extractable semi-volatile above 0.05µg/g of material	
	ISO10993-18 HPLC-MS	No extractable non-volatile above 0.25µg/g of material	
	ISO10993-18 ICP-MS	No extractable metallic ions above 39 elements reporting limits	
Heavy metals	ASTM2820 ICP-MS	<1 ppm each	<1 ppm each

Figure 2: Biocompatibility tests performed with IMPE**KK** materials.

Discussion: In addition to biocompatibility results, mechanical data existing for PEKK and recently generated application data with IMPE**KK** are supporting the use of Seqens' materials for implantable use. Among several preliminary case studies, IMPE**KK** materials have demonstrated unique properties.

Optimization of Fused Filament Fabrication (FFF) Process Parameters for PEEK and PEKK Biomaterials for Orthopedic Medical Device Application

Abigail Tetteh, Daniel Porter, Matthew Di Prima, Steven Kurtz

Introduction:

The disparity in mechanical properties between materials used in joint arthroplasty and bone has been linked to stress shielding and bone loss. As a result, aseptic loosening continues to be one of the frequently reported causes of revisions. High-performance thermoplastics like Poly-ether-ether-ketone (PEEK) and Poly-ether-ketone-ketone (PEKK) exhibiting mechanical properties comparable to surrounding bone can be used to fabricate 3D printed orthopedic load bearing devices. Therefore, this study aims to optimize fused filament fabrication (FFF) process parameters for PEEK and PEKK.

Methods and Materials:

A Taguchi L9-orthogonal array (4 factors and 3 levels) with 4 replicates was employed as the experimental design. PEEK (VESTAKEEP® i4 3DF-T, Evonik) and PEKK (IMPEKK® 3D-F, Sequens) were evaluated to determine optimal process parameters (print temperature, chamber temperature, layer height, print speed) that maximize compressive mechanical properties (compressive strength, modulus, and yield strength). Cylindrical samples were printed in the z-direction on a high-temperature 3d printer (EXT 220 MED, 3D Systems). Compression testing was performed following ASTM D695 standard on an Instron testing machine (Instron 68FM-100) at 1.3mm/min crosshead speed. Minitab 21.4.3 software was utilized to calculate signal-to-noise ratios for optimal parameters and to conduct ANOVA for assessing statistical significance at $p<0.05$.

Results:

Compressive strength ranged from 136-173 MPa, compressive modulus from 2.6-3.5 GPa, and 0.2% yield strength from 85-94 MPa for PEEK samples. Compressive strength ranged from 108-120 MPa, compressive modulus from 2.8-3.4 GPa, and 0.2% yield strength from 80-93 MPa for PEKK samples. The four process parameters (Figure 1) investigated had varying effects on the two materials and their compressive properties. For PEEK, print temperature impacted compressive strength ($p = 0.013$) and yield strength ($p = 0.048$), layer height impacted compressive modulus ($p = 0.000$), print speed impacted yield strength ($p = 0.048$) and compressive modulus ($p = 0.000$), and chamber temperature showed no significant effect on any of the output metrics. For PEKK on the other hand, all process parameters significantly affected yield strength ($p < 0.05$), and chamber temperature impacted compressive strength ($p = 0.003$) and compressive modulus ($p = 0.047$). The main effects plots for signal-to-noise ratios highlighting optimal process parameter levels for PEEK and PEKK are shown in Figure 2 and 3 respectively. Due to the intended application of both materials for orthopedic devices, compressive yield strength was chosen as the failure criterion.

Conclusions:

Print temperature, print speed and layer height influenced the compressive properties of PEEK while all process parameters influenced the properties of PEKK. The optimal process parameters for yield strength (the chosen material strength metric) were; the highest tested print temperature (410˚C PEEK, 410˚C PEKK); the highest tested chamber temperature (210˚C PEEK, 150˚C PEKK), and the lowest tested layer height (0.1mm PEEK, 0.1mm PEKK). However, unlike the preceding parameters where the optimal levels were similar for both materials, the optimal print speed differed for both materials. Specifically, the optimal print speed was 2000mm/min, the highest tested for PEEK, and 1500mm/min, the middle speed tested for PEKK. The current results can be used to guide the design and printing process for FFF medical devices.

Process Parameter - Factor	**PEEK** **Process Parameter - Level**	**PEKK** **Process Parameter – Level**
Print Temperature (˚C)	390, 400, 410	390, 400, 410
Chamber Temperature (˚C)	170, 190, 210	110, 130, 150
Layer Height (mm)	0.1, 0.2, 0.3	0.1, 0.2, 0.3
Print Speed (mm/min)	1000, 1500, 2000	1000, 1500, 2000

Figure 1: FFF process parameters (factors and corresponding levels) for PEEK and PEKK used in the study.

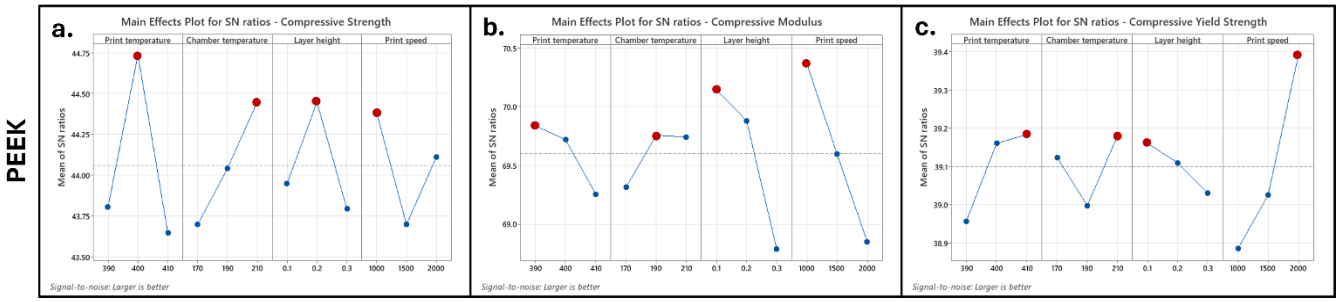

Figure 2: Main effects plot for signal-to-noise ratios for **a.** compressive strength, **b.** compressive modulus, and **c.** yield strength of PEEK (9 runs with 4 replicates, n = 36 samples tested).

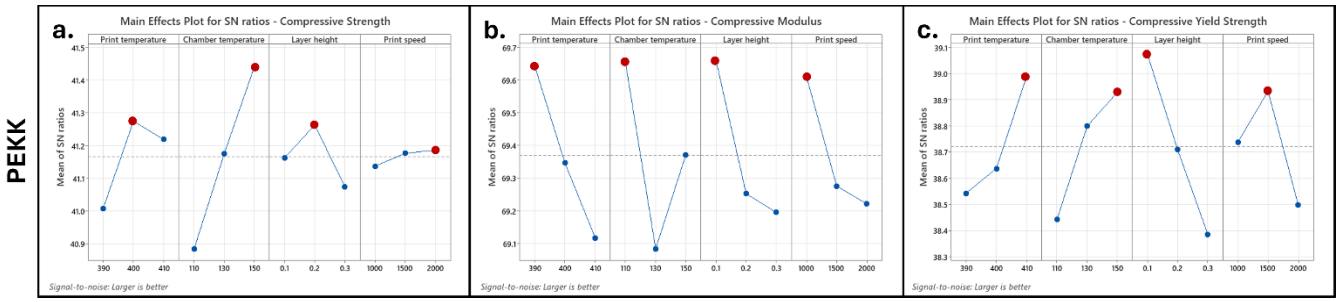

Figure 3: Main effects plot for signal-to-noise ratios for **a.** compressive strength, **b.** compressive modulus, and **c.** yield strength of PEKK (9 runs with 4 replicates, n = 36 samples tested).

Fabrication of 3D printed surface- porous PAEK structures

Yaan Liu[1], Yu Chen[1], Richard Davies[1], Oana Ghita[1]
[1] Faculty of Environment, Science and Economy, University of Exeter, Exeter, EX4 4QF, UK
y.liu@exeter.ac.uk

Introduction:

Polyetheretherketone (PEEK) is a biocompatible polymer that has been widely studied and successfully applied in orthopaedics, neurosurgery, trauma, joint replacement, and craniomaxillofacial reconstruction [1-8]. However, in spite of its use, PEEK is sometimes associated with a poor osseointegration, leading to the formation of a layer of fibrous connective tissue between the implant and the host tissue [6, 9]. Porous features showed to offer an improved osteogenic response, thereby using a porous PEEK surface is an effective way to improve osseointegration [10]. A porous structure is recognised to have a range of benefits from an increased surface area and more space for osteoblasts to develop, to vascularisation, biological response with interconnected pores and ingrowth of blood vessels and biomechanical compatibility – matching the modulus of elasticity of PEEK with the one of the bones.

Achieving a surface-porous PEEK structure is not trivial, over the years various methods had been tried using traditional processing methods such as extrusion [6] and compression [11], combined with various porogen materials. Alternatively, a sulfonation treatment on PEEK was employed as another way to obtain porous PEEK structures on the surface [12, 13]. Evans et al. [6] introduced surface porous PEEK using a melt extrusion technique. By leaching the sodium chloride crystal, a porous layer thickness of 399.6 ± 63.3 μm, a mean pore size of 279.9 ± 31.6 μm and porosity of 67.3 ± 3.1% have been achieved. A more recent study [11] combined the sulfonation process with 'cold pressing' treatment using sodium chloride as a porogenic agent to form surface porous structures. The sulfonation treatment formed small pores of 0.5 to 10 μm, which aid in cell adhesion, and the porogen material introduced the pores ranging from 100-200 μm, facilitating cell/tissue ingrowth.

In this study, powder bed fusion (PBF) was used to create a porous PEEK structure at first and then additional structure was printed through the material extrusion (MEX) process to obtain a surface-porous PEEK structure. Using an optimised mix of PEEK powder and sodium chloride crystals as porogen, the PBF process was applied for fabrication of porous PEEK structures. Using material extrusion (MEX) process, solid PEEK was next printed onto the porous PEEK structure to simulate the manufacture of a solid PEEK implant with a porous surface.

Methods and Materials:

PEEK 450PF powder (Victrex Plc, UK) was used for the powder bed fusion (PBF) process of porous PEEK component. A heat treatment on the powder was carried out at 250°C for 24 h in an air-ventilated oven to improve the powder flow. 70 wt% of sieved sodium chloride (sieved below 125 μm) was mixed with the treated PEEK powder to achieve high porosity. A Microtrac Sync size & shape analyser (Microtrac, UK) was used to measure powder size distribution (PSD).

The PBF process was carried out using EOSINT P800 (EOS, Germany) with a laser power of 12W, an energy density (ED) of 0.024 J, a laser speed of 2550 mm/s, a layer thickness of 0.12 mm and a hatching distance of 0.2 mm.

Fabricated porous PEEK structures were characterised by micro-CT (VERSA XRM-500; Zeiss, Germany) and a high resolution of 2.03 μm per voxel was achieved. Compression test on the porous PEEK structures were preformed by using the Lloyd LR3000k Universal Materials Testing Machine (Lloyd Instruments, UK) according to the ISO 604 standard with a test speed of 1 mm/min. Three potin bending test was performed by using a mechanical testing machine (Lloyd Instrument EZ20, UK) according to the ISO 178 standard. The span size was 64 mm and the test speed was 5 mm/min. Three repeats for each test were conducted and the average data was obtained.

Following the PBF process, the printed parts were transferred into water and stirred in water for 24 hours to remove the salt. After the leaching process, the porous PEEK parts were dried in an oven at 100°C for 24 hours. Further details can be found in a previous study [14].

Two PAEK grades, PEEK 151 and AM 200 both supplied by Victrex Plc, were tested for fabrication of solid PAEK structures onto the porous PEEK surface using an INTAMSYS FUNMAT PRO 40 printer. The printing parameters are listed in Table 1.

Table 1. Printing parameters used on the INTAMSYS FUNAMT POR 40 printer.

Parameters	Values
Printing speed (mm/s)	10 for initial layer and 20 for the rest
Infill density (%)	25, 50 or 100
Nozzle diameter (mm)	0.4
Printing raster angle (°)	± 45, 0 and 90
Layer thickness	0.4 for initial layer and 0.2 for the rest
Nozzle temperature (°C)	435
Chamber temperature (°C)	85
Build platform temperature (°C)	110

The interface of porous/solid PEEK structures was characterised by SKYSCAN 1273 (Bruker, UK) and digital microscope VHX-7000 (KEYENCE LTD, UK). Scanning electron microscopy (SEM) images were obtained by a Tescan VEGA3 SEM (Tescan, UK).

Results and Discussion

PEEK 450PF powder was heat-treated at 250°C for 24 hours to improve the powder flow for the PBF process [15]. The sieved sodium chloride (<125 µm) was mixed with the treated PEEK powder in a 70/30% (NaCl/PEEK ratio). The sodium chloride particles had in a wider PSD with the smallest size being 5.5 µm (Figure 1). The mixed powder had a suitable flow and spreadability for use in the EOS P800.

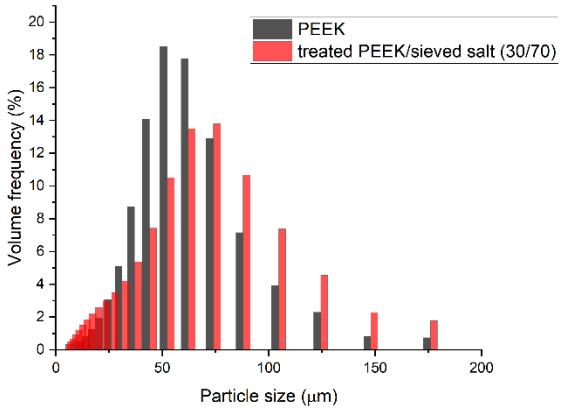

Figure 1. PSD of PEEK powder and the mixture of treated PEEK/sieved NaCl (30/70).

Figure 2 (a) shows the printed porous structures with dimensions from 10×1×10 to 10×10×10 mm. Figure 1(b) shows the micro-CT of PEEK framework with calculated porosity of 83.5%. Figure 2 (c-e) shows the SEM images of fracture surfaces (three-point bending fractured samples) of porous PEEK. Some large connect pores around a few hundred microns were found in low magnification images. In higher magnification images, round pores of approximately 50 µm and smaller pores of a few microns were randomly generated after the salt leaching process.

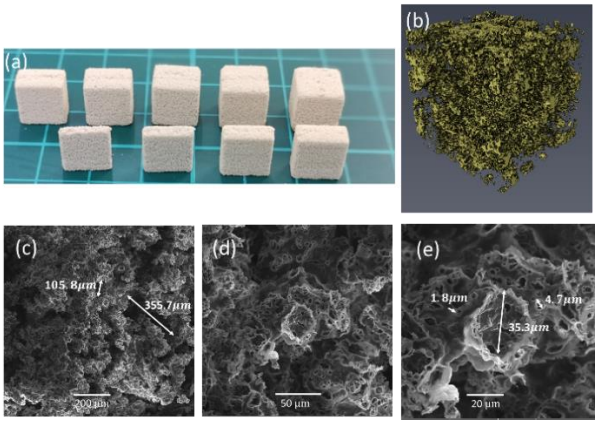

Figure 2. (a) Photo of printed porous PEEK samples with dimensions from 10×1×10 to 10×10×10 mm; (b) micro-CT scan of porous PEEK structure (500 × 500 × 500 µm cubic structures were extracted) and (c)-(e) SEM images of fractured surface of the porous PEEK with different magnifications.

The mechanical properties of the printed porous PEEK structures are summarised in Table 2. Compared with the literature data [16], the porous PEEK structures obtained here are promising in compressive properties. Samples fabricated by compression moulding using sodium chloride as a porogen with comparative porosities to the current study (84% tapped salt and 79% dry mixing salt) achieved compressive yield strength values of 1.22 MPa (tapped salt) and 1.85 MPa (dry mixing salt) and yield strain of ~5% [16].

Table 2. Mechanical properties of printed porous PEEK materials.

Compression Yield Stress (MPa)	**Compression Yield Strain (%)**
4.1 ± 0.2	64 ± 2.1
Flexural Stress (MPa)	**Flexural Modulus (MPa)**
0.217 ± 0.004	6.085 ± 0.757

Two different grades of PEEK were used for printing onto the porous printed PEEK structure: PEEK 151 and AM200. The two PEEK grades differ in crystallisation kinetics and viscosity, both properties being important in the MEX process. PEEK 151 has a lower viscosity (130 Pa·s) [17] compared to AM200 (245 Pa·s) [18]. The lower viscosity of PEEK 151 was assumed to result in better diffusion into the porous PEEK structure. Although no significant difference in diffusion of the molten polymer into the porous structure was noticed, the printing results indicated that AM200 led to less warpage compared to the PEEK 151 material due to the slow crystallizing nature of the AM 200. Figure 3 (a) shows a PEEK structure with 100% infill printed using the PEEK 151 filament onto a porous PEEK structure. In Figure 3 (b), PEEK structures with 50% and

25% infill were separately printed on two sides of a porous PEEK structure.

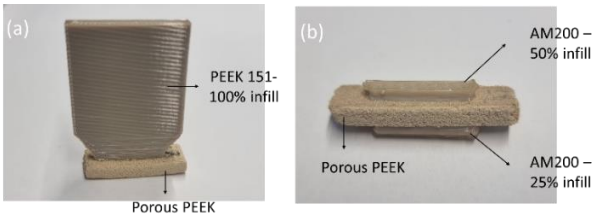

Figure 3. (a) A PEEK 151 structure with 100% infill was printed onto a porous PEEK structure and (b) AM 200 structures with 50% and 25% infill were separately printed on two sides of a porous PEEK structure.

Figure 4 shows digital microscope images of the interface between a solid MEX printed AM200 structure (100% infill) and a porous PBF printed PEEK structure. Printing layers are clearly observed in the images. The first layer was measured to be 0.4 mm thick with subsequent layers thicknesses of 0.2 mm, matching the printing details shown in Table 1. The images have demonstrated the effective infusion of solid PEEK material into the porous structures.

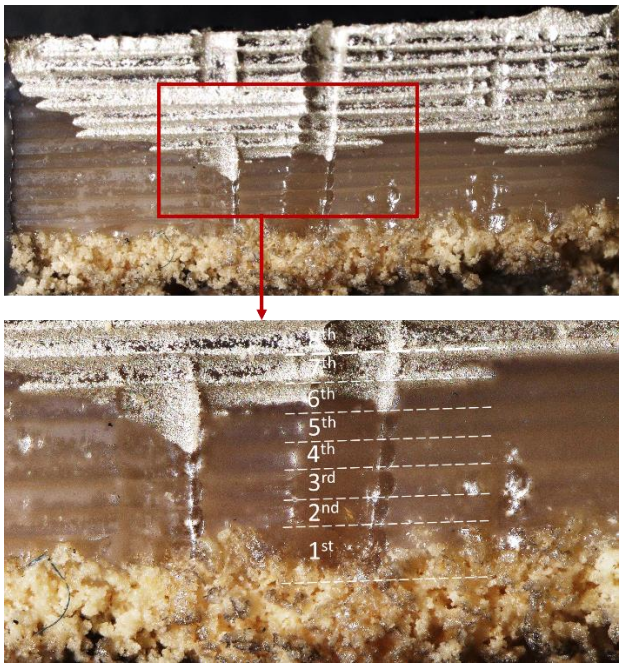

Figure 4. Digital microscope images of the interface between a solid PEEK structure (AM200 with 100% infill) and a porous PEEK structure. First layer thickness: 0.4 mm and subsequent layer thickness: 0.2 mm.

Conclusions

In this study, a blend of sodium chloride crystals and PEEK powder was formulated to create highly porous PEEK structures via the PBF process. The incorporation of the sodium chloride as a porogen material was used to generate open pores, resulting in porous structures with good mechanical performance. PAEK structures were then MEX printed onto the porous PEEK, demonstrating effective material infusion at the interface. The combination of random pore size distribution and solid structure combined with the design freedom and customisation suggests promising applications in the implant industry. The findings from this feasibility study demonstrate the viability of fabricating porous PEEK structures through an innovative, hybrid AM approach that integrates two distinct AM technologies in a sequential, two-stage process.

References

[1] S.M. Kurtz, J.N. Devine, PEEK biomaterials in trauma, orthopedic, and spinal implants, Biomaterials 28(32) (2007) 4845-4869.
[2] J.M. Toth, M. Wang, B.T. Estes, J.L. Scifert, H.B. Seim, A.S. Turner, Polyetheretherketone as a biomaterial for spinal applications, Biomaterials 27(3) (2006) 324-334.
[3] W.R. Walsh, N. Bertollo, C. Christou, D. Schaffner, R.J. Mobbs, Plasma-sprayed titanium coating to polyetheretherketone improves the bone-implant interface, The Spine Journal 15(5) (2015) 1041-1049.
[4] Y.-C. Chou, D.-C. Chen, W.A. Hsieh, W.-F. Chen, P.-S. Yen, T. Harnod, T.-L. Chiou, Y.-L. Chang, C.-F. Su, S.-Z. Lin, S.-Y. Chen, Efficacy of anterior cervical fusion: Comparison of titanium cages, polyetheretherketone (PEEK) cages and autogenous bone grafts, Journal of Clinical Neuroscience 15(11) (2008) 1240-1245.
[5] M. Roskies, J.O. Jordan, D. Fang, M.-N. Abdallah, M.P. Hier, A. Mlynarek, F. Tamimi, S.D. Tran, Improving PEEK bioactivity for craniofacial reconstruction using a 3D printed scaffold embedded with mesenchymal stem cells, Journal of Biomaterials Applications 31(1) (2016) 132-139.
[6] N.T. Evans, F.B. Torstrick, C.S.D. Lee, K.M. Dupont, D.L. Safranski, W.A. Chang, A.E. Macedo, A.S.P. Lin, J.M. Boothby, D.C. Whittingslow, R.A. Carson, R.E. Guldberg, K. Gall, High-strength, surface-porous polyether-ether-ketone for load-bearing orthopedic implants, Acta Biomaterialia 13 (2015) 159-167.
[7] S.M. Kurtz, J. Day, K. Ong, Chapter 14 - Isoelastic Polyaryletheretherketone Implants for Total Joint Replacement, in: S.M. Kurtz (Ed.), PEEK Biomaterials Handbook, William Andrew Publishing, Oxford, 2012, pp. 221-242.
[8] S. Lovald, S.M. Kurtz, Chapter 15 - Applications of Polyetheretherketone in Trauma, Arthroscopy, and Cranial Defect Repair, in: S.M. Kurtz (Ed.), PEEK Biomaterials Handbook, William Andrew Publishing, Oxford, 2012, pp. 243-260.
[9] B. Yuan, Q. Cheng, R. Zhao, X. Zhu, X. Yang, X. Yang, K. Zhang, Y. Song, X. Zhang, Comparison of osteointegration property between PEKK and PEEK: Effects of surface structure and chemistry, Biomaterials 170 (2018) 116-126.
[10] C. Liao, Y. Li, S.C. Tjong, Polyetheretherketone and Its Composites for Bone Replacement and Regeneration, Polymers (Basel) 12(12) (2020).
[11] Z. Chen, Y. Chen, Y. Wang, J. Deng, X. Wang, Q. Wang, Y. Liu, J. Ding, L. Yu, Polyetheretherketone implants with hierarchical porous structure for boosted osseointegration, Biomaterials Research 27(1) (2023) 61.
[12] Y. Zhao, H.M. Wong, W. Wang, P. Li, Z. Xu, E.Y.W. Chong, C.H. Yan, K.W.K. Yeung, P.K. Chu, Cytocompatibility, osseointegration, and bioactivity of three-dimensional porous and nanostructured network on polyetheretherketone, Biomaterials 34(37) (2013) 9264-9277.
[13] J. Wu, L. Li, C. Fu, F. Yang, Z. Jiao, X. Shi, Y. Ito, Z. Wang, Q. Liu, P. Zhang, Micro-porous polyetheretherketone implants decorated with BMP-2 via phosphorylated gelatin coating for enhancing cell adhesion and osteogenic differentiation, Colloids and Surfaces B: Biointerfaces 169 (2018) 233-241.
[14] Multiscale Porous Poly (Ether-Ether-Ketone) Structures Manufactured by Powder Bed Fusion Process, 3D Printing and Additive Manufacturing 11(1) (2024) 219-230.
[15] S. Berretta, K.E. Evans, O. Ghita, Processability of PEEK, a new polymer for High Temperature Laser Sintering (HT-LS), European Polymer Journal 68 (2015) 243-266.
[16] A.R. Siddiq, A.R. Kennedy, Porous poly-ether ether ketone (PEEK) manufactured by a novel powder route using near-spherical salt bead porogens: Characterisation and mechanical properties, Materials Science and Engineering: C 47 (2015) 180-188.
[17] VICTREX™ PEEK POLYMER 150G, Victrex Manufacturing Limited. https://www.victrex.com/en/downloads/datasheets/victrex-peek-150g.
[18] VICTREX AM™ 200 FIL datasheet, Victrex Manufacturing Limited. https://www.victrex.com/en/downloads/datasheets/victrex-am-200-fil.

Use of AI-based software for rapid optimization of printing parameters for a novel 3D printer with thermal radiation heating for the production of PEEK samples in small dimensions

Jiandong Li[1], Franziska Schmidt[1], Jamila Yassine[1], Adam Rumjahn[2], Marien Wolthuis[2], Pavel Cacivkin[3], Matthias Kaiser[3], Andreas Dominik Schwitalla[1,4]

[1] Charité – Universitätsmedizin Berlin, Corporate Member of Freie Universität Berlin and Humboldt- Universität zu Berlin, Dental Materials and Biomaterial Research, Department of Prosthodontics, Geriatric Dentistry and Craniomandibular Disorders, Aßmannshauser Str. 4-6, 14197, Berlin, Germany
[2] Orion Additive Manufacturing GmbH, c/o Start-A-Factory, Gustav-Meyer-Allee 25/Gebäude 17/3, 13355 Berlin, Germany
[3] Exponential Technologies, Dzērbenes iela 14, Rīga, LV-1006, Latvia
[4] Einstein Center Digital Future (ECDF), Robert-Koch-Forum, Wilhelmstr. 67, 10117 Berlin, Germany

jiandong.li@charite.de, franziska.schmidt2@charite.de, jamila.yassine@charite.de, adam@orion-am.com, marien@orion-am.com, pavel.cacivkin@x-t.ai, matthias.kaiser@x-t.ai, andreas.schwitalla@charite.de

Introduction: Additive manufacturing, particularly of small components made of polyether ether ketone (PEEK) via material extrusion (MEX), continues to pose a major challenge. At the same time, many different parameters have a major influence on the quality of the manufactured components, such as nozzle temperature, chamber temperature, print speed, etc., so that numerous experiments are theoretically necessary to determine the ideal printing parameters. Therefore, the aim of the present study was to determine the ideal printing parameters regarding the mechanical properties of very small dimensioned components with the help of an artificial neuronal network (ANN) in order to minimize the number of necessary experiments.

Methods and Materials: 6 different parameter combinations were suggested by AI-based software (xT SAAM, Exponential Technologies, Riga, Latvia). With the help of these, n=2 samples in the form of small rods (1 x 2 x 15 mm) were produced by MEX and subjected to 3-point bending tests. The parameter combination that showed the best mechanical properties was used to produce a further n=14 samples, which were again subjected to 3-point bending tests. A parameter combination that had been evaluated in preliminary tests was used as a control group, with which n=14 samples were also produced and subjected to 3-point bending tests.

Results: The n=14 specimens based on the production using the optimized parameter setting showed a flexural modulus of 2989.3 ± 141 MPa and a flexural strength of 154.8 ± 4.8 MPa, while the n=14 specimens of the control group showed a flexural modulus of 2704.3 ± 239.6 MPa and a flexural strength of 139 ± 11.7 MPa.

Discussion: With the help of the AI-based software, an ideal combination of parameter settings for the additive manufacturing of small PEEK-based components via MEX could be found with a small number of experiments.

Further optimization experiments were not pursued, as the mechanical properties of the additively manufactured samples already exceeded those of industrially extruded PEEK.

Theoretically, in order to continue the search for further optimized parameters, the results of the tests must be entered into the software as feedback, whereby it was previously determined which result has the highest importance. The software then ranks the experimental groups based on this and suggests new experimental groups with new parameter combinations, which are then used to produce new samples. This procedure can be repeated until no further optimization is found.

Taguchi Optimization of Additively Manufactured PEKK and Silicon Nitride Loaded PEKK for Medical Device Applications

Tabitha Derr, Cemile Basgul, Paul DeSantis, Ryan M. Bock, Steven M. Kurtz

Introduction:

Periprosthetic joint infection remains a prevalent issue in modern joint arthroplasty. Silicon nitride, known to exhibit anti-bacterial properties and support osteoblast maturation, provides an effective method of combating infection. Incorporating silicon nitride with polyetherketoneketone (PEKK) enables it to exploit PEKK's favorable mechanical properties and advantageous manufacturability using extrusion-based additive manufacturing. Hence, silicon nitride loaded polyetherketoneketone (SN PEKK) composites may be of potential value in creating infection-resistant patient-specific medical implants. Our objective was to determine optimal fused filament fabrication (FFF) parameters for PEKK and SN PEKK.

Methods:

Taguchi optimization (L9 array, n=5) was performed on PEKK (IMPEKK® 3D-F, Seqens) and SN PEKK to assess the impact of printing parameters (layer height, nozzle temperature, bed temperature, and chamber temperature) on ultimate tensile strength (UTS). Z-directional tensile specimens were printed on a medical FFF printer (EXT 220 MED, 3D Systems). Specimens underwent tensile testing according to ASTM D638. Signal/noise ratios for UTS were calculated and ANOVA (Minitab 21.4.2) was used to assess statistical significance ($p<0.05$).

Results:

Layer height had the greatest impact on UTS (signal/noise range: PEKK, 2.0 and SN PEKK, 4.4). Optimal nozzle and chamber temperatures were 400 ºC and 130 ºC for both materials, while optimal layer height was 0.1 mm for both materials. Optimal bed temperature for PEKK and SN PEKK were 150 ºC and 170 ºC, respectively. For PEKK, differences in all parameters were significant except bed temperature, while for SN PEKK all parameters were significant except nozzle temperature. Models with a layer height of 0.1 mm required 3 hours 23 minutes to print, while those with a layer height of 0.3 mm needed 1 hour 9 minutes. The specimens with optimum statistically significant parameters showed the highest UTS for both PEKK (91 ± 2 MPa) and SN PEKK (76 ± 3 MPa).

Conclusions:

Layer height is the most influential printing variable for both PEKK and SN PEKK; however, low layer height significantly increases print time. The optimal PEKK printing condition has a UTS comparable to that of injection molded specimens, but SN PEKK achieved only 84% of the injection molded value for neat PEKK. Further research is needed to understand SN dispersion in the composite tensile specimens and its potential implications on the behavior of medical implants.

3D-Printing at the Point-of-Care:
Patient-Specific PEKK Ankle Fusion Implants for Diabetic Patients

Pearle M. Shah

Failed total ankle arthroplasty (TAA), ankle trauma, or health conditions such as Charcot neuroarthropathy are just a few reasons that may lead to ankle fusion surgeries or ankle arthrodesis. Specifically, diabetes affects 11.6% of the adult U.S. population and has a significant impact on bone health and healing, putting diabetic individuals at a high risk for such surgeries. In one cohort of diabetic patients requiring primary arthrodesis from ankle fractures, an overall complication rate exceeding 75% was found, including issues such as reoperation, infection, non-union, and amputation. Current off-the-shelf ankle fusion cages fail to address the complex anatomies of ankle defects, while customized 3D-printed metal cages pose challenges like metal allergies, cage subsidence, or long manufacturing times. To address complex ankle defect anatomies in diabetic patients and long implant manufacturing times, this study aims to define the design envelope for the development of patient-specific tibiotalar cages using polyetherketoneketone (PEKK) for 3D-printing at the point-of-care (3DP-POC).

A dataset of patient CT scans with a primary cause of death from diabetes was segmented using CT segmentation software (DICOM to Print). Rectangular cages were fitted into each reconstructed anatomical model in Shapr3D based on the boundaries for resection to determine the lower and upper bound cages (extremes of the design envelope). These rectangular cages were refined and customized to fit the exact anatomies of the corresponding patients in Geomagic Freeform. The 3DGence slicing software was then utilized to add porosity and walls to enhance osseointegration and mechanical stability. A high-precision FDM printer, 3DGence Industry F421, was used to print the cages with Kimya PEKK-A filament.

Dimensional analysis, porosity calculations, and static axial compression tests (ASTM F2077) were conducted. All cages fell within the desired printing tolerances of PEKK-A, indicating good dimensional accuracy. A high porosity (>50%) and mechanical stability (>3.6 kN per ASTM F2665) were also achieved. The final cage designs were evaluated by a surgeon who determined their clinical relevance for diabetic patients needing a fusion grid after ankle arthroplasty. This approach strives to shift current clinical standards for ankle fusion surgeries, especially in diabetic patients, through patient-specific 3DP-POC PEKK tibiotalar implants.

Antibacterial Properties of 3D Printed PEKK

Porteus, JS[1]
[1]Oxford Performance Materials Inc., CT, USA
jporteus@oxfordpm.com

Introduction: Per the CDC, on any given day, about 1 in 31 hospital patients has at least one healthcare-associated infection. Infection is a significant risk for patients receiving a medical device implant, as it can lead to complications such as patient harm, failure of the implant, and the need for revision surgery. Prevention of implant-associated infections is crucial for a successful outcome.

Antibacterial properties of PEKK were previously reported by Wang et al., and the study found significant decreases of *Staphylococcus epidermidis* and *Pseudomonas aeruginosa* attachment and growth on the PEKK surface after five days of culture when compared to PEEK.[1]

The objectives of the present *in vitro* study were (1) to determine bacteria colonization and antibacterial activity on PEKK samples fabricated by OPM's OsteoFab additive manufacturing process as compared to PEEK and titanium and (2) to determine the mechanism(s) of the antibacterial properties of PEKK.

Methods and Materials: For the antibacterial activity experiments, bacteria studied included *S. epidermidis*, *P. aeruginosa*, and methicillin-resistant staphylococcus aureus (MRSA), obtained from the American Type Culture Collection as 35984, 25668, and 36794, respectively. PEKK, PEEK, and titanium disc samples (n=12 discs per material per bacterium) were sterilized, bacteria were rehydrated in Luria broth (LB) supplemented with 10% fetal bovine serum and inoculated on the sample surface, and bacteria functions were determined at 1, 5, and 7 days. Three assays were used to determine bacteria functions: crystal-violet staining, live/dead assay, and spreading and plating method for CFU determination.

For the mechanism experiments, it was postulated that surface roughness and the related surface energy of the materials modulated the adsorption of endogenous antibacterial proteins, including mucin, casein, and lubricin, and that increased protein adsorption would be correlated to greater antibacterial effect. Surface roughness and surface energy of the PEKK, PEEK, and titanium materials were first determined using atomic force microscopy and contact angle measurements, respectively. To measure protein adsorption, disc samples were sterilized and placed in culture media (LB with 10% fetal bovine serum) for 24 hours. After 24 hours, proteins were extracted from the samples by soaking in 10% sodium dodecyl sulfate (SDS) for five minutes. ELISA was then used to analyze the protein eluant supernatant to determine type and quantity of adsorbed proteins, with a focus on mucin, casein, and lubricin.

To correlate the increased adsorption of key proteins from the culture media on the samples to inhibition of bacteria, additional samples were coated with 10 micrograms/ml of proteins that demonstrated an increased adsorption trend on the sample through simple soaking. Bacteria experiments performed for the antibacterial activity experiments were then repeated on the protein pre-adsorbed samples (n=3 discs per protein per bacterium) using a single 24-hour time point. Crystal-violet staining, live/dead assay, and spreading and plating assays were again used to determine bacteria functions.

All PEKK samples were manufactured via OPM's proprietary OsteoFab® additive manufacturing process, which is the laser sintering of polyetherketoneketone (PEKK) polymer to produce functional parts. PEEK and titanium (Ti-6Al-4V ELI) materials were obtained and used as controls.

Results: Results from the antibacterial activity study showed significant reductions in colonization of *S. epidermidis*, *P. aeruginosa*, and MRSA on PEKK compared to PEEK and titanium after nearly all time points of the study when measured via colony forming units, crystal violet staining, and live/dead staining. Importantly, the greatest reduction in colonization on PEKK was seen with MRSA, as shown in Figure 1. Live/dead staining further showed that of those bacteria that were counted on the PEKK surface, significantly less were alive when compared to PEEK and titanium.

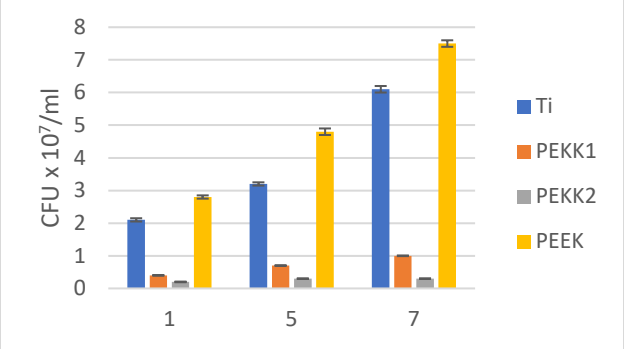

Figure 1. Results of MRSA colonization on PEKK, PEEK, and titanium at 1, 5, and 7 days.

Results from the mechanism experiments showed that the surface energy of PEKK is more similar to the surface energies of mucin, casein, and lubricin versus PEEK and titanium (Table 1). PEKK adsorbed up to 6x, 8x, and 3x more casein, mucin, and lubricin protein, respectively, versus PEEK and titanium (Table 2). Bacteria inhibition testing of the protein pre-adsorbed samples correlated increased protein adsorption to increased bacteria

inhibition on PEKK; in all assays for all nine combinations of bacteria and protein tested, colonization on PEKK was significantly decreased compared to PEEK and titanium. CFU results for the MRSA and mucin combination are shown in Figure 2. Live/dead staining again showed that of those bacteria that were counted on the PEKK surface, significantly less were alive when compared to PEEK and titanium.

Table 1. Surface energies of test samples and proteins.

	Surface Energy/Surface Tension (mN/m)
Ti	62.5
PEEK	16.3
PEKK	35.7
Casein	48.0[2]
Mucin	42-46[3]
Lubricin	40[4]

Table 2. Protein adsorption to test samples (ELISA intensity).

	Casein	Mucin	Lubricin
Ti	0.1	0.2	0.1
PEEK	0.1	0.1	0.1
PEKK	0.6	0.8	0.3

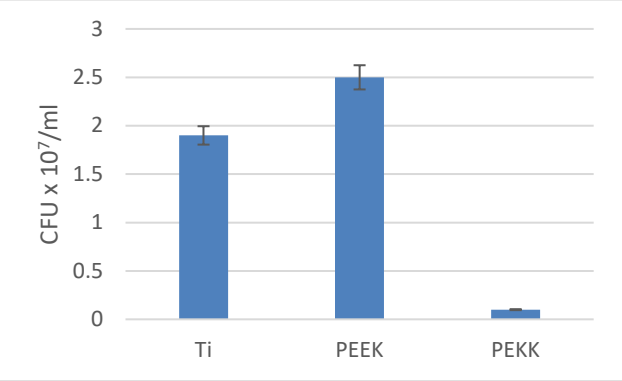

Figure 2. CFU count results after 24 hours of MRSA colonization on PEKK, PEEK, and titanium samples pre-adsorbed with mucin.

Discussion: Results from these studies provide significant evidence of the antibacterial properties of PEKK, without the use of antibiotics, and a mechanism of action of decreased colonization: (1) the surface energy of PEKK is closer in value to key proteins (casein, mucin, and lubricin) known to inhibit bacteria colonization, (2) increased adsorption of casein, mucin, and lubricin on PEKK versus PEEK and titanium, and (3) decreased bacteria colonization by *S. epidermidis*, *P. aeruginosa*, and MRSA on PEKK when coated with casein, mucin, and lubricin. Further, the live/dead assays demonstrated that of the lower overall numbers of bacteria counted on PEKK, more were dead compared to PEEK and titanium, further demonstrating the potential for decreased bacterial colonization on the surface of PEKK as compared to other implant materials.

References:

1. Wang, M., Bhardwaj, G., & Webster, T. (2017). Antibacterial properties of PEKK for orthopedic applications. International Journal Of Nanomedicine, Volume 12, 6471-6476.
2. Colloid and Interface Chemistry for Nanotechnology, CRC Press, 2014.
3. Nagyová B, Tiffany JM. Components responsible for the surface tension of human tears. Curr Eye Res. 1999 Jul;19(1):4-11.
4. Zappone B, Ruths M, Greene GW, Jay GD, Israelachvili JN. Adsorption, lubrication, and wear of lubricin on model surfaces: polymer brush-like behavior of a glycoprotein. Biophys J. 2007 Mar 1;92(5):1693-708.

Lycopene and nano-CaO_2 decorated porous polyetheretherketone scaffold for anti-tumor and osteogenesis

Dongmei Yu[1,2], Chaozong Liu[1], Zheng Guo[2]
[1] Institute of Orthopaedics and Musculo-Skeletal Science, University College London, The Royal National Orthopaedic Hospital, Stanmore, HA7 4LP, UK
[2] Department of Orthopedics, Tangdu Hospital, Fourth Military Medical University, Xi'an, 710038, China
dongmei.yu@ucl.ac.uk; chaozong.liu@ucl.ac.uk; guozheng@fmmu.edu.cn

Introduction: Osteosarcoma (OS), the most commonly occurring primary bone malignant tumor, mainly emerged in children and adolescents. The bottleneck is that the current clinical strategy with a combination of neoadjuvant chemotherapy and surgical resection, does not realize the time-sequential treatment requirement for postsurgical OS administration. Firstly, surgical resection could hardly remove tumor tissues completely, while postsurgical chemotherapy fails to efficiently suppress the tumor recurrence. Secondly, surgical resection leads to extensive bone defect, which is hard to repair. The clinical postsurgical OS treatment faces big challenges for the staged therapeutic requirements of early anti-tumor and long-lasting osteogenesis. Calcium (Ca) as one of the most abundant elements in bone can noteworthy enhance osteogenesis. The released H_2O_2 initiates chemodynamic therapy to induce apoptosis in tumor cells. Lycopene due to special structure composed of 89.45 % carbon and 10.51 % hydrogen ($C_{40}H_{56}$) and containing 11 linear conjugated bonds and 2 non-conjugated double bonds, provides a strong antioxidant activity. Based on above-mentioned consideration, nano-CaO_2 and lycopene decorated porous polyetheretherketone (PEEK) scaffold was designed to realize anti-tumor and osteogenesis.

Methods and Materials: Porous PEEK scaffolds were fabricated using a fused filament fabrication with pore size of 600 μm and the interconnected PEEK struts width of 400 μm. Porous PEEK scaffolds were immersed in concentrated sulfuric acid (98%) at room temperature for 5 min to activate surface via sulfonation reaction (SPEEK). Thereafter, SPEEK was immersed in norepinephrine dissolved in Tris-HCl buffer solution, and then soaked in saturated nano-CaO_2 solution followed by washing with distilled water. Subsequently, lycopene gel is used to immerse above-mentioned sample to acquire lycopene and nano-CaO_2 decorated porous SPEEK scaffold.

Results: Lycopene and nano-CaO_2 decorated porous polyetheretherketone scaffold was successfully fabricated and occurred time-sequential release of lycopene and nano-CaO_2. On one hand, lycopene and O_2-generating source of nano-CaO_2 could efficiently eliminate the residual OS cells, as verified by live/dead staining assay, showing red fluorescence positive dying cells. The intracellular ROS levels of Saos-2 cells may elevate after incubating with an extract diluent medium of lycopene and nano-CaO_2 decorated scaffolds, as detected by a ROS probe DCFH-DA, suggesting brighter green fluorescence. The excess ROS damaged cells by randomly attacking the intracellular components, which would initiate the execution of cell death. Suppressing performance for postsurgical tumor recurrence on a subcutaneous OS mouse model in vivo was monitored by imaging system and tumor volume measurement. It revealed that lycopene and nano-CaO_2 decorated porous SPEEK scaffold prominently eliminated the remaining tumor relapse as shown by fluorescence images. Lycopene regulated polarization to M2 phenotype of macrophages, as demonstrated by representative immunofluorescence and immunohistochemistry staining. Furthermore, lycopene and nano-CaO_2 promoted osteogenesis visualized by alkaline phosphatase (ALP) staining, alizarin red (AR) staining and gene expression level. The osteoimmune microenvironment changes in vivo as bone healing progressed, showing excellent anti-inflammatory capacity of lycopene and nano-CaO_2 decorated porous SPEEK scaffold. The mineral apposition rate (MAR) and the new bone formation rate (BFR/BS) calculated by bone histomorphometry indicated higher bone defect repair capability of above-mentioned composite scaffold compared to the control.

Discussion: The repair process after lycopene and nano-CaO_2 decorated porous SPEEK scaffold implantation in the defect area can be divided into an early ROS-dominated period and a long-term Ca^{2+}-dominated period. Lycopene release and a large amount of ROS accumulates led to in situ tumor cell death. Moreover, the early action of ROS promoted M1-type macrophages to inhibit tumor cell growth. With the decreased and finally exhausted release of ROS, the released Ca^{2+} dominantly polarized the M2-type macrophages and ultimately promoted the repair of bone defects via Wnt3a/GSK-3β/β-catenin signaling pathway. In summary, lycopene and nano-CaO_2 decorated porous SPEEK scaffold time-sequentially resulted in tumor cell death, regulated microenvironment, and promoted osteogenesis.

Mechanical, morphological, calorimetric and spectroscopic characterization of 3D printed and annealed PEEK and carbon-fiber reinforced PEEK specimens

Medel, F.J.[1,+*], Pascual F.J.[2,+], Martínez-Nogués V.[3], Alconchel A.[3], Hornero C.[4], Fernández, J.M.[5]
[1]Dpt. Mechanical Engineering- [+]Aragon Institute of Engineering Research (I3A), University of Zaragoza, Spain.
[2]Centro Universitario de la Defensa de Zaragoza, CUD-AGM, Spain
[3]R&D Department, TECNOPACKAGING, Spain.
[4]Advanced Materials Department, Moses Productos, Spain.
[5]R&D Department, AITIIP Centro Tecnológico, Spain.
[*]*fjmedel@unizar.es*

Introduction: Additive manufacturing of poly-ether-ether-ketone (PEEK) components is becoming very popular in the biomedical engineering and orthopedic fields, not only for prototypes, but even for end-use products [1]. In this context, the characterization of mechanical and structural properties of 3D printed PEEK products is paramount to ensure the fabrication process has imparted the desired properties. In this work, we present an extensive characterization of PEEK and carbon fiber-reinforced PEEK samples before and after a post-3D printing annealing treatment.

Methods and Materials: Uniaxial tensile test specimens were 3D printed from PEEK and carbon fiber-reinforced PEEK (CF-PEEK) filaments (diameter 1.75 mm; TreeD filaments; Italy) using a Intamsys Funmat HT (INTAMSYS Technology GmbH, Germany). The selected 3D printing parameters were nozzle sizes 0.4 and 0.5 mm, for PEEK and CF-PEEK, respectively, bed temperature 160 ºC, nozzle temperature 400-415 ºC, print speed 35-40 mm/s, layer thickness 0.2 mm and infill density 100%. After manufacturing, some of the tensile samples were subjected to a thermal treatment at 240 ºC for 4 hours in vacuum (Qualivac Vacuum Oven; LTE-Scientific, UK). Tensile tests (n=6) were carried out to fracture at a displacement rate of 5 mm/min in an Instron 5565. Fracture surfaces were observed under the scanning electron microscope (Merlin FESEM; Carl Zeiss). Then, differential scanning calorimetry (DSC) experiments were conducted using a DSC3+, (Mettler Toledo; Spain) to evaluate the crystallinity of samples obtained from different regions of the 3D printed specimens. Melting temperatures and fusion enthalpy areas were obtained from the first heating run from 25 to 450 °C (heating rate 10 °C/min). Crystallinity percentages were calculated based on the following formula: $X_c(\%)= \Delta H_m/(w_p \Delta H^0_m)$, where ΔH_m was the enthalpy of melting, ΔH^0_m is the standard enthalpy of fusion of a 100% crystalline PEEK sample (130 J/g) and w_p is the PEEK content (85% for CF-PEEK). Finally, Raman spectroscopy was performed to obtain spectra of different regions using an Alpha 300 M+ confocal Raman spectrometer (Oxford Instruments; UK), working with a 785 nm laser. The height ratio between peaks at about 1146 cm^{-1} and 1598 cm^{-1} was chosen to monitored crystallinity variations within 3D printed samples before and after annealing [2].

Results: 3D printed PEEK tensile samples withstood average yield and fracture stresses of 82.1±5.7 and 71.3±3.7 MPa, respectively, and a strain to fracture close to 10% (Figure 1a; Table 1). On the other hand, CF-PEEK specimens fractured very close to the yield point (64.2±7.7 MPa) and they exhibited a remarkably lower fracture strain close to 4%. Annealed PEEK specimens experienced an increase in both yield and fracture stresses (92.4±1.0 and 86.8±1.3, respectively), but the fracture strain decreased below 8% (Figure 1b; Table 1). In the case of CF-PEEK specimens, the thermal treatment increased about a 10% their maximum stress (71.7±7.6 MPa) and provoked a slight reduction in fracture strain. SEM images of fracture surfaces revealed the layer structure of 3D printed specimens. Fracture surfaces of as-3D printed and annealed PEEK were very similar and they exhibited few ripples at high magnification (Figure 2). Fracture surfaces of 3D printed CF-PEEK had a different appearance, as the layer structure and especially the filaments were less evident (Figure 3). High magnification SEM images revealed the presence of carbon fibers and holes of different sizes (10-80 μm). Thermally treated CF-PEEK samples still exhibited holes, but they appeared to be smaller (10-50 μm). DSC results confirmed the PEEK filament had a slightly higher crystallinity (17.6%) than the CF-PEEK one (14.7%). Samples obtained from the perimeter shell of 3D printed PEEK specimens exhibited higher crystallinity (22.7 %), but it was much lower for the inner region (9.6%). After annealing, crystallinity decreased in the perimeter (18.7%), but increased in the inner region (12.2%). DSC experiments of CF-PEEK samples also revealed regional differences in crystallinity. Nevertheless, the variability of DSC results was considerable (Figure 4). Finally, Raman spectra (Figure 5) confirmed that the 1146 cm^{-1} /1598 cm^{-1} height ratio increased after annealing for both PEEK (1.44±0.21 and 1.51±0.09, before and after annealing, respectively) and CF-PEEK samples (1.47±0.32 and 1.54±0.08, respectively).

Discussion: Our study has shown the annealing process improved the maximum stress that 3D printed PEEK specimens withstand. DSC and Raman spectroscopy characterizations confirmed 3D printed specimens are very heterogeneous from the crystallinity point of view and annealing may contribute to homogenize them. Besides 3D printing parameter selection, the choice of appropriate characterization techniques and methods is of great importance.

References: [1] Basgul et al. *J Biomed Mater Res* 2021
[2] Doumeng et al. *Wear* 2019; 426-427 (PartB),1040

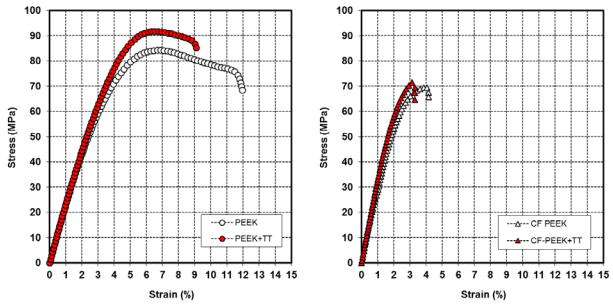

Figure 1. Typical stress-strain curves for unfilled (left) and carbon fiber loaded (right) 3D printed PEEK before (white) and after (red) thermal treatment.

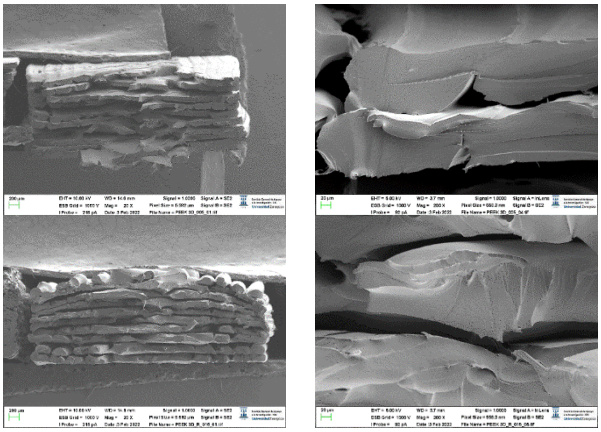

Figure 2. SEM images of 3D printed PEEK fracture surfaces before (above) and after (below) thermal treatment.

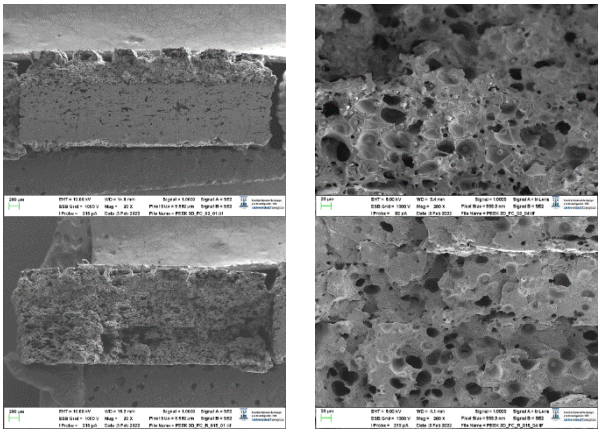

Figure 3. SEM images of 3D printed CF-PEEK fracture surfaces before (above) and after (below) thermal treatment.

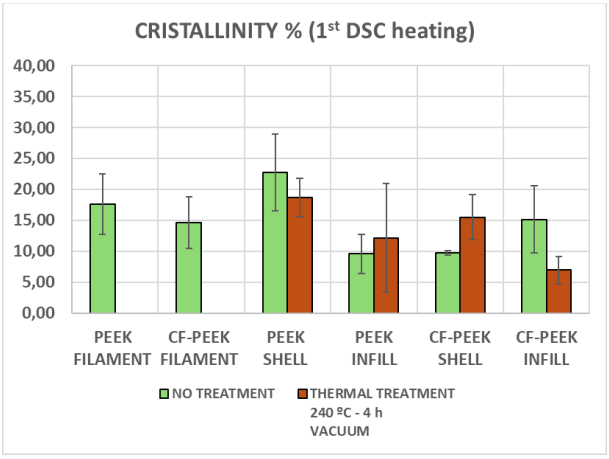

Figure 4. Crystallinity contents for samples obtained from filaments and different regions of tensile specimens before and after thermal treatment.

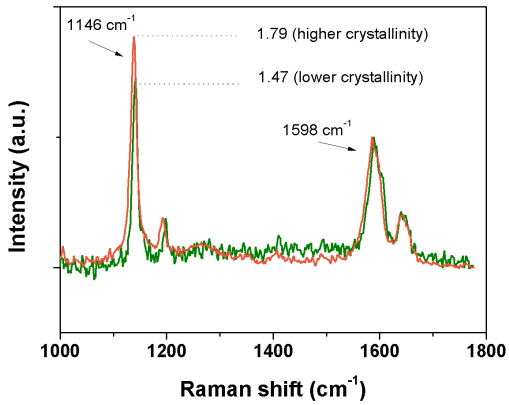

Figure 5. Raman spectra of regions within PEEK and carbon-fiber reinforced PEEK showing different crystallinities (1146 cm^{-1}/1598 cm^{-1} peak height ratios).

Table 1. Mechanical properties from tensile tests (n=6).

	Secant Modulus (GPa)	Yield/ Max. Stress (MPa)	Strain at Yield/ Max. Stress (MPa)	Fracture Stress (MPa)	Fracture Strain (%)
PEEK	2.1±0.1	82.1±5.7	6.6±0.3	71.3±3.7	10.5±2.3
PEEK + TT	2.2±0.2	92.4±1	7.4±1.6	86.8±1.3	7.9±0.9
CF-PEEK	2.5±0.3	64.2±7.7	3.6±0.3	60.7±8.0	3.7±0.4
CF-PEEK + TT	2.8±0.3	71.7±7.6	3.4±0.4	65.0±7.0	3.5±0.4